NRL Memorandum Report 4078

NRL Memorandum Report 4078
EOTPO Report 55

Passive Infrared Surveillance: New Methods of Analysis

RICHARD A. STEINBERG

Electro-Optical Technology Program Office
Management Information and Special Programs Organization

September 24, 1979

ELECTRO-OPTICAL TECHNOLOGY PROGRAM OFFICE
Naval Research Laboratory
Washington, D.C. 20375

DISCLAIMER NOTICE

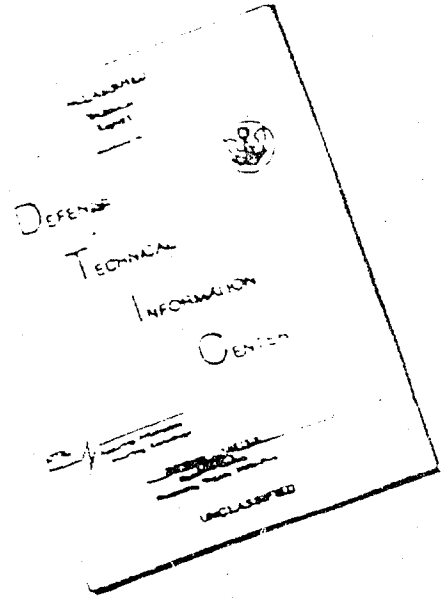

THIS DOCUMENT IS BEST QUALITY AVAILABLE. THE COPY FURNISHED TO DTIC CONTAINED A SIGNIFICANT NUMBER OF PAGES WHICH DO NOT REPRODUCE LEGIBLY.

Reviewed and Approved by

Dr. John M. MacCallum, Jr.

Head, Electro-Optical Technology Program Office

SECURITY CLASSIFICATION OF THIS PAGE (When Data Entered)

REPORT DOCUMENTATION PAGE

READ INSTRUCTIONS BEFORE COMPLETING FORM

1. REPORT NUMBER: NRL Memorandum Report 4078
2. GOVT ACCESSION NO.
3. RECIPIENT'S CATALOG NUMBER

4. TITLE (and Subtitle): PASSIVE INFRARED SURVEILLANCE: NEW METHODS OF ANALYSIS
5. TYPE OF REPORT & PERIOD COVERED: Interim report on a continuing NRL problem.
6. PERFORMING ORG. REPORT NUMBER: EOTPO Report 55

7. AUTHOR(s): Richard A. Steinberg
8. CONTRACT OR GRANT NUMBER(s)

9. PERFORMING ORGANIZATION NAME AND ADDRESS: Naval Research Laboratory, Washington, D.C. 20375
10. PROGRAM ELEMENT, PROJECT, TASK AREA & WORK UNIT NUMBERS: NRL Problem N01-29

11. CONTROLLING OFFICE NAME AND ADDRESS
12. REPORT DATE: September 26, 1979
13. NUMBER OF PAGES: 166

14. MONITORING AGENCY NAME & ADDRESS(if different from Controlling Office)
15. SECURITY CLASS. (of this report): UNCLASSIFIED
15a. DECLASSIFICATION/DOWNGRADING SCHEDULE

16. DISTRIBUTION STATEMENT (of this Report)

Approved for public release; distribution unlimited.

17. DISTRIBUTION STATEMENT (of the abstract entered in Block 20, if different from Report)

18. SUPPLEMENTARY NOTES

19. KEY WORDS (Continue on reverse side if necessary and identify by block number)

Infrared technology
Electro-Optical Technology Program Office (EOTPO)
Electro-optics
Surveillance

20. ABSTRACT (Continue on reverse side if necessary and identify by block number)

A new theoretical procedure is presented for calculating the performance of scanning background-limited (BLIP) infrared sensors with adaptive threshold signal processing logic. The performance predictions obtained with this model are background-conditional, i.e., are valid only for a given infrared background scene, presumably specified as a radiance map of arbitrary (but deterministic) structure. The non-stationary statistical nature of the photocurrent is explicitly taken into account. The basic approach involves a combination of some results from optical communications theory with a formalism

(Continues)

DD FORM 1 JAN 73 1473 EDITION OF 1 NOV 65 IS OBSOLETE
S/N 0102-014-6601

SECURITY CLASSIFICATION OF THIS PAGE (When Data Entered)

20. Abstract (Continued)

for the threshold-crossing statistics of nonstationary noises, originally developed by Rice, Cramer, and Leadbetter.

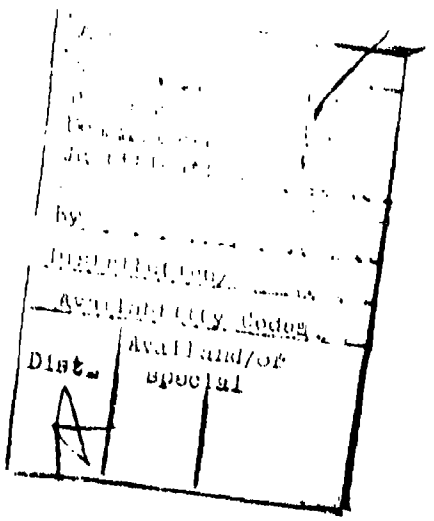

CONTENTS

Appendices

PASSIVE INFRARED SURVEILLANCE: NEW METHODS OF ANALYSIS

I. INTRODUCTION

A. Background

This paper describes an analytical model for predicting the performance of a particular class of infrared sensors, generically described as Infrared Search and Track (IRST) devices. An IRST system generally consists of one or more photodetectors located in the focal plane of a scanning optical telescope, and a complement of signal processing electronics to process the detected photocurrents. The signal processors' task is to determine whether or not an object of a particular type (a "target") is anywhere in the sensors' field of view, while keeping the frequency of false target reports (i.e., the "False Alarm Rate," FAR) to an acceptably low level.

The IRST is a nonimaging device, as contrasted with Forward Looking Infrared (FLIR) imaging systems. [1,2] The search and track device may be required to keep a full hemisphere (2π steradians) under constant observation, have a resolution of one milliradian or less, and operate without human assistance in a fully autonomous mode for weeks at a time. The challenge this presents to the system designer is magnified still further by the abundant opportunities for target/background confusion offered by such typical background scenes as cloudy skies and cities.

Manuscript submitted July 5, 1979.

Previous attempts to model background effects on IRST system performance have focused on the Wiener spectrum approach,[3-8] a frequency domain technique originally developed for calculating the noise variance in communication circuits. Unfortunately, unlike the noise processes typically assumed in statistical communication theory,[9] the IRST photocurrent is apt to be a highly non-stationary random process, inadequately characterized simply in terms of its variance. As the sensor scans across a structured background, the spatially non-uniform scene brightness is mapped into a photocurrent whose mean, variance, and other statistics, are all functions of time. The inadequacy of the Wiener spectrum method under these conditions has been appreciated for many years.[10,11]

The approach taken in this paper brings together and generalizes some results from the theories of optical communications[12] and stochastic processes.[13] In particular, the formulation for "threshold crossing rates" originally derived by Rice[13] for stationary processes is generalized in Section III.B to accomodate such nonstationary processes as arise when nonuniform scenes are scanned by an IRST sensor. A crossing rate formulation similar to that of Section III.B has been previously derived by Cramer and Leadbetter,[14] as discussed in Appendix D.

The general crossing rate formalism is particularized to non-stationary Gaussian statistics in Section III.C, appropriate to the description of the photocurrents of present interest.[12,15]

Some asymptotic approximations to the complete crossing rate integral are developed in Section III.D.

Numerical examples are given in Section V that compare a number of approximate formulations with the rigorous formulation developed in Section III.C. An original analysis of adaptive threshold IRST sensors is presented in Section VI.

Previous works describing analysis techniques for IRST systems are restricted in applicability to uniform scenes. Moreover, these works generally prescribe a totally different formulation for the calculation of FAR than for the calculation of the target detection probability, P_D.[16] The original contribution of this paper is two-fold:

1. An original analysis is presented that unifies the previous work, by showing that the earlier techniques for calculating FAR and P_D are actually both derivable as special cases of a more general formulation, eq. (51).
2. More importantly, an original method for calculating FAR and P_D is presented that is inherently applicable to non-uniform scenes.

B. A Basic Threshold Receiver

In order to provide a frame of reference for the following discussion it is necessary to describe a simple IRST receiver structure, and to define the parameters used to characterize IRST performance.

A basic threshold comparison receiver is shown in Fig. 1. The current X(t) at the output of the detector is input to an electrical filter of transfer function H(f). The output current Y(t) of the electrical filter is compared with a threshold $y_o(t)$. If Y(t) exceeds the threshold, the presence of a "target" is declared; otherwise, no target declaration is made.

The probability that the IRST device makes a target declaration when a target is in fact in the sensors' field of view is called the Probability of Detection (P_D). The rate at which false target declarations occur is termed the "False Alarm Rate (FAR)."

One may correctly infer from the statistical nature of the two principal IRST performance measures (FAR and P_D) that the IRST detection problem is inherently statistical.

The means by which the threshold y_o in Fig. 1 is established will not be considered until Section VI. For the purposes of the present discussion, while the possibility of time variation is retained, the threshold $y_o(t)$ is assumed to be deterministic.[a]

---

[a] Consistent with a convention of random process theory, stochastic quantities are assigned capital letters, with sample values designated by the corresponding lower case letters. E.g., a sample function of the random process Y(t) is designated y(t).

Analysis of threshold comparison receivers with stochastic thresholds $Y_o(t)$ is also of interest, particularly when $Y_o(t)$ is derived as a function of the photocurrent $X(t)$. The "adaptive threshold" radar[17,18] and sonar[19] receivers are of this variety. An IRST adaptive threshold processor analysis is presented in Section VI.

II. OUTLINE OF RESULTS

A. Objectives

The objective of the following section is to outline a new method for predicting the expected number of times that the photocurrent from an infrared sensor will cross a time-varying threshold, as the sensor scans a non-uniform scene. The method is based on the development in Section III.B of an expression for the "threshold crossing rate" $\dot{m}_J(t)$ of the random current Y(t) (cf. Fig. 1). The rate $\dot{m}_J$ is integrated to derive the probable number of threshold crossings $m_J(O,T)$ during a time interval T_O:

$$m_J(O,T) = \int_{T_O} \dot{m}_J(t)dt \qquad (1)$$

where T_O is the time interval $|t| < T/2$.

The expected number of threshold crossings $m_J(O,T)$ on the time interval T_O may be related to the usual False Alarm Rate (FAR) and Probability of Detection (P_D) statistics typically used to characterize the performance of IRST devices, as discussed in Appendix C.

An expression for the threshold crossing rate $\dot{m}_J(t)$ will be presented in Section II.C. An approximate asymptotic formulation for m_J is presented in Section II.B. The approximate expression for m_J has sufficient accuracy in many cases and eliminates the need to perform the integral of eq. (1). The asymptotic result given here is derived in Section III.D.

It is assumed that the average photocurrent $m_X(t)$ of the current X(t) (cf. Fig. 1) is a known function of time.

As discussed in Appendix A, $m_x(t)$ is a function of the aperture irradiance, the Modulation Transfer Function, and several other sensor parameters of the system to be modeled (the "model sensor").

B. Asymptotic Formulation for m_J

The basic quantities needed to perform the calculation for the expected number of threshold crossings m_J are

a) The time-varying average value $m_x(t)$ of the random current X(t) (cf. Fig. 1), and

b) The transfer function H(f) of the post-detector filter in Fig. 1.

Equivalently, the Fourier transform of H(f) can be specified in place of H(f):

$$h(t)=\mathcal{F}\{H(f)\} \tag{2}$$

The function h(t) is called the "impulse response" of the post-detector filter, and $\mathcal{F}\{\ \}$ denotes the Fourier transform of the bracketed quantity.

As discussed in Appendix A, H(f) is presumed to include the frequency characteristic of the photodetector. Thus, the photodetector in Fig. 1 is "idealized," in the sense that it is presumed to have a perfect all-pass electrical frequency characteristic, the frequency-dependent part of the detector responsivity having been lumped together with H(f).

As shown in Appendix A, the average value $m_x(t)$ of the random current X(t) in Fig. 1 is derivable in terms of:

a) high spatial resolution radiometric imagery of the infrared scene, in the optical passband of interest

b) the postulated modulation transfer function (MTF) of the optical train of the model system

c) the quantum efficiency and physical dimensions of the focal plane detectors, and

d) the focal plane scan velocity.

The basic equation for obtaining $m_x(t)$ is eq (A-14).

The asymptotic expression for the expected number of threshold crossings m_J can be expressed in terms of the quantities m_y, σ_y, m_z, and σ_z, each of which can be derived as a function of $m_x(t)$. The definitions of m_y, σ_y, and σ_z, are as follows:

$$m_y(t) = E\{Y(t)\} \tag{3a}$$

$$m_z(t) \equiv E\{\dot{Y}(t)\} = \dot{m}_y \tag{3b}$$

$$\sigma_y^2(t) = E\{[Y(t) - m_y(t)]^2\} \tag{4}$$

$$\sigma_z^2(t) = E\{[\dot{Y}(t) - m_z(t)]^2\} \tag{5}$$

Thus, m_y is the mean value of the output Y(t) of the post-detector filter (cf. Fig. 1); σ_y^2 is the variance of Y(t), and σ_z^2 is the variance of $\dot{Y}$.* The expectation operators in eqs. (3)-(5) denote ensemble averages over the photon fluctuation noise. It is assumed throughout the analysis that photon noise is the dominant noise mechanism; in this case, the detector is said to be operating in the "background limited performance" (BLIP) regime.

---

*In the following analysis a dotted quantity denotes the time derivative of the corresponding undotted quantity. Also, $E\{\cdot\}$ denotes the expected value of the bracketed quantity.

As shown in Appendix B, m_y, σ_y, and σ_z bear the following functional relationships to $m_x(t)$:

$$m_y(t) = h(t) \circledast m_x(t) \qquad (6)$$

$$\sigma_y^2(t) = e\ h^2(t) \circledast m_x(t) \qquad (7)$$

$$\sigma_z^2(t) = e\ \left[\dot{h}(t)\right]^2 \circledast m_x(t) \qquad (8)$$

where $h(t)$ is given by eq. (2), e is the electronic charge, and $\circledast$ denotes the process of convolution:

$$a(t) \circledast b(t) = \int_{-\infty}^{\infty} a(\mu)\, b(t-\mu)\, d\mu \qquad (9)$$

The asymptotic formulation for m_J requires knowledge of m_y, σ_y, and σ_z at a discrete set of times. In order to illustrate the two types of time points that have special significance, reference is made to Fig. 2. Fig. 2a is an illustrative example showing the mean value $m_x(t)$ of the random current $X(t)$, as a function of time. The corresponding $m_y(t)$, as obtained from eq. (6), might appear as in Fig. 2b. As shown in Fig. 2b, the threshold function y_o is taken as a constant in order to simplify the discussion of this section; generalization of

the present results to time-varying thresholds is performed in succeeding sections.

With reference to Fig. 2b, times t_1 and t_2 are of special significance in performing the calculation for $m_J(0,T)$.

At time t_2 the mean current m_y crosses the threshold y_o with a positive slope.

As shown in Section III.D., the crossing counter m_J is incremented by unity at time t_2. It may be seen that the following equations are satisfied at time t_2:

$$m_y(t_2) = y_o$$
$$\dot{m}_y(t_2) > 0 \qquad (12)$$

When there are no solutions to eq. (12) during the time interval of interest, the value of m_J is generally dominated by contributions to the integral in eq. (1) that occur near local maxima in $m_y(t)$, such as the maximum at time t_1 in Fig. 2b. The asymptotic expression for the increment in m_J associated with the local maximum of m_y at t_1 can be written as:

$$m_J(t_1,\tau) \approx \dot{m}_J(t_1) \cdot \delta t_1 \qquad (13)$$

where $\dot{m}_J(t_1)$ is the threshold crossing rate at time t_1, and δt_1 is the effective time interval during which $m_y(t)$ remains at its closest proximity to the threshold y_o. The time τ in eq (13) is relatively unimportant; the choice $\tau > 3\delta t_1$ is generally adequate to capture the principal contribution to m_J that occurs in the neighborhood of t_1.

A reasonable approximation to $\dot{m}_J(t_1)$ valid when the time fluctuations in $m_x(t)$ and $m_y(t)$ are slow compared to a characteristic fluctuation time for h(t) is given by:

$$\dot{m}_J(t_1) \doteq \frac{1}{2\pi} \left[\frac{\sigma_z(t_1)}{\sigma_y(t_1)}\right] \exp\left[-u^2(t_1)/2\right] \qquad (14)$$

where $\sigma_y(t_1)$ and $\sigma_z(t_1)$ are obtained from eqs (7) and (8), evaluated at time t_1, and

$$u(t) \equiv \frac{y_o - m_y(t)}{\sigma_y(t)} \qquad (15)$$

Eq. (14) is Rice's original equation for the mean threshold crossing rate of a stationary Gaussian noise.

The effective proximity time δt_1 in eq (13) is given by

$$\delta t_1 = \left[\frac{2\pi}{\dot{u}(t_1)\ \ddot{u}(t_1)}\right]^{\frac{1}{2}} \qquad (16)$$

where $\ddot{u}(t_1)$ is the second derivative of $u(t)$ with respect to time, evaluated at $t = t_1$.

C. The Exact Expression for $\dot{m}_J$

Eq (13), while simple to evaluate, is not always an accurate approximation for m_J. As borne out in the numerical examples of Section V., eq. (13) becomes progressively less accurate as:

a) the target/background contrast decreases, and

b) the width of the peak at t_1 (cf. Fig. 2a) decreases.

The implication of a) and b) is that eq. (13) is unsuitable for analyzing IRST performance in the regime where the clutter discrimination problem is likely to be most serious. The objective of this section is to present the complete expression, eq. (17), for the mean crossing rate $\dot{m}_J$ derived in Section III.C. The exact expression for $\dot{m}_J$ is not subject to limitations a) and b) above. In addition, the derivation leading to eq. (17) is used to guide the derivation in Section VI of a rigorous formulation for adaptive threshold processors.

The exact expression for the mean crossing rate derived in Section III.C., appropriate for non-stationary Gaussian random processes, is

$$\dot{m}_J(t|y_o,\dot{y}_o) = \left(\frac{\sigma_z}{\sigma_y}\right)(1-r^2)^{\frac{1}{2}}\,\phi(u)\,\{\phi(p) + p_1\,\Phi(p)\} \qquad (17)$$

where $\sigma_y(t)$, $\sigma_z(t)$, and $u(t)$ are given by equations (7), (8), and (15), respectively. The functions $\phi(.)$ and $\Phi(.)$ are the Gaussian density function and its integral, respectively:

$$\phi(x) = (2\pi)^{-\frac{1}{2}} \exp(-x^2/2) \tag{18}$$

$$\Phi(x) = \int_{-\infty}^{x} \phi(z)\, dz \tag{19}$$

The quantities p and p_1 in eq (17) are defined by:

$$p = [\sigma_z(1-r^2)^{\frac{1}{2}}]^{-1} \{m_z + ru\sigma_z - \dot{y}_o\, \mu(\dot{y}_o)\} \equiv \begin{cases} p_o & , \dot{y}_o < 0 \\ p_1 & , \dot{y}_o > 0 \end{cases} \tag{20}$$

with m_y given by eq (6), and $\mu(.)$ defined as the unit step function:

$$\mu(x) = \begin{cases} 0 & x \leq 0 \\ 1 & x > 0 \end{cases} \tag{21}$$

Eq (17) is applicable even for time-varying thresholds $y_o(t)$, as may be inferred by noting the presence of $\dot{y}_o(t)$ in eq. (20). The reason for including $y_o(t)$ and $\dot{y}_o(t)$ as arguments of m_J in eq. (17) is explained in Section II.E.

The only still-undefined quantity in eqs. (17) and (20) is r(t), defined now as:

$$r(t) \equiv C_{yz}(t) / (\sigma_y\, \sigma_z) \tag{22}$$

where C_{yz} is the cross covariance function of Y(t) and $\dot{Y}(t)$ (cf. eqs (3)-(5)):

$$C_{yz} \equiv E\{[Y(t) - m_y(t)]\, [\dot{Y}(t) - m_z(t)]\} \tag{23}$$

As shown in Appendix B,

$$C_{yz}(t) = \sigma_y(t)\,\dot{\sigma}_y(t) \tag{24}$$

Thus, from eqs (22) and (24)

$$r(t) = (\dot{\sigma}_y/\sigma_z) \tag{25}$$

It may be noted that eq. (17) was derived subject to the assumption that the photocurrent Y(t) (cf. Fig. 1) is a non-stationary Gaussian process. The justification for this assumption and the constraints it imposes on the validity of eq. (17) are discussed in Appendix F.

For the special case of uniform scenes and stationary thresholds, it follows from eqs. (6) and (7) that

$$m_z = \dot{\sigma}_y = \dot{y}_o = 0 \tag{26}$$

From eqs. (20), (25), and (26)

$$r = p = p_1 = 0 \tag{27}$$

From (17) and (27)

$$\dot{m}_J(t) = (\sigma_z/\sigma_y)\,(2\pi)^{-\frac{1}{2}}\,\phi(u) \tag{28}$$

which is identical to eq. (14). Thus, eq. (17) reduces correctly to Rice's original equation (14), appropriate to the case of stationary Gaussian noise.

Eq. (17) appears almost identical to an equation derived by Cramer and Leadbetter.[14] The relationship between eq. (17) and the corresponding equation in Ref. [14] is discussed in Appendix D.

D. The Character of the Results

The character of the results obtained with eq. (17) is illustrated with the aid of Figs. 2-5. Once again, the fact that the process Y(t) (cf. Fig. 1) has a time-varying mean $m_y(t)$ qualifies Y(t) generically as a "non-stationary" process. Also, while the theory developed in this paper is general enough to accomodate both time-varying and stochastic threshold functions, the present example is simplified by the assumption of a constant threshold y_o (as depicted in Fig. 2b).

Figures 3 and 4 depict, respectively, the crossing rate $\dot{m}_J$ and expected number of threshold crossings m_J corresponding to the mean current $m_y(t)$ and constant threshold y_o of Fig. 2b. The following general observations are made with respect to figures 2-4.

1. As seen in Fig. 3, the function $\dot{m}_J(t)$ is appreciably non-zero over only a very small fraction of the total time interval. The pulse-like waveforms in Fig. 3 are much narrower than the corresponding peaks in Fig. 2.

2. If solutions exist to the equation

$$m_y(t_s) = y_o \tag{29}$$

subject to the constraint that *

$$\dot{m}(t)>0 \quad , \text{ at } t = t_s \tag{30}$$

than the character of m_J is determined almost entirely by the behavior of $\dot{m}_J$ in the near-neighborhood of the times t_s.

*By convention, dotted quantities denote time derivatives of the corresponding undotted quantities.

For each solution of equation (29) that satisfies constraint (30), i.e., for each positive slope threshold crossing by the mean current $m_y(t)$, the expected number of crossings m_J is incremented by unity. Time t_2 in figures 2-4 is an example of this effect.

3. If $m_y(t)$ lies below y_o on the interval $|t|<T/2$, i.e., if no solutions exist to eq. (29), then the character of m_J is determined almost entirely by the behavior of m_J in the near-neighborhood of the local maxima of m_y. Time t_1 in Figures 2-4 illustrates this effect.

4. The precise form of $m_y(t)$ is typically unimportant. For example, the $m_y(t)$ of Fig. 5 might yield effectively the same m_J as the $m_y(t)$ of Fig. 2, subject only to the constraints that the peak value and curvature of m(t) at time t_1 and the values of t_1, t_2, and y_o are the same in figures 2 and 5.

It is assumed throughout much of the analysis that the comparator device in Fig. 1 recognizes only those threshold crossings for which the following two inequalities are observed:

$$\dot{y}(t) > \dot{y}_o(t) \tag{31}$$

and

$$\dot{y}(t) > 0 \tag{32}$$

This assumption on the nature of the comparator device has been incorporated into the analysis in such a way that the analytical expression for $\dot{m}_J$ is insensitive to downcrossings, such as that at time t_3 in Fig. 2. In fact, similar formulations for the crossing rate may be developed subject to different assumptions than (31) and (32), e.g., that the comparator device is sensitive only to downcrossings, or both upcrossings and downcrossings. In general, it might be desirable to incorporate both upcrossing and downcrossing sensitive detectors in a single IRST receiver, in order to develop an estimator of object size.

It should be recognized that a hardware implementation of the crossing detectors analyzed in this paper must first estimate quantities $y(t)$ and $\dot{y}(t)$ before tests (31) and (32) can be performed.

E. Adaptive Threshold Processors

The results described thus far pertain to calculations of the crossing rate performance of processors configured as in Fig. 1, having time-variable, deterministic, threshold functions $y_o(t)$. However, as discussed in Section VI and Appendix E, potential performance advantages accrue to the use of threshold-establishing circuitry that adapts the value of the threshold to the prevailing background conditions. These "adaptive threshold" processors, such as that shown in Fig. 20, give rise to threshold functions that are not only time-varying, but are also inherently stochastic.

By choosing a suitably large value for the delay time T_d in Fig. 20, the filtered current process $Y(t)$ and the threshold process $Y_o(t)$ are rendered statistically independent. As shown in Section VI.B., it follows that:

$$\dot{m}_J(t) = E_{y_o\dot{y}_o}\{\dot{m}_J(t|y_o\dot{y}_o)\} \tag{205}$$

with $\dot{m}_J(t|y_o,\dot{y}_o)$ given by eq. (17). The expectation operator $E_{y_o\dot{y}_o}$ in eq. (205) is defined by:

$$E_{y_o\dot{y}_o}\{.\} = \int\int d\zeta d\eta\, f_{y_o\dot{y}_o}(\zeta,\eta)\,\{.\} \tag{207}$$

where $f_{y_o\dot{y}_o}$ is the joint density function of the threshold process Y_o and it's time derivative $\dot{Y}_o$.

Happily, the crossing rate expression for time-varying deterministic thresholds, eq. (17), is found to be also applicable to the stochastic threshold-crossing rate, eq. (205).

Eq. (205) is further developed in Section VI.C, and the following approximate result is obtained:

$$\dot{m}_J(t) = \dot{m}_J(t \mid m_{y_o}, m_{\dot{y}_o}) \left[1 + \left(\frac{\sigma_{y_o}}{\sigma_y}\right)^2 \varepsilon_1 + \left(\frac{\sigma_{\dot{y}_o}}{\sigma_{\dot{y}}}\right) \varepsilon_2\right] \qquad (225)$$

where σ_y^2 and $\sigma_{\dot{y}}^2$ are calculated from eqs. (7) and (8), respectively. Expressions for m_{y_o}, σ_{y_o}, and $\sigma_{\dot{y}_o}$, are obtained by straightforward analogy to eqs. (6)-(8):

$$m_{y_o}(t) = K\, h_o(t-T_d) \circledast m_x(t) \qquad (189)$$

$$\sigma^2_{y_o}(t) = eK\, h_o^2\,(t-T_d) \circledast m_x(t) \qquad (190)$$

$$\sigma^2_{\dot{y}_o}(t) = eK \left[\dot{h}_o(t-T_d)\right]^2 \circledast m_x(t) \qquad (191)$$

The gain constant K, time delay T_d, and impulse response $h_o(t)$, in eqs. (189)-(191) are design parameters of the adaptive threshold scheme shown in Fig. 20. Expressions for the terms ε_1 and ε_2 in eq. (225) appear as eqs. (226) and (227) in Section VI.C.

As discussed in Section VI.D., the threshold variance factors $\sigma^2_{y_o}$ and $\sigma^2_{\dot{y}_o}$ in eq. (225) represent a "False Alarm Penalty" that causes the false alarm performance of adaptive threshold schemes to be inherently inferior to fixed threshold schemes, against uniform background scenes.

It is also noted that:

a) The analysis of Section VI is applicable to a considerable variety of adaptive threshold processors, including the structures depicted in Figs. 22-24.

b) A list of important design parameter trade-off issues is identified at the end of Section VI.D. The only important obstacle to performing these analyses is the lack of high spatial resolution, radiometric, infrared background imagery.

III. ANALYSIS

A. Introduction

The objective of section III.B. is to derive an expression for the expected value of the number of times a nonstationary noise Y(t) crosses a nonstationary stochastic threshold $Y_o(t)$. The main result of section III.B., eq. (42), is not used in its complete generality until the adaptive threshold processer analysis of Section VI. Eq. (42) is particularized at the end of Section III.B. to the case of deterministic, time-varying thresholds $y_o(t)$.

The crossing rate equation that results, eq. (48), requires knowledge of the joint density function $f_{y\dot{y}}(y,\dot{y})$ of the current Y(t) and its time derivative $\dot{Y}(t)$.

As discussed in Section III.C., the current Y(t) is a non-stationary Gaussian process. It follows that Y(t) and $\dot{Y}(t)$ are jointly Gaussian processes. The joint density $f_{y\dot{y}}$ can then be expressed in terms of five characteristic statistics.

The explicit expression for the jointly Gaussian $f_{y\dot{y}}$ is then used with the general crossing rate expression (48) derived in Section III.B. to derive an explicit expression for the crossing rate, eq. (70). The expressions for the five important current statistics given in Section III.C. are derived in Appendix B. The complete expression for the

expected number of crossings, eq. (72), generally requires the numerical integration of a somewhat complicated integrand. Section III.D. is devoted to deriving some approximations to eq. (72) that don't require numerical integration, and that have greater intuitive appeal.

B. A Basic Equation for Curve Crossing Rates

The first objective of this section is to derive eq. (39) for the average zero-crossing rate of a random process G(t).

The process G(t) is not required to be either stationary or Gaussian. Fig. 6 depicts a sample function g(t) of the process G(t). It is noted that g(t) has a zero-crossing at time t_o:

$$g(t_o) = 0 \tag{33}$$

It follows from (33) and the well-known properties of the Dirac delta-function, $\delta(.)$, that

$$1 = \int_{-\varepsilon_1}^{\varepsilon_2} \delta(g)\, dg = \int_{t_o-\Delta}^{t_o+\Delta} \delta[g(t)]\ |\dot{g}(t)|\, dt \tag{34}$$

where ε_1, ε_2, and Δ are defined in Fig. 6.

It follows from (34) that the total number of zero crossings of the sample function g(t) on the time interval $|t| < T/2$ is given by:

$$J = \int_{T_o} \delta(g)\ |\dot{g}(t)|dt \tag{35}$$

In writing (35) it is assumed that g(t) does not have a zero-crossing either at $t = \pm T/2$. Defining $m_J(0,T)$ as the expected value of J on the time interval T_o:

$$m_J(0,T) = E\{J\} \tag{36}$$

and operating on eq. (35) with the expectation operator $E\{.\}$, one obtains

$$m_J(0,T) = \int_{T_o} dt\ E\{\delta(g)|\dot{g}(t)|\} \equiv \int_{T_o} \dot{m}_J(t)dt \tag{37}$$

with the interval T_o defined by $|t| < T/2$.

From (37)

$$\dot{m}_J(t) = E\{\delta(g)|\dot{g}|\} = \int d\dot{g} \int dg\ f_{G\dot{G}}(g,\dot{g})\{\delta(g)|\dot{g}|\} \tag{38}$$

where $f_{G\dot{G}}(g,\dot{g})$ is the joint probability density function of the process G and its time derivative $\dot{G}$.

The first basic result of this section is the following expression for the zero-crossing rate $\dot{m}_J$:

$$\dot{m}_J(t) = \int |\dot{g}|\ f_{G\dot{G}}(0,\dot{g})\ d\dot{g} \tag{39}$$

Eq. (39) is well-known; however, most references to (39) appear to impose a stationarity requirement on G that is not actually necessary. The applicability of (39) to nonstationary processes appears to have first been recognized by Cramér and Leadbetter.[14]

The domain of integration in eq. (39) is a matter of some interest. If one wishes to calculate only the expected number of positive slope zero-crossings, i.e., the expected number of times that both

$$G(t_o) = 0 \tag{40}$$

and

$$\dot{G}(t_o) > 0 \tag{41}$$

are both satisfied on the interval $|t| < T/2$, the lower and upper limits of integration in (39) should be chosen as 0 and ∞, respectively. The resulting expression for $m_J(0,T)$:

$$m_J(0,T) = \int_{T_o} dt \left\{ \int_o^\infty d\dot{g} \; |\dot{g}| f_{G\dot{G}}(0,\dot{g}) \right\} \tag{42}$$

does not include zero-crossings of the type depicted in Fig. 6, for which $\dot{g} < 0$. Apparently, $\hat{m}_J$ is sensitive only to the "right type" of zero crossing, as defined by the limits of integration in eq. (39).

The process G(t) is now assumed to be formed as the difference of two stochastic processes Y(t) and $Y_o(t)$:

$$G(t) \equiv Y(t) - Y_o(t) \tag{43}$$

where $Y_o(t)$ is referred to as the "threshold process". Without making any assumptions with respect to the statistics of Y(t) and $Y_o(t)$ (e.g., each process may be both non-stationary and non-Gaussian) it follows from (43) that:

$$f_{G\dot{G}}(0,\dot{g}) = \iint d\zeta d\eta \; f_{y\dot{y}y_o\dot{y}_o}(\zeta, \dot{g} + \eta, \zeta, \eta) \tag{44}$$

The proof of (44) is straight-forward (cf. ref. [21], p.131). Eqs. (42) and (44) are the basis of the adaptive threshold processer analysis of Section VI. For the present, it suffices to specialize (44) to the case of non-random thresholds, for which the fourth-order joint density $f_{y\dot{y}y_o\dot{y}_o}$ becomes

$$f_{y\dot{y}y_o\dot{y}_o}(\zeta,\dot{\xi}+\eta,\zeta,\eta) = f_{y\dot{y}}(\zeta,\dot{\xi}+\eta)\,\delta(y_o-\zeta)\,\delta(\dot{y}_o-\eta) \quad (44a)$$

From (44a) and (44)

$$f_{G\dot{G}}(0,\dot{\xi}) = f_{y\dot{y}}(y_o,\dot{\xi}+\dot{y}_o) \quad (45)$$

From (39) and (45)

$$\nu_J(t) = \int|\dot{\xi}|\, f_{y\dot{y}}(y_o,\dot{\xi}+\dot{y}_o)d\dot{\xi} \quad (46)$$

Changing variables:

$$z \equiv \dot{\xi} + \dot{y}_o \quad (47)$$

(46)may be written as

$$\nu_J(t) = \int|z-\dot{y}_o|f_{y\dot{y}}(y_o,z)dz \quad (48)$$

The quantity ν_J, previously interpreted as the zero-crossing rate of the process G (cf. eq. (39)), is now interpreted as the threshold crossing rate of the process Y(t).

The domain of integration of eq. (48) is defined by assuming that the hardware implementation of the threshold counter is sensitive only to those crossings for which the following two inequalities are satisfied simultaneously:

$$\dot{y}(t) > \dot{y}_o(t) \tag{49}$$

and

$$\dot{y}(t) > 0 \tag{50}$$

For the example of Fig. [7] this particular type of detector would increment its "crossing counter" at time t_1, but, by design, would fail to indicate threshold crossings at times t_2, t_3, and t_4.

It follows from eqs. (48) - (50) that

$$\dot{m}_J(t) = I(\infty) - \mu(\dot{y}_o)\ I(\dot{y}_o) \tag{51}$$

Where $\mu(.)$ is given by eq. (21), and

$$I(x) \equiv \int_o^x (z-\dot{y}_o)\ f_{y\dot{y}}(y_o,z)dz \tag{52}$$

The crossing rate $\dot{m}_J$ could just as well have been formulated subject to different constraints than (49) and (50). For example, the hardware implementation of the threshold counter may be sensitive to all crossings for which

$$\dot{y}(t) > 0$$

regardless of the relative magnitudes of $\dot{y}(t)$ and $\dot{y}_o(t)$.

In this case eq. (48) is still subject to the constraint of eq. (50), but the constraint of eq. (49) is no longer in force. It may then be shown that the following expression obtains, instead of eq. (51):

$$\dot{m}_J(t) = I(\infty) - 2\mu(\dot{y}_o)\, I(\dot{y}_o) \qquad (53)$$

with $I(.)$ given by (52).

When $\dot{y}_o < 0$, satisfaction of (50) assures satisfaction of (49). One then expects $\dot{m}_J$ and $\dot{\mathfrak{m}}_J$ to be equal. Inspection of eqs. (51) and (53) shows that this is indeed the case:

$$\dot{\mathfrak{m}}_J(t) = \dot{m}_J(t) = I(\infty) \qquad , \dot{y}_o(t) < 0$$

However, when $\dot{y}_o > 0$ condition (49) is more restrictive than (50). One then expects $\dot{m}_J$ to be greater than $\dot{\mathfrak{m}}_J$. From (51) and (53):

$$\dot{m}_J(t) = \dot{\mathfrak{m}}_J(t) - I(\dot{y}_o) \qquad , \dot{y}_o(t) > 0$$

Since $I(\dot{y}_o)$ is inherently negative (cf. (52)), it follows that $\dot{m}_J > \dot{\mathfrak{m}}_J$, as expected, when $\dot{y}_o > 0$.

With respect to Fig. 7, it can be shown that the integral m_J of eq. (53) is incremented by unity both at time t_1 and t_2. By comparison, $\mathfrak{m}_J$ is incremented by unity only at time t_1; $\mathfrak{m}_J$ does not "count" the crossing time t_2, for which condition (49) is violated. Neither $\mathfrak{m}_J$ nor m_J registers

a crossing at times t_3 and t_4 in Fig. 7, since condition (50) is violated at times t_3 and t_4.

Plots of m(t) and $\dot{m}(t)$ corresponding to Fig. 7 are depicted in Figs. 8a and 8b, respectively.

The analysis that follows in Sections III - V is based on development of eq. (51) rather than eq. (53), i.e., it is assumed that the signal processer hardware being modelled requires the satisfaction of both (49) and (50) before it will register a threshold crossing.

C. NON-STATIONARY GAUSSIAN PROCESSES

Further development of eq. (48) for the crossing rate $\dot{n}_J$ is contingent on obtaining a suitable expression for the joint density $f_{y\dot{y}}$. The objectives of this section are:

1) to evaluate eq. (48) for the particular case of a bivariate Gaussian density, eq. (55), and

2) to introduce the expressions derived in Appendix B for the five basic statistics that appear as parameters in eq. (55).

The justification for assuming a Gaussian distribution for f_y (and hence for $f_{\dot{y}}$ and $f_{y\dot{y}}$ as well) is given in Appendix F.

The approximation:

$$F_y(y) \simeq \Phi\left(\frac{y-m_y}{\sigma_y}\right)$$

has been considered by Gilbert and Pollack,[22] where $\Phi(.)$ is the Gaussian distribution function, eq. (65), m_y and $\sigma_{\dot{y}}$ are defined by eqs. (56) and (58), and $F_y(y)$ is the distribution function of the process Y(t):

$$F_y(y) = \int_{-\infty}^{y} f_y(y')dy'$$

A summary of Gilbert and Pollacks' results is given in Ref. (15).

The problem addressed in Appendix F is different, and much simpler, than the problem of Ref. (22). It is shown in Appendix F that the relative error in $\hat{m}_J$ is approximately equal to the relative error ε in the density function of Y(t):

$$f_y(y) \approx \sigma_y^{-1} \phi\left(\frac{y-m_y}{\sigma_y}\right) \quad (1 + \varepsilon)$$

where $\phi(.)$ is the Gaussian density function, eq. (64). The Edgeworth series expansion[13] of $f_y(y)$ provides a simple and easily evaluated expression for the relative error ε. Sample calculations described in Appendix F show that ε is negligibly small for typical system and background parameter values.

Based on the analysis of Appendix F, the joint density $f_{y\dot{y}}$ is now assumed to have the following bivariate normal form:

$$f_{y\dot{y}}(y_o,z) = \{2\pi\sigma_y\sigma_z(1-r^2)^{\frac{1}{2}}\}^{-1} \exp\left\{-\left[\frac{u^2 + v^2 - 2ruv}{2(1-r^2)}\right]\right\} \quad (55)$$

where:

$$m_y \equiv E\{Y\} \quad (56)$$

$$m_z = E\{\dot{Y}\} \quad (57)$$

$$\sigma_y^2 \equiv E\{(Y-m_y)^2\} \quad (58)$$

$$\sigma_z^2 \equiv E\{(\dot{Y}-m_z)^2\} \quad (59)$$

$$r\sigma_y\sigma_z \equiv E\{(Y-m_y)(\dot{Y}-m_z)\} \equiv C_{yz} \quad (60)$$

$$u \equiv (y_o-m_y)/\sigma_y \quad (61)$$

$$v \equiv (z-m_z)/\sigma_z \quad (62)$$

It may be shown from eqs (52) and (55) that

$$I(x) = \left(\frac{\sigma_z}{\sigma_y}\right) (1-r^2)^{\frac{1}{2}} \phi(u)\{[\phi(p_o) - \phi(p_x)] + p_1[\Phi(p_o)-\Phi(p_x)]\} \quad (63)$$

where σ_y, σ_z, r, and u, are given by eqs (58), (59), (60), and (61), respectively. The functions $\phi(.)$ and $\Phi(.)$ in (63) are defined as follows:

$$\phi(x) \equiv (2\pi)^{-\frac{1}{2}} \exp(-x^2/2) \quad (64)$$

$$\Phi(x) \equiv \int_{-\infty}^{x} \phi(z)dz \quad (65)$$

The quantities p_o, p_1, and p_x in (63) are defined as:

$$p_o \equiv [(1-r^2)^{\frac{1}{2}} \sigma_z]^{-1} (m_z + ru\sigma_z) \quad (66)$$

$$p_1 \equiv [(1-r^2)^{\frac{1}{2}} \sigma_z]^{-1} (m_z + ru\sigma_z - y_o) \quad (67)$$

$$p_x \equiv [(1-r^2)^{\frac{1}{2}} \sigma_z]^{-1} (m_z + ru\sigma_z - x) \quad (68)$$

From eq. (68), (64), and (65)

$$\lim_{x\to\infty} \phi(p_x) = \lim_{x\to\infty} \Phi(p_x) = 0 \quad (69)$$

From eqs. (51), (63), and (69):

$$\dot{m}_J(t) = \left(\frac{\sigma_z}{\sigma_y}\right)(1-r^2)^{\frac{1}{2}}\ \phi(u)\ \{\phi(p) + p_1\Phi(p)\} \tag{70}$$

where by definition

$$p \equiv \begin{cases} p_o & \dot{y}_o < 0 \\ p_1 & \dot{y}_o > 0 \end{cases} \tag{71}$$

with p_o and p_1 given by eqs. (66) and (67).

The expected number of threshold crossings on the time interval T_o, defined by $|t| < T/2$, is given by:

$$m_J(O,T) = E\{J\} = \int_{T_o} \dot{m}_J(t)dt \tag{72}$$

with $\dot{m}_J(t)$ given by eq. (70). In order to complete the formal calculational procedure for m_J, it is necessary to specify values for the five functions $m_y(t)$, $m_z(t)$, $\sigma_y(t)$, $\sigma_z(t)$, and $r(t)$, defined by eqs. (56) - (60). It is shown in Appendix B that for background-limited (BLIP) detection,

$$m_y(t) = h(t) \circledast m_x(t) \tag{73}$$

$$\sigma_y^2(t) = e\ h^2(t) \circledast m_x(t) \tag{74}$$

$$\sigma_z^2(t) = e\ [h(t)]^2 \circledast m_x(t) \tag{75}$$

$$m_z(t) = \dot{m}_y(t) \tag{73a}$$

$$r(t) = \dot{\sigma}_y(t)/\sigma_z(t) \tag{76}$$

where e is the electronic charge, h(t) is the impulse response of the post-detector filter (cf Fig. 1), $m_X(t)$ is the mean value of the current X(t) (cf. Fig. 1), and $\circledast$ is the convolution operator:

$$f(t) \circledast g(t) \equiv \int_{-\infty}^{\infty} f(t-x)g(x)dx \qquad (77)$$

The relationship of $m_X(t)$ to the radiance of the scene under observation and the optical parameters of the IRST sensor is discussed in Appendix A, and expressed quantitatively by eq. (A-14). Eqs. (A-14), (70), and (72)-(76), taken together, represent a prescription for calculating the performance of a time-variable threshold IRST sensor against a non-uniform scene.

In principal, it remains only to model, measure, or otherwise specify the radiance distributions of typical targets and background scenes. This aspect of the IRST modeling problem is not considered in this paper.

It may be noted that eq. (70) appears almost identical to an equation in Ref. (14). The relationship between eq. (70) and the corresponding equation in Ref. (14) is discussed in Appendix D.

D. Asymptotic Approximations

1. Introduction

Evaluation of eq. (72) for the mean number of threshold crossings m_J generally requires a numerical integration of $\dot{m}_J$, as given by eq. (70). It is now shown that a relatively simple approximation for m_J can be developed that eliminates the need to perform this numerical integration, and has greater intuitive appeal than the original formulation. Some numerical examples comparing the numerical integral of eq. (70) with the approximate result developed here are presented in part V of this paper. Eq. (72), with eq. (70) substituted for $\dot{m}_J$, is now written as:

$$m_J(0,T) = \int_{T_o} a(t)e^{-b(t)}dt \tag{78}$$

where T_o is the time interval $|t| < T/2$, and where

$$b(t) \equiv u^2(t)/2 \tag{79}$$

$$a(t) \equiv \left(\frac{\sigma_z}{\sigma_y}\right)(1-r^2)^{\frac{1}{2}}\{\phi(p) + p_1\,\Phi(p)\}(2\pi)^{-\frac{1}{2}} \tag{80}$$

Experience with the numerical evaluation of eq. (78) has led to the conclusion that $\dot{m}_J$ is appreciably non-zero only over very brief intervals of time (cf., for example, Fig. 3). Since the principal contribution to the integral m_J of $\dot{m}_J$ accrues over those same short intervals (cf. Fig. 4), eq. (78) may be written as:

$$m_J(0,T) \simeq \sum_n m_J(t_n,\tau_n) \tag{81}$$

where

$$m_J(t_n,\tau_n) \equiv \int_{T_n} a(t)e^{-b(t)}dt \tag{82}$$

where T_n is the time interval $|t-t_n| < \tau_n/2$.
The interval T_n is presumed to be large enough for the integral in eq. (82) to capture the principal contribution to $m_J(0,T)$ made by the n^{th} term in the summation of eq. (81).

Experience with the numerical evaluation of eq. (78) has also shown that the rapid time variation of m_J in the neighborhood of the discrete times t_n is mainly due to the exponential factor, the function $a(t)$ varying much more slowly with time. Eq. (82) is thus approximated as:

$$m_J(t_n,\tau_n) \simeq a_n I_n \tag{83}$$

where $a_n \equiv a(t_n)$, and

$$I_n \equiv \int_{T_n} e^{-b(t)}dt \tag{84}$$

where T_n is the time interval $|t-t_n| < \tau_n/2$

The usual first-order saddle point method is now used to obtain approximations for I_n. The saddle points t_n are found by solving for the roots of the equation:

$$B(t_n) = u(t_n)\dot{u}(t_n) = 0 \tag{85}$$

Eq. (85) has two distinctly different types of solutions, corresponding to solutions of the following two equations:

$$\dot{u}(t_n) = 0 \tag{86}$$

$$u(t_n) = 0 \tag{87}$$

Each root of eq. (85) gives rise to a discrete contribution to the approximate formulation for m_J, the form of which depends on whether the root is a solution to eq. (86) or eq. (87).

Solutions of eq. (86), such as time t_1 in Fig. 2b, will be referred to as "saddle points." Solutions of eq. (87), such as time t_2 in Fig. 2b, will be referred to as "mean crossing times."

The next objective is the development of approximations to the integral I_n of eq. (84).

2. Saddle Points

The function u(t) in eq. (79) is now given a Taylor expansion about a time t_n:

$$u(t) \cong u_n + \dot{u}_n(t-t_n) + \ddot{u}_n (t-t_n)^2/2 \tag{88}$$

Assuming that t_n is a "saddle point", i.e., a solution of eq. (86), eq. (88) becomes:

$$u(t) \cong u_n + \ddot{u}_n(t - t_n)^2/2 \tag{89}$$

From eqs. (79) and (89), dropping the fourth-order term:

$$b(t) \cong u_n^2/2 + u_n \ddot{u}_n (t-t_n)^2/2 \tag{90}$$

From eqs. (84), (90), and (79):

$$I_n \cong \exp(-b_n) \int_{-\varepsilon_n/2}^{\varepsilon_n/2} \exp(-u_n \ddot{u}_n t^2/2) dt \tag{91}$$

where $b_n \equiv b(t_n)$.

Making use of the fact that

$$\int_{-\infty}^{\infty} \exp(-\pi x^2) dx = 1 \tag{92}$$

and assuming that ε_n in (91) is chosen sufficiently large, eq. (91) can be approximated as

$$I_n \cong (2\pi/u_n \ddot{u}_n)^{\frac{1}{2}} \exp(-b_n) \tag{93}$$

From (83) and (93)

$$m_J(t_n, \tau_n) \cong \left[a_n \exp(-b_n)\right] (2\pi/u_n \ddot{u}_n)^{\frac{1}{2}} \tag{94}$$

Comparison of eqs. (78) and (72) shows that

$$\bar{m}_J(t) \equiv a(t) \exp\left[-b(t)\right] \tag{95}$$

With the definition:

$$\delta t_n \equiv (2\pi/u_n \ddot{u}_n)^{\frac{1}{2}} \tag{96}$$

It follows from (94)-(96) that:

$$m_J(t_n,\tau_n) \cong \dot{m}_J(t_n)\ \delta t_n \tag{97}$$

From eqs. (81) and (97)

$$m_J(0,T) \cong \sum_n \dot{m}_J(t_n)\ \delta t_n \tag{98}$$

It is relatively straightforward to show that:

$$\dot{u}(t) \equiv d/dt\ \{(y_o-m_y)/\sigma_y\} = -\sigma_z(1-r^2)^{\frac{1}{2}}\ p_1/\sigma_y \tag{99}$$

Thus, from (86) and (99)

$$p_1(t_n) = 0 \tag{100}$$

From (80) and (100)

$$a_n = (\sigma_z/\sigma_y)(1-r^2)^{\frac{1}{2}}\ \phi(p_n)\ (2\pi)^{-\frac{1}{2}} \tag{101}$$

From (100), (66), (67), and (71)

$$p_n = \begin{cases} p_o = \left[(1-r^2)^{\frac{1}{2}}\ \sigma_z\right]^{-1}\ \dot{y}_o & ,\dot{y}_o < 0 \\ p_1 = 0 & ,\dot{y}_o > 0 \end{cases} \tag{102}$$

at $t = t_n$.

From (95), (101), and (79)

$$\dot{m}_J(t_n) = \{(2\pi)^{-\frac{1}{2}}\ (\sigma_z/\sigma_y)\ \phi(u_n)\}\ \{\left[2\pi(1-r^2)\right]^{\frac{1}{2}}\ \phi(p_n)\} \tag{103}$$

The desired approximation to m_J is given by eq. (98), with δt_n and $\dot{m}_J(t_n)$ given by eqs. (96) and (103), respectively.

The first bracketed quantity on the left-hand-side of eq. (103) is identical to Rice's equation for the threshold crossing rate of stationary Gaussian noise. The second bracketed quantity in eq. (103) is always less than unity. For constant threshold processors ($\dot{y}_o = 0$) the second bracketed quantity is equal to $(1-r^2)^{\frac{1}{2}}$, which is nearly unity whenever the fluctuations in the mean current $m_x(t)$ are slow compared to the impulse response $h(t)$ of the post-detector filter.

For constant threshold processors, the quantity δt_n in eqs. (96) and (98) can be interpreted as the effective time interval during which the filtered mean current $m_y(t)$ remains in the neighborhood of its peak.

It should be noted that the approximation (98) may be incomplete, since the discrete terms in the summation all correspond to roots of eq. (86). As discussed in the following section, roots of eq. (87), assuming such roots exist, each make an additional discrete contribution to m_J.

3. Mean-Crossing Times

Instead of eq. (86), it is now assumed that eq. (85) is satisfied because

$$u(t_n) = \{[y_o(t_n) - m_y(t_n)]/\sigma_y(t_n)\} = 0 \qquad (104)$$

The saddle points obtained as solutions of eq. (104) correspond to times when the mean current $m_y(t)$ crosses the threshold $y_o(t)$. Thus, in the vicinity of t_n,

$$\left[y_o(t) - m_y(t)\right] \cong \left[\dot{y}_o(t_n) - \dot{m}_y(t_n)\right] \ (t-t_n) \tag{105}$$

From eqs. (105) and (79)

$$b(t) \cong \left[y_o(t_n) - \dot{m}_y(t_n)\right]^2 (t-t_n)^2/2\sigma_y^2(t_n) \tag{106}$$

Evaluating eq. (84) for I_n, with b(t) now given by (106) rather than (90), it can be shown that

$$m_J(t_n,\tau_n) \cong (1-r^2)^{\frac{1}{2}}\ \phi(p_n)\left|\frac{\sigma_z}{\dot{y}_o-\dot{m}_y}\right| + \Phi(p_n)\ \mathrm{sgn}\ (\dot{m}_y-\dot{y}_o) \tag{107}$$

Where sgn(.) denotes the sign of the bracketed quantity, | | denotes the absolute value of the enclosed quantity, and

$$p_n = \begin{cases} \left[\sigma_z(1-r^2)^{\frac{1}{2}}\right]^{-1} \dot{m}_y & , \ \dot{y}_o < 0 \\ \left[\sigma_z(1-r^2)^{\frac{1}{2}}\right]^{-1} (\dot{m}_y-\dot{y}_o) & , \ \dot{y}_o > 0 \end{cases} \tag{108}$$

The assumption is now made that:

$$|p_n| \gg 1 \tag{109}$$

Subject to assumption (109), it follows from eq. (108) that

$$\phi(p_n) \cong 0 \tag{110}$$

and

$$\Phi(p_n) \cong \begin{cases} \mu(\dot{m}_y) & \dot{y}_o < 0 \\ \mu(\dot{m}_y - \dot{y}_o) & \dot{y}_o > 0 \end{cases} \tag{111}$$

where $\mu(.)$ denotes the unit step function

$$\mu(x) = \begin{cases} 0 & , \quad x < 0 \\ 1 & , \quad x > 0 \end{cases} \tag{112}$$

Eq. (111) can also be written as

$$\Phi(p_n) \cong \mu(\dot{m}_y)\ \mu(\dot{m}_y - \dot{y}_o) \tag{113}$$

Noting that

$$\mu(\dot{m}_y - \dot{y}_o)\ \text{sgn}\ (\dot{m}_y - \dot{y}_o) \equiv \mu(\dot{m}_y - \dot{y}_o) \tag{114}$$

it follows from eqs. (107), (110), (113), and (114), that

$$m_J(t_n, \tau_n) \cong \mu\left[\dot{m}_y(t_n)\right]\ \mu\left[\dot{m}_y(t_n) - \dot{y}_o(t_n)\right] \tag{115}$$

subject to assumption (109), with p_n given by (108).

It follows from eq. (115) that if the mean current $m_y(t)$ crosses the threshold $y_o(t)$ at time t_n, then the crossing count m_J will be incremented by unity if the following two conditions are both satisfied:

1) the slope of $m_y(t)$ at time t_n (i.e., $\dot{m}(t_n)$) must be positive, and

2) the slope of $m_y(t)$ must be greater than that of $y_o(t)$ at time t_n

--assuming that the slopes of $m_y(t)$ and $y_o(t)$ at time t_n aren't nearly the same, i.e., that $m_y(t)$ and $y_o(t)$ don't run nearly parallel in the neighborhood of their crossing point t_n. (This last assumption is expressed quantitatively by inequality (109).)

Thus, the asymptotic result for mean-crossing times reflects the limitations on the domain of integration in eq. (48) imposed by inequalities (49) and (50).

IV. INFINITE CONTRAST POINT TARGETS

A. Introduction

The mean crossing rate formalism developed in Section III.C requires adherence to the following prescription:

1. The mean current $m_x(t)$ must be specified. (It is shown in Appendix A how $m_x(t)$ may be calculated in terms of the radiance distribution of the scene.)
2. The post-detector filter impulse response $h(t)$ must be specified.
3. Eqs. (73)-(76) must be evaluated for the five functions $m_y(t)$, $\sigma_y^2(t)$, $\sigma_z^2(t)$, $m_z(t)$, and $r(t)$.
4. The mean crossing rate $\dot{m}_J(t)$ is obtained from eq. (70), and integrated over time to obtain the expected number of crossings.

The difficult calculational problem generally posed by step 3 above can be circumvented by making the following choice for $m_x(t)$:

$$m_x(t) = x_o\ \delta(t-t_o) \tag{116}$$

Eq. (116) is the limiting case of an infinite contrast point target, assuming an ideal optical MTF, and point detectors in the focal plane.

The final result of this section will be an expression for $m_J(0,T)$ that is formally identical to the usual expression for the probability of detection P_D[16]:

$$P_D = 1 - \Phi\left\{\frac{y_o - m_y(t_p)}{\sigma_y(t_p)}\right\} \qquad (117)$$

Where $\Phi(.)$ is the Gaussian distribution function, and t_p is the time at which the post-detector filter output current assumes its peak value.

The application of eq. (117) to P_D calculations was previously derived[16] subject to the assumption of internal amplifier-noise-limited operation, for which the filtered current Y(t) is a stationary random process. The surprising result is now obtained that eq. (117) is also applicable to P_D calculations for BLIP sensors, for which the current Y(t) is a nonstationary random process. The only important distinction between the calculational procedures for P_D for amplifier-noise-limited or background-limited operations lies in the means for obtaining $\sigma_y(t_p)$. For BLIP sensors, $\sigma_y(t_p)$ is calculated from eq. (146).

B. Analysis

Eqs. (116) and (73)-(76)lead immediately to the following equations for the five basic current statistics:

$$m_y(t) = x_o h(t-t_o) \tag{118}$$

$$\sigma_y^2(t) = x_o\, e\, h^2(t-t_o) \tag{119}$$

$$\sigma_z^2(t) = x_o\, e \left[\hbar(t-t_o)\right]^2 \tag{120}$$

$$\dot{m}_y(t) = x_o\, \hbar(t-t_o) \tag{121}$$

$$r(\cdot)\, \sigma_y(t)\, \sigma_z(t) = x_o\, e\, h(t-t_o)\, \hbar(t-t_o) \tag{122}$$

From eqs. (119) and (120):

$$\sigma_y(t) = (x_o e)^{\frac{1}{2}} \, |h(t-t_o)| = (x_o e)^{\frac{1}{2}} \, h(t-t_o) \, \text{sgn} \left[h(t-t_o)\right] \quad (123)$$

$$\sigma_z(t) = (x_o e)^{\frac{1}{2}} \, |\hat{h}(t-t_o)| = (x_o e)^{\frac{1}{2}} \, \hat{h}(t-t_o) \, \text{sgn} \left[\hat{h}(t-t_o)\right] \quad (124)$$

where the function sgn (.) denotes the sign of its argument.
From eqs. (122)-(124):

$$r(t) = \text{sgn} \left[h(t-t_o) \, \hat{h}(t-t_o)\right] \quad (125)$$

Thus, from (125):

$$|r(t)| = 1 \quad (126)$$

Unity correlation coefficient, eq. (126), invalidates the bivariate density eq. (55). (Note the factor $(1-r^2)^{\frac{1}{2}}$ in eq. (55).) Thus, a new expression for f_{yz} must be found that is valid for the case r = 1, and used to evaluate eq. (52).

It may be shown that eq. (126) implies the following relationship between $\dot{Y}(t) \equiv Z(t)$ and Y(t):

$$Z(t) = a(t) \, Y(t) \quad (127)$$

where

$$a(t) \equiv \{\hat{h}(t-t_o)/h(t-t_o)\} \quad (128)$$

It follows, in turn, that:

$$f_{YZ}(y,z) = f_Y(y)\ \delta(z - ay) \tag{129}$$

Where $\delta(.)$ is the Dirac delta function, a is given by (128), and

$$f_Y(y) = \sigma_y^{-1}\ \phi(u) \tag{130}$$

with

$$\phi(x) \equiv (2\pi)^{-\frac{1}{2}} \exp\ (-x^2/2) \tag{131}$$

and

$$u(t) \equiv \left[y_o(t) - m_y(t)\right] / \sigma_y(t) \tag{132}$$

From eqs. (52) and (129):

$$I(x) = (ay_o - \dot{y}_o)\ f_Y(y_o)\ \{\mu(ay_o) - \mu(ay_o - x)\} \tag{133}$$

with the unit step function $\mu(.)$ defined by eq. (112). Assuming a constant threshold processor,

$$\dot{y}_o = 0 \tag{134}$$

it follows from eqs. (51) and (133) that

$$\dot{m}_J\ (t) = I(\infty) = ay_o\ f_Y\ (y_o)\ \mu(ay_o) \tag{135}$$

From eqs. (72), (135), and (130)-(132),

$$m_J(0,T) = \int_{t_o}^{T/2} dt\ a y_o\ \mu(a y_o)\ \sigma_y^{-1}\ \phi(u) \tag{136}$$

With the following change of variable

$$q \equiv \left[y_o - x_o h(t-t_o)\right] \left[(x_o e)^{\frac{1}{2}}\ h(t-t_o)\right]^{-1} \tag{137}$$

eq. (136) may be written as

$$m_J(0,T) = \int_{q(t_o)}^{q(T/2)} \mu\left[h(t-t_o) y_o / h(t-t_o)\right]\ \text{sgn}\ \left[h(t-t_o)\right] \phi(q)dq \tag{138}$$

It is now assumed that the threshold is positive

$$y_o > 0 \tag{139}$$

and that h(t) has the form shown in Fig. 9.. Eq. (138) then may be written as:

$$m_J(0,T) = -\int_{q(t_o)}^{q(t_1)} \phi(q)dq \tag{140}$$

From eq. (137)

$$q(t_o) = \lim_{h(0)\to 0^+} \left\{\frac{y_o - x_o\ h(0)}{(x_o e)^{\frac{1}{2}}\ h(0)}\right\} \to \infty \tag{141}$$

Also, from eq. (137) and Fig. 9:

$$q(t_1) = \left[\frac{y_o - x_o\, h_{max}}{(x_o e)^{\frac{1}{2}} h_{max}}\right] = \frac{y_o - m_{y_{max}}}{\sigma_{y_{max}}} \qquad (142)$$

From (140)-(142)

$$m_J(O,T) = \int_{q(t_1)}^{\infty} \phi(q)dq \qquad (143)$$

Defining the Gaussian distribution function $\Phi(.)$ as in eq. (65), eq. (143) may be written as:

$$m_J(O,T) = 1 - \Phi\{q(t_1)\} \qquad (144)$$

with $q(t_1)$ given by eq. (142). Eq. (144) is the desired result.

Eq. (144) may be generalized somewhat, by allowing h(t) to have the form shown in Fig. 10. With the following definitions:

$$m_{y\,max}(j) = x_o\, h_{max}(j) \quad j = 1,2,3,\ldots \qquad (145)$$

$$\sigma_{y\,max}(j) = (x_o e)^{\frac{1}{2}} h_{max}(j) \quad j = 1,2,3,\ldots \qquad (146)$$

$$q(t_j) = \frac{y_o - m_{ymax}(j)}{\sigma_{ymax}(j)} \qquad j = 1,2,3,\ldots \qquad (147)$$

It follows that

$$m_J(O,T) = \sum_j \{1 - \Phi\left[q(t_j)\right]\} \qquad (148)$$

According to (148), m_J has a discrete contribution from each of the peaks in h(t).

V. SAMPLE CALCULATIONS

A. A Model Filter and Model Background

In order to calculate the threshold crossing rate $\dot{m}_J$, it is generally necessary to first numerically evaluate eqs. (73)-(76) for the functions $m_y(t)$, $\sigma_y^2(t)$, $\sigma_z^2(t)$, $m_z(t)$, and $r(t)$, since analytical evaluation of eqs. (73) - (76) is generally not possible.

In order to obviate the need for numerical evaluation of (73) - (76), it is assumed in this section that the impulse response $h(t)$ and mean current $m_x(t)$ have the following forms:

$$h(t) = (2/t_o) \exp\{-\pi(t/t_o)^2\} \cos 2\pi f_o t \tag{149}$$

$$m_x(t) = x_o \{1 + x_1 \exp\left[-\pi(t/\tau)^2\right]\} \tag{150}$$

Eq. (149) is a two-parameter family of functions, with parameters t_o and f_o. Eq. (150) is a three-parameter family, with parameters x_o, x_1, and τ. Eqs. (149) and (150) are particularly convenient, as they allow analytical evaluation of eqs. (73) - (76), and have a large enough number of parameters to illustrate many of the effects that one would expect to observe with more general $h(t)$ and $m_x(t)$.

Taking the Fourier transform of eq. (149) results in the following expression for the transfer function $H(f)$:

$$H(f) = \mathcal{F}\{h(t)\} = \{\exp\left[-\pi(f-f_o)^2 t_o^2\right] + \exp\left[-\pi(f+f_o)^2 t_o^2\right]\} \qquad (151)$$

Representative plots of eqs. (150) and (151) are given in Figs. (11) and (12).

It is seen from Fig. 11 that the parameters x_o, x_1, and τ of $m_x(t)$ correspond respectively to a constant background brightness level, the object/background peak contrast, and the size of the non-uniformity. It follows from Fig.12 that the model filter has a bandpass characteristic centered at the frequency f_o. From eq. (149), the parameter t_o is a damping constant for the filter. Thus, while not completely general, eqs. (149) and (150) permit the exploration of a considerable variety of possible background/filter interaction effects.

Assuming that

$$\exp\left(-4\pi f_o^2 t_o^2\right) >> 1 \qquad (152)$$

it follows from eq. (151) that

$$\max_f H(f) \approx 1 \qquad (153)$$

The factor $(2/t_o)$ on the right-hand-side of eq. (149) was chosen to normalize H(f) to a peak value of unity.

The only major deficiency in eq. (151) as a model filter characteristic is the inability to control the filters' low frequency roll-off independently of the center-frequency parameter f_o and noise bandwidth parameter t_o.

The derivations of the analytical expressions that result

from evaluating eqs. (73)-(76) with the assumed functional forms for h(t) and $m_x(t)$ are available from the author.

Figs. 13-17 are illustrative evaluations of $m_y(t)$, $m_z(t)$, $\sigma_y^2(t)$, $C_{yz}(t)$, and $\sigma_z^2(t)$, assuming the following choices for the five model background/filter parameters:

$$x_o = 134. \text{ namps} \tag{154}$$

$$x_1 = 0.5 \tag{155}$$

$$\tau = 159. \ \mu\text{sec.} \tag{156}$$

$$f_o = 6.91 \text{ kHz} \tag{157}$$

$$t_o = 225 \ \mu\text{sec.} \tag{158}$$

The rationale behind the choice of parameter values (154) - (158) is discussed in Appendix G.

B. Crossing Count Calculations

In this section the value obtained for $m_J(0,T)$ by integrating eq. (70) numerically will be compared with the value obtained for $m_J(0,T)$ by three approximate methods. In every case, it will be assumed that $h(t)$ and $m_x(t)$ have the forms specified by eqs. (149) and (150), and that the threshold y_o is independent of time.

The first approximation to $m_J(0,T)$ is given by:

$$m_{QS}(0,T) = \int_{T_o} \dot{m}_{QS}(t)dt \tag{159}$$

where

$$\dot{m}_{QS}(t) \equiv (2\pi)^{-\frac{1}{2}} (\sigma_z/\sigma_y)\ \phi(u) \tag{160}$$

and T_o is the interval $|t| < T/2$.

Comparing eq. (160) and eq. (14), it is seen that eq. (159) is simply the integral of Rice's original expression for the crossing rates of stationary processes, transmuted into a function of time through the use of time-variable expressions for the basic current statistics, m_y, σ_y and σ_z.

It is generally found that the estimate

$$m_{QS} \approx m_J \tag{161}$$

improves monotonically as the parameter τ in eq. (150) is made larger. Eq. (159) defines what will be referred to as the "quasi-stationary" (Q-S) approximation to the mean crossing count m_J.

The second approximation to $m_J(0,T)$ that will be evaluated in this section is the asymptotic approximation derived in Section III.D:

$$m_A(0,T) \cong \dot{m}_J(t_s)\delta t_s \tag{162}$$

The saddle point t_s is obtained from eqs. (100) and (67) as the solution of

$$m_z(t_s) + r(t_s)\, u(t_s)\, \sigma_z(t_s) = 0 \tag{163}$$

since it is assumed that $\dot{y}_o(t) = 0$ in this section in order to simplify the numerical examples. It has been found that (163) is effectively equivalent to

$$m_z(t_s) = 0 \tag{164}$$

due to the very small value of $r(t_s)$ for the examples that have been worked. It follows from eq. (164) and inspection of Fig. 14 that $t_s = 0$ for the example of eqs. (154) - (158). The same saddle point condition has also been found to hold for the other numerical cases discussed in this section:

$$t_s = 0 \tag{165}$$

corresponding to the time of closest approach of $m_y(t)$ to y_o, for the assumed expressions (149) and (150) for h(t) and $m_x(t)$. It follows from the above discussion and the analysis of sectionIII.D that the appropriate asymptotic approximation to $m_J(0,T)$ is given by

$$m_A(0,T) = \dot{m}_{QS}(0)\ \delta t_s \tag{166}$$

where $\dot{m}_{QS}$ is given by eq. (160), and δt_s is given by eq. (96):

$$\delta t_s = \{2\pi/\ddot{u}(0)\ u(0)\}^{\frac{1}{2}} \tag{167}$$

where

$$u(0) = \frac{y_o - m_y(0)}{\sigma_y(0)} \tag{168}$$

and

$$\ddot{u}(0) \equiv d^2u(t)/dt^2\Big|_{t=0} \tag{169}$$

The third and final approximation to $m_J(0,T)$ is effectively a modified version ofGenoud's method[24]for the calculation of probability of detection:

$$m_{PS}(0,T) = 1 - \Phi\{u(0)\} \tag{170}$$

where $\Phi(.)$ is the Gaussian distribution function, as given by eq. (65).

As will presently be shown, eq. (170) becomes increasingly accurate as an approximation to m_J:

$$m_{PS}(O,T) \approx m_J(O,T) \tag{171}$$

as the object contrast x_1 is made progressively larger and the object extent τ is made progressively smaller. This is not at all surprising, in light of the fact that the mean threshold count for infinite contrast point targets, eq. (144), is identical to eq. (170). The quantity m_{PS} will be called the "point source approximation" to m_J.

Fig.18 is a plot of the base ten logarithms of $m_J(O,T_F)$, $m_{PS}(O,T_F)$, and $m_A(O,T_F)$, as a function of the normalized peak threshold level u_p:

$$u_p \equiv u(0) \tag{172}$$

where $u(0)$ is given by eq. (168), and assuming the background radiance and filter parameters of eqs. (154)-(158).

As discussed in Appendix G, parameters (154)-(158) correspond to the following more basic parameter choices:

$$\begin{aligned}
&\alpha_o = 1 \text{ mrad} && \text{(object angular subtense)}\\
&\alpha_T = 1 \text{ mrad} && \text{(instantaneous field-of-view)}\\
&T_F = 1 \text{ sec} && \text{(frame time)} \qquad (173)\\
&H(0) = 10^{-3} && \text{(transfer function zero ordinate)}
\end{aligned}$$

$$\begin{aligned}
&\eta = 0.6 && \text{(quantum efficiency)}\\
&\bar{\lambda} = 4.0\mu\text{m} && \text{(optical wavelength)} \qquad (174)\\
&A_{ap} = 500 \text{ cm}^2 && \text{(aperture area)}
\end{aligned}$$

and

$$L_B = 0.14 \text{ mw cm}^{-2} \text{ sr}^{-1} \quad \text{(background radiance)} \qquad (175)$$

Specifying $\alpha_o = \alpha_T$ qualifies the object described by eq. (150) as "target-like" in character (cf. Appendix G).

It is seen from Fig. 18 that the point source approximation m_{PS} provides an excellent fit to the crossing count function m_J, for the target-like object described by eqs. (154)-(158). However, the asymptotic approximation m_A underestimates m_J by nearly an order of magnitude for the target-like object.

It is now assumed that the object is clutter-like, rather than target-like:

$$\alpha_o = 5\,\alpha_T = 5 \text{ mrad.}$$

instead of the previously assumed values $\alpha_o = \alpha_T = 1$ mrad. It follows that

$$\tau = 795\ \mu\text{sec.}$$

replaces eq. (156). The other background and filter parameter values, eqs. (154), (155), (157), and (158) are left unchanged. Fig. 19 is a plot of the base ten logarithms of the corresponding values of $m_J(0,T_F)$, $m_{PS}(0,T_F)$, and $m_A(0,T_F)$ for the clutter-like object.

It is seen from Fig. 20 that the asymptotic approximation m_A is effectively equal to m_J, providing a much better approximation than m_{PS} for the clutter-like object.

It has generally been found for a fairly wide range of background and filter parameters that

a) m_{PS} provides an excellent approximation to m_J, and is superior to m_A, when the time scale of fluctuation of $m_x(t)$ is comparable to that of $h(t)$.

b) m_A provides an excellent approximation to m_J, and is superior to m_{PS}, when the time scale of fluctuation of $m_x(t)$ is slower than that of $h(t)$.

Finally, it is noted that the quasi-static approximation m_{QS} usually provides at least as good an approximation to m_J as either m_{PS} or m_λ. For example, plots of m_{QS} are virtually coincident with m_J on both of Figs. 18 and 19. However, evaluation of m_{QS} requires the numerical integration of eq. (159). By contrast, the calculations for m_{PS} and m_λ don't require numerical integration, and thus require far less computation time than calculations for m_{QS}.

VI. Adaptive Threshold Processors

A. Introduction

The basic IRST processor under consideration up to this point is described in Section I.B, and depicted in Fig. 1. It has been shown in Section V that the threshold crossing performance of the receiver in Fig. 1 is strongly dependent on the threshold function $y_o(t)$. Thus, it is highly desirable that the IRST processor suppress clutter-induced threshold crossings by increasing $y_o(t)$ when $m_x(t)$ is "clutter-like".

Rather than allow $y_o(t)$ to take on an a priori constant or functional value, it is necessary to establish the threshold by some means that "adapts" $y_o(t)$ to the prevailing background conditions.

A similar type of signal processing problem has been addressed in the radar[17,18] and sonar[19] literatures. A candidate adaptive threshold scheme adapted from the earlier work[25] is depicted in Fig. 20.

The block with transfer function $\exp(-j2\pi fT_d)$ introduces a delay of T_d seconds. The triangular-shaped block in Fig. 20 denotes an ideal all-pass amplifier of gain K. It is seen that the delay time T_d, gain K, and transfer functions $H_o(f)$ and $H(f)$ are all design variables. Strategies for choosing the design variables in order to satisfy particular performance requirements or optimization criteria will not be discussed. The remainder of this section is devoted to developing a formulation for the expected number of threshold crossings for IRST receivers structured as in Fig. 20 under the assumption that the design variables have all been specified.

Eq. (225) for the crossing rate $\dot{m}_J$ is the principal result of this section.

B. Analysis

The starting point for the adaptive threshold analysis is eq. (39):

$$\dot{m}_J(t) = \int |\dot{g}| \; f_{G\dot{G}}(0,\dot{g})d\dot{g} \tag{176}$$

where, from eq. (43):

$$f_{G\dot{G}}(0,\dot{g}) = \int\int d\zeta d\eta \; f_{y\dot{y}y_o\dot{y}_o}(\zeta,\dot{g}+\eta,\zeta,\eta) \tag{177}$$

Assuming that the processes, $y, \dot{y}$, y_o, and $\dot{y}_o$, are jointly Gaussian (cf. Appendix F for justification), their joint density can be expressed in terms of their covariance matrix[21] $\underset{\approx}{\Lambda}$. The matrix $\underset{\approx}{\Lambda}$ has four rows and four columns, for a total of sixteen elements. Written in partitioned form:

$$\underset{\approx}{\Lambda} = \left[\begin{array}{c|c} \underset{\approx}{C} & \underset{\approx}{C}_1^T \\ \hline \underset{\approx}{C}_1 & \underset{\approx}{C}_o \end{array}\right] \tag{178}$$

where the superscript T in (178) denotes the matrix transpose operation. The sub-matrices $\underset{\approx}{C}$, $\underset{\approx}{C}_o$, and $\underset{\approx}{C}_1$ in eq. (178) are defined as follows:

$$\underset{\approx}{C} = \begin{vmatrix} \sigma_y^2(t) & C_{y\dot{y}}(t,t) \\ C_{\dot{y}y}(t,t) & \sigma_{\dot{y}}^2(t) \end{vmatrix} \tag{179}$$

$$\underset{\approx}{C}_o = \begin{vmatrix} \sigma_{y_o}^2(t) & C_{y_o\dot{y}_o}(t,t) \\ C_{\dot{y}_o y_o}(t,t) & \sigma_{\dot{y}_o}^2(t) \end{vmatrix} \tag{180}$$

$$\underset{\approx}{C}_1 = \begin{vmatrix} C_{y_o y}(t,t) & C_{y_o \dot{y}}(t,t) \\ C_{\dot{y}_o y}(t,t) & C_{\dot{y}_o \dot{y}}(t,t) \end{vmatrix} \tag{181}$$

The scalar covariances that comprise the elements of (179)-(181) are defined by

$$C_{AB}(t_1,t_2) \equiv E\{\left[A(t_1)-m_A(t_1)\right]\left[B(t_2)-m_B(t_2)\right]\} \tag{182}$$

where A and B take on the values Y, $\dot{Y}$, Y_o, and $\dot{Y}_o$, as appropriate. Also,

$$m_A(t) \equiv E\{A(t)\} \tag{183}$$

and

$$\sigma_A^2(t) \equiv C_{AA}(t,t) \tag{184}$$

It follows from (182) that $C_{\dot{y}y}(t,t) = C_{y\dot{y}}(t,t)$ and $C_{\dot{y}_o y_o}(t,t) = C_{y_o \dot{y}_o}(t,t)$. Thus, the matrices $\underset{\approx}{C}$ and $\underset{\approx}{C}_o$ are symmetric.

The elements of $\underset{\approx}{C}$ are obtained directly from eqs. (B-17), (B-20), and (B-23):

$$\sigma_y^2(t) = e\{m_x(t) \circledast h^2(t)\} \tag{185}$$

$$\sigma_{\dot{y}}^2(t) = e\{m_x(t) \circledast [\dot{h}(t)]^2\} \tag{186}$$

$$C_{y\dot{y}}(t,t) = \sigma_y(t)\, \delta_y(t) \tag{187}$$

Expressions for the elements of (180) may be obtained as direct adaptations of (185)-(187). It follows from Fig. 20 that

$$Y_o(t) = K\{h_o(t-T_d) \circledast X(t)\} \tag{188}$$

where $h_o(t)$ is the Fourier inverse of $H_o(f)$. Taking the expected value of both sides of (188):

$$m_{y_o}(t) = K\{h_o(t-T_d) \circledast m_x(t)\} \tag{189}$$

analagous to eq. (B-30). It may also be shown, analagous to (185)-(187) that:

$$\sigma_{y_o}^2(t) = eK\{m_x(t) \circledast h_o^2(t-T_d)\} \tag{190}$$

$$\sigma_{\dot{y}_o}^2(t) = eK\{m_x(t) \circledast \left[\dot{h}_o(t-T_d)\right]^2\} \tag{191}$$

$$C_{y_o\dot{y}_o}(t,t) = \sigma_{y_o}(t)\,\dot{\sigma}_{y_o}(t) \tag{192}$$

It remains only to formulate similar expressions for the elements of $\underset{\sim}{C}_1$ in order to complete the specification of the joint density $f_{yy\dot{y}_o\dot{y}_o}$.

The analysis this requires is so similar to Appendix B that it will only be outlined here.

It may be shown that:

$$C_{y_oy}(t_1,t_2) = eK\int_{-\infty}^{\infty} d\mu\; m_x(\mu)h_o(t_1-T_d-\mu)\; h(t_2-\mu) \tag{193}$$

Also,

$$C_{\dot{y}_oy}(t_1,t_2) = \partial_{t_1}\{C_{y_oy}(t_1,t_2)\} \tag{194}$$

and

$$C_{y_o\dot{y}}(t_1,t_2) = \partial_{t_2}\{C_{y_oy}(t_1,t_2)\} \tag{195}$$

$$C_{\dot{y}_o\dot{y}}(t_1,t_2) = \partial_{t_1}\partial_{t_2}\{C_{y_oy}(t_1,t_2)\} \tag{196}$$

From (193)-(196):

$$C_{y_o y}(t,t) = eK\{m_x(t) \circledast \left[h_o(t-T_d)h(t)\right]\} \tag{197}$$

$$C_{\dot{y}_o y}(t,t) = eK\{m_x(t) \circledast \left[\dot{h}_o(t-T_d)h(t)\right]\} \tag{198}$$

$$C_{y_o \dot{y}}(t,t) = eK\{m_x(t) \circledast \left[h_o(t-T_d)\dot{h}(t)\right]\} \tag{199}$$

$$C_{\dot{y}_o \dot{y}}(t,t) = eK\{m_x(t) \circledast \left[\dot{h}_o(t-T_d)\dot{h}(t)\right]\} \tag{200}$$

It may readily be seen by inspection of Fig. 22 that

$$h_o(t-T_d)h(t) \cong 0 \tag{201}$$

for sufficiently large delay times T_d. It follows from (197)-(201) that

$$C_{y_o y}(t,t) = C_{\dot{y}_o y}(t,t) = C_{y_o \dot{y}}(t,t) = C_{\dot{y}_o \dot{y}}(t,t) = 0 \tag{202}$$

for sufficiently large T_d. It is assumed that T_d is chosen large enough to validate eq. (202). Since uncorrelated Gaussian processes are necessarily statistically independent[21] it follows from eq. (202) that:

$$f_{y\dot{y}y_o\dot{y}_o}(y,\dot{y},y_o,\dot{y}_o) = f_{y\dot{y}}(y,\dot{y})f_{y_o\dot{y}_o}(y_o,\dot{y}_o) \tag{203}$$

From eqs. (176), (177), and (203)

$$\dot{m}_J(t) = \int\int d\zeta d\eta \; f_{y_o \dot{y}_o}(\zeta,\eta)\{\int d\dot{\zeta} |\dot{\zeta}| f_{y\dot{y}}(\zeta,\dot{\zeta}+\eta)\} \tag{204}$$

With the change of variable $z = \dot{\zeta} + \eta$, eq.(204) may be written

$$\dot{m}_J(t) = E_{y_o \dot{y}_o}\{\dot{m}_J(t|y_o,\dot{y}_o)\} \tag{205}$$

where, by definition,

$$\dot{m}_J(t|y_o,\dot{y}_o) \equiv \int |z-\dot{y}_o| f_{y\dot{y}}(y_o,z)dz \tag{206}$$

$$E_{y_o \dot{y}_o}\{.\} \equiv \int\int d\zeta d\eta \; f_{y_o \dot{y}_o}(\zeta,\eta)\{.\} \tag{207}$$

and $f_{y\dot{y}}$ is obtained by analogy to eq. (55).

Happily, eq. (206) is seen to be identical to eq. (48). Thus, the entire analysis of sections IV.B and IV.C, originally applicable only for deterministic thresholds, is now found to be directly applicable for stochastic thresholds as well. From eqs.(70) and (71):

$$\dot{m}_J(t|y_o,\dot{y}_o) = \left(\frac{\sigma_{\dot{y}}}{\sigma_y}\right)(1-r^2)^{\frac{1}{2}}\,\phi(u)\{\Phi(p) + p_1\,\Phi(p)\} \tag{208}$$

where

$$p = \left[\sigma_{\dot{y}}(1-r^2)^{\frac{1}{2}}\right]^{-1}\left[\dot{m}_y + ru\sigma_{\dot{y}} - \dot{y}_o\mu(\dot{y}_o)\right] = \begin{cases} p_o & \dot{y}_o<0 \\ p_1 & \dot{y}_o>0 \end{cases} \tag{209}$$

Eq. (205) represents a formal means of calculating the mean threshold crossing performance of the adaptive threshold processor depicted in Fig. 20. However, the evaluation of eq. (205) appears to present some significant calculational difficulties. These difficulties are obviated by means of the approximate method of evaluation pursued in the following section.

C. Approximations for $\mathfrak{m}_J$

Following ref. (26), p. 141, $\mathfrak{m}_J(t|\, y_o, \dot{y}_o)$ is given a truncated Taylor expansion about the values $y_o = m_{y_o}$ and $\dot{y}_o = \mathfrak{m}_{\dot{y}_o}$:

$$\mathfrak{m}_J(t|\, y_o, \dot{y}_o) \approx A + B + C/2 \tag{210}$$

where

$$A \equiv \mathfrak{m}_J(t|m_{y_o}, \mathfrak{m}_{\dot{y}_o}) \equiv \mathfrak{m}_J(t|\,.) \tag{211}$$

$$B \equiv (y_o - m_{y_o})\, \partial_{y_o} \mathfrak{m}_J(t|\,.) + (\dot{y}_o - \mathfrak{m}_{\dot{y}_o})\, \partial_{\dot{y}_o} \mathfrak{m}_J(t|\,.) \tag{212}$$

$$C \equiv (y_o - m_{y_o})^2\, \partial^2_{y_o y_o} \mathfrak{m}_J(t|\,.) + (\dot{y}_o - \mathfrak{m}_{\dot{y}_o})^2\, \partial^2_{\dot{y}_o \dot{y}_o} \mathfrak{m}_J(t|\,.) \tag{213}$$

The following notation has been employed in eqs. (212) and (213):

$$\partial_{y_o} m_J(t|.) = \left\{\frac{\partial}{\partial y_o} m_J(t|y_o,\dot{y}_o)\right\}\Bigg|_{\substack{y_o = m_{y_o} \\ \dot{y}_o = m_{\dot{y}_o}}} \tag{214}$$

$$\partial^2_{y_o y_o} m_J(t|.) = \left\{\frac{\partial^2}{\partial y_o^2} m_J(t|y_o,\dot{y}_o)\right\}\Bigg|_{\substack{y_o = m_{y_o} \\ \dot{y}_o = m_{\dot{y}_o}}} \tag{215}$$

From eqs. (205) and (210)

$$m_J(t) = E_{y_o\dot{y}_o}\{A\} + E_{y_o\dot{y}_o}\{B\} + \tfrac{1}{2} E_{y_o\dot{y}_o}\{C\} \tag{216}$$

From eqs. (207) and (211)-(213):

$$E_{y_o\dot{y}_o}\{A\} = m_J(t|.) \tag{217}$$

$$E_{y_o\dot{y}_o}\{B\} = 0 \tag{218}$$

$$E_{y_o\dot{y}_o}\{C\} = \sigma^2_{y_o}\,\partial^2_{y_o y_o} m_J(t|.) + \sigma^2_{\dot{y}_o}\,\partial^2_{\dot{y}_o\dot{y}_o} m_J(t|.) \tag{219}$$

From (216)-(219):

$$m_J(t) = \{1+\tfrac{1}{2}(\sigma^2_{y_o}\,\partial^2_{y_o y_o} + \sigma^2_{\dot{y}_o}\,\partial^2_{\dot{y}_o\dot{y}_o})\}\, m_J(t|.) \tag{220}$$

Further development of eq. (220) is simplified by employing eq. (D-6) for $\dot{m}_J$, rather than the crossing rate function of eq. (208). From eqs. (D-4) and (209):

$$\dot{m}_{CL}(t|y_o,\dot{y}_o) = \left(\frac{\sigma_{\dot{y}}}{\sigma_y}\right) \phi(u) \{\phi(p_1) + p_1 \Phi(p_1)\} \tag{221}$$

where

$$p_1 \simeq (\dot{m}_y - \dot{y}_o)/\sigma_{\dot{y}} \tag{222}$$

Consistent with the numerical results obtained thus far, terms of first and higher order in r have been dropped in writing eqs. (221) and (222).

From eqs. (220) and (221):

$$\dot{m}_J(t) = \left(\frac{\sigma_{\dot{y}}}{\sigma_y}\right) \left[1 + \tfrac{1}{2} (\sigma^2_{y_o} \partial^2_{y_o y_o} + \sigma^2_{\dot{y}_o} \partial_{\dot{y}_o \dot{y}_o})\right] \phi(u) L \Big|_{y_o = m_{y_o}} \tag{223}$$

where

$$L = \phi(p_1) + p_1 \Phi(p_1) \tag{224}$$

It may be shown from (223) and (224) that:

$$\dot{m}_J(t) = \dot{m}_{CL}(t|m_{y_o},\dot{m}_{y_o}) \left[1 + \left(\frac{\sigma_{yo}}{\sigma_y}\right)^2 \varepsilon_1 + \left(\frac{\sigma_{\dot{y}o}}{\sigma_{\dot{y}}}\right)^2 \varepsilon_2\right] \tag{225}$$

where

$$\varepsilon_1 \equiv \tfrac{1}{2}(u^2 - 1)\Big|_{y_o = m_{y_o}} \tag{226}$$

and

$$\varepsilon_2 \equiv \phi(p_1)/2L \Big|_{y_o = m_{y_o}} \tag{227}$$

The quantities $m_{y_o}(t)$, $\sigma_{y_o}(t)$, and $\sigma_{\dot{y}_o}(t)$ in eq. (225) are calculated by means of eqs. (189), (190), and (191), respectively. Finally, the expected number of threshold crossings in a time interval T_o may be obtained as:

$$m_J(O,T) = \int_{T_o} \dot{m}_J(t)dt \tag{228}$$

with $\dot{m}_J$ given by eq. (225).

Eq. (225) provides the basis for analyzing a much broader range of possible adaptive threshold schemes than Fig. 20 might suggest. For example, straightforward generalizations of eq. (225) may be applied to the structures of Figs. 22-24. Further numerical analysis along the lines of Sec.V for various model backgrounds and candidate processor structures is indicated, but has not been pursued thus far.

Some qualitative discussion of eq. (225) follows in the next (and concluding) section of this paper.

D. Discussion

The advantages and disadvantages that accrue to the use of an Adaptive Threshold (AT) processor may be evaluated by comparing eq. (225) with the corresponding crossing rate function for Fixed Threshold (FT) processors:

$$\dot{m}_{FT}(t) = \dot{m}_{CL}(t|y_o,0) \tag{229}$$

The most important consideration in computing the False Alarm Rate (FAR) of FT processors is the factor:

$$\phi(u) = \exp\left[-(m_y-y_o)^2/2\sigma_y^2\right](2\pi)^{-\frac{1}{2}} \tag{230}$$

that enters eq. (229) through eq. (221). As shown in the numerical examples of Section V, constant threshold processors operating against non-uniform scenes are most susceptible to false alarms in the immediate neighborhood of the local maxima of $m_y(t)$, i.e., local minima of $u^2(t)$. It follows from eq. (230) that the false alarm rate is an extremely sensitive function of m_y, increasing at a tremendous rate as the mean current $m_y(t)$ approaches y_o.

The potential advantage of AT schemes may be seen by comparing eq. (230) with the corresponding factor in eq. (225):

$$\phi(u)\Big|_{y_o=m_{y_o}} = (2\pi)^{-\frac{1}{2}} \exp\left[-(m_y-m_{y_o})^2/2\sigma_y^2\right] \tag{231}$$

If the filter $H_o(f)$ in Fig. 20 can be chosen such that $m_{y_o}(t)$ "tracks" the background-induced variations in $m_y(t)$, the performance-destroying local minima in $u^2(t)$ can be eliminated.

It should be noted that the adaptive threshold performance advantage just described is only realized when the background scene is non-uniform. The performance of AT processors is generally inferior to the performance of FT processors when the background scene is uniform and of known brightness. In this case:

$$FAR_{AT} = FAR_{FT}(1 + FAP) > FAR_{FT} \tag{232}$$

where

$$FAP \equiv (\sigma_{y_o}/\sigma_y)^2 \varepsilon_1 + (\sigma_{\dot{y}_o}/\sigma_{\dot{y}})^2 \varepsilon_2 \tag{233}$$

The threshold variance terms, eq. (233), contribute a False Alarm Penalty (FAP) whenever an AT processor is used when it truly isn't needed.

According to eq. (232), the adaptive threshold false alarm rate (FAR_{AT}) is greater (i.e., worse) than the fixed threshold false alarm rate (FAR_{FT}), assuming that the adaptive threshold gain K in Fig. 20 has been adjusted to achieve

equivalent target detection sensitivities for the two processors, rendering the false alarm rate comparison of eq. (232) a meaningful one.*

---

*It is assumed that the threshold filter $H_0(f)$ responds too slowly to suppress fast rise-time target-induced threshold crossings. Cf., for example, the interpolating threshold scheme of Fig. 22.

For uniform backgrounds, it is not hard to show that:*

$$(\sigma_{y_o}/\sigma_y)^2 = (\Delta f_o/\Delta f) \tag{236}$$

and

$$(\sigma_{\dot{y}_o}/\sigma_{\dot{y}})^2 \simeq (\Delta f_o/\Delta f)^3 \tag{237}$$

where Δf is the noise bandwidth of $H(f)$, and Δf_o is the noise bandwidth of $H_o(f)$ (cf. Fig.20). It follows from eqs. (233), (236), and (237), that:

$$FAP \simeq (\Delta f_o/\Delta f)\ \{\varepsilon_1 + (\Delta f_o/\Delta f)^2\ \varepsilon_2\} \tag{238}$$

Generally, Δf_o should be chosen smaller than Δf to minimize the false alarm penalty, eq. (238), and to prevent a too-rapid threshold response that would tend to suppress target-induced threshold crossings. On the other hand, Δf_o should be chosen large enough to allow the threshold to accurately follow most of the structure in the background scene. Clearly, the choice for Δf_o involves degrading system performance against uniform backgrounds for the sake of improved performance against non-uniform backgrounds.

---

*Eq. (237) is derived by assuming a rectangular-shaped $H(f)$, having an upper cut-off frequency f_u, and a noise bandwidth $\Delta f \simeq f_u$.

It appears likely that a more favorable trade-off could be achieved with the receiver structure shown in Fig. 22, both from the standpoint of

a) decreasing the false alarm penalty, eq. (233), and

b) improving the background tracking properties of $m_{y_o}(t)$.

Eq. (225) and the entire analysis of the preceding section is easily adapted to the structures of Figs. 22-24. The false alarm penalty, eq. (233), decreases roughly as $(2N)^{-\frac{1}{2}}$ for the detector of Fig. 23. The improvement in uniform background performance thus obtained for large values of N is gained at the expense of degraded performance against cluttered scenes, as compared to detectors with small values of N. The good background-tracking capability of the structure in Fig. 22 combined with the low false alarm penalty of the structure of Fig. 23 can be obtained by employing a two-dimensional detector array with Time-Delay and Integration (TDI) logic.

In order to put this discussion on a concrete quantitative basis, particular background and target radiance distributions must be chosen, and the mean current $m_x(t)$ calculated by means of eq. (A-14). The target detection and clutter rejection capabilities of a given candidate adaptive threshold processor can than be analyzed by means of eq. (225). Intercomparisons of the numerical results thus obtained for a variety of different processor structures should than allow quantitative conclusions to be drawn concerning such issues as:

a) the performance penalty caused by failing to match the sensor's instantaneous field-of-view to the angular size of the target.

b) the potential performance advantages of time-delay and integration (TDI).

c) the best value of N, and the desireability of having different transfer functions $H_n(f)$ for each of the 2N taps in the tapped delay line structure of Fig. 24.

d) the advantages that may be gained by employing simple two-dimensional threshold processing, in which the "target signal" Y(t) and threshold function $Y_o(t)$ are derived from detectors scanning at different elevations.

e) the possible advantages of including power-law devices, or other instantaneous non-linear devices in the threshold-establishing circuitry. It is noted that the propagation of mean values and variances through non-linear processing elements may be treated by relatively straightforward means.[29] Thus, the calculation of m_{y_o}, and $\sigma^2_{y_o}$ for use in eq. (225) is not difficult, for a specified non-linear relationship between $Y_o(t)$ and X(t).

The only important obstacle to performing analyses of the kind described above is the lack of high spatial resolution, radiometric, infrared background imagery.

REFERENCES

1. J. M. Lloyd, "Thermal Imaging Systems", New York: Plenum Press, 1975.

2. Fred Rosell, "Thermal Imaging Systems", NRL Formal Report, Naval Research Laboratory, Washington, D.C.: to be published.

3. William L. Wolf, editor, "Handbook of Military Infrared Technology", Washington, D.C.: U.S. Gov't. Printing Office, 1965.

4. Khalil Seyrafi, "Electro-Optical Systems Analysis", Los Angeles: Electro-Optical Research Company, 1973.

5. Lucien M. Biberman, "Reticles in Electro-Optical Devices", London: Pergamon Press, 1966.

6. J. A. Jamieson et al., "Infrared Physics and Engineering", New York: McGraw-Hill, 1963.

7. Hans Samuelsson, "Infrared Systems: I. Expressions for Signal and Background Induced Noise with Space Filters", IEEE Transactions on Aerospace and Electronic Systems, Vol. AES-7, No. 1, Jan. 1971, p. 27.

8. Hans Samuelsson, "Infrared Systems: II. Accuracy of Angle Measurement", IEEE Transactions on Aerospace and Electronic Systems, Vol. AES-7, No. 1, Jan. 1971, p. 34.

9. Harry L. Van Trees, "Detection, Estimation, and Modulation Theory, Part I.", New York: John Wiley & Sons, 1968.

10. David Z. Robinson, "Methods of Background Description and Their Utility", London: Proceedings of the IRE, 1959,p.1554.

11. Lucien M. Biberman, "Background Considerations in Infrared System Design", Applied Optics, Vol. 4, No. 3, p. 343, March 1965.

12. Robert M. Gagliardi, Sherman Karp, "Optical Communications", New York: John Wiley & Sons, 1976.

13. S. O. Rice, "Mathematical Analysis of Random Noise", Selected Papers on Noise and Stochastic Processes, edited by Nelson Wax, New York: Dover Publications, 1954.

14. Harald Cramer, M.R. Leadbetter, "Stationary and Related Stochastic Processes". New York: John Wiley & Sons, 1967.

15. William K. Pratt, "Laser Communications Systems", New York: John Wiley & Sons, 1969.

16. "Electro-Optics Handbook", Radio Corporation of America, Burlington, Massachusetts: RCA, 1968.

17a. Ramon Nitzberg, "Constant-False-Alarm-Rate Signal Processors for Several Types of Interference", IEEE Transactions on Aerospace and Electronic Systems, Vol. AES-8, No. 1, Jan. 1972, p. 27.

17b. Ramon Nitzberg, "Constant-False-Alarm-Rate Processors for Locally Nonstationary Clutter", IEEE Transactions on Aerospace and Electronic Systems, Vol. AES-9, No. 3, May 1973, p. 399.

17c. Ramon Nitzberg, "Analysis of the Arithmetic Mean CFAR Normalizer for Fluctuating Targets", IEEE Transactions on Aerospace and Electronic Systems, Vol. AES-14, No. 1, Jan. 1978, p. 44.

18. John T. Rickard, George M. Dillard, "Adaptive Detection Algorithms for Multiple-Target Situations", IEEE Transactions on Aerospace and Electronic Systems, Vol. AES-13, No. 4, July 1977, p. 338.

19. D. V. Gupta, J.F. Vetelino, T.J. Curry, J.T. Francis, "An Adaptive Threshold System for Nonstationary Noise Backgrounds", IEEE Transactions on Aerospace and Electronic Systems, Vol. AES-13, No. 1, Jan. 1977, p. 11.

20. Athanasias Papoulis, "Probability, Random Variables, and Stochastic Processes", New York: McGraw-Hill, 1965.

21. James L. Melsa and Andrew P. Sage, "An Introduction to Probability and Stochastic Processes", New Jersey: Prentice-Hall, Inc., 1973.

22. E.N. Gilbert and H.O. Pollak, "Amplitude Distribution of Shot Noise", Bell System Technical Journal, page 333, March 1960.

23. Ian F. Blake and William C. Lindsey, "Level-Crossing Problems for Random Processes", IEEE Transactions on Information Theory, Vol. IT-19, No. 3, May 1973, p. 295.

24. R. H. Genoud, "Infrared Search-System Range Performance", Proc. Inst. Radio Engrs., Vol. 47, page 1581, 1959.

25. Don J. Torrieri, "Adaptive Thresholding Systems", IEEE Transactions on Aerospace and Electronic Systems, May 1977, p. 273.

26. Paul L. Meyer, "Introductory Probability and Statistical Applications",Reading, Massachusetts: Addison-Wesley, 1970.

27. J. S. Bendat, "Principles and Applications of Random Noise Theory", New York: Wiley, 1958.

28. W. Tam and R. Corriveau, "Infrared Spectral Radiance of the Sky", Infrared Physics, Vol. 16,pp. 129-134, 1976.

29. W. B. Davenport and W. L. Root, "An Introduction to the Theory of Random Signals and Noise", New York, McGraw-Hill, 1958.

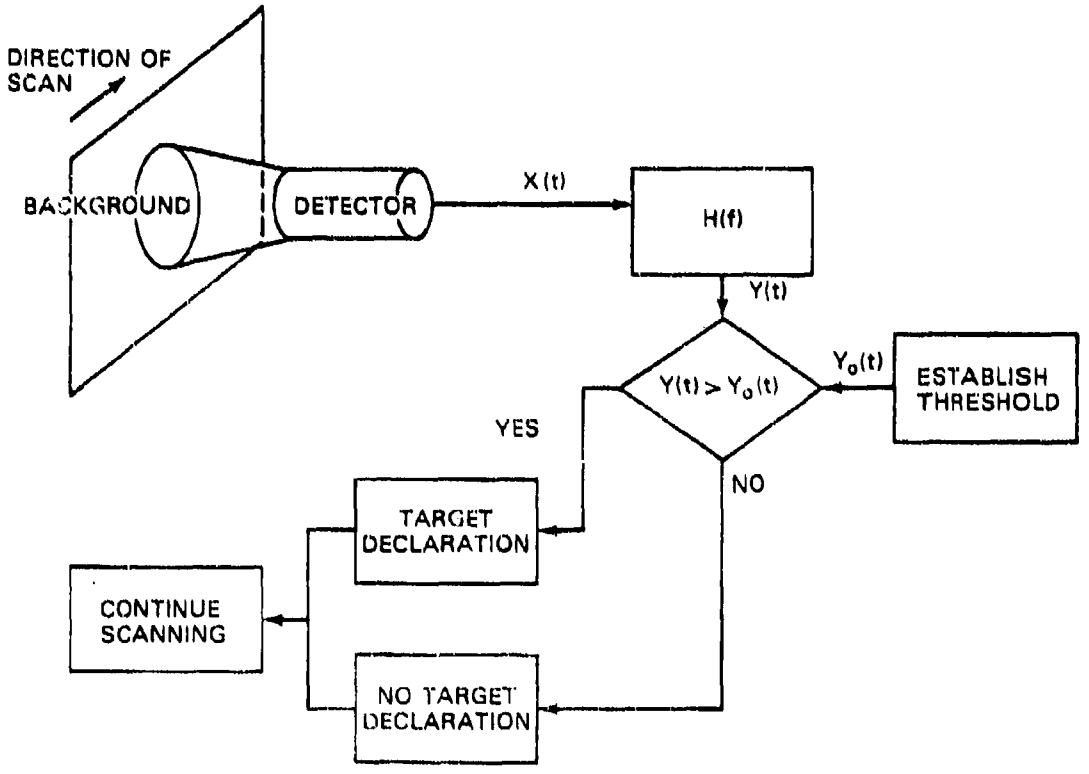

Figure 1

A basic threshold comparison receiver. The photodetector in this figure is "idealized", in the sense that it is presumed to have a perfect all-pass electrical frequency characteristic; the frequency-dependent part of the detector responsivity is lumped together with the transfer function of the post-detector filter to obtain H(f). A "target declaration" is made whenever the filtered current Y(t) exceeds the threshold level $Y_o(t)$.

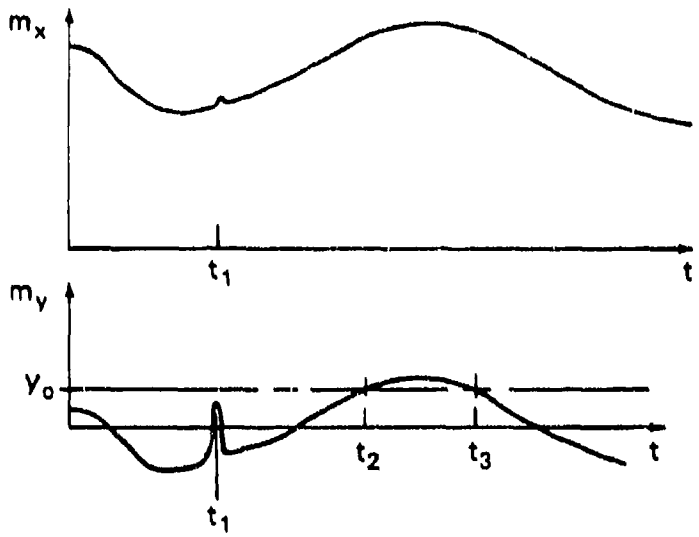

Figure 2

Part a) of this figure is an illustrative example showing the mean value $m_x(t)$ of the random current $X(t)$, as a function of time. A small "target-like" (i.e., short-duration) disturbance occurring at time t_1 is superposed on a larger amplitude, more slowly varying background. The corresponding mean current $m_y(t)$ at the output of the post-detector filter (cf. Fig. 1) is shown in part b) of this figure. The slowly-varying background part of $m_x(t)$ is greatly attenuated. By contrast, the target pulse is attenuated very little, since its bandwidth is matched to that of the post-detector filter.

A constant threshold of amplitude y_o appears as a horizontal line in Fig. 2b). The time t_2, where the mean current $m_y(t)$ crosses the threshold with a positive slope, is referred to as a "mean-crossing time" in the text. The time t_1, where $\left[y_o - m_y(t)\right]$ has a local minimum, is called a "saddle point" in the text.

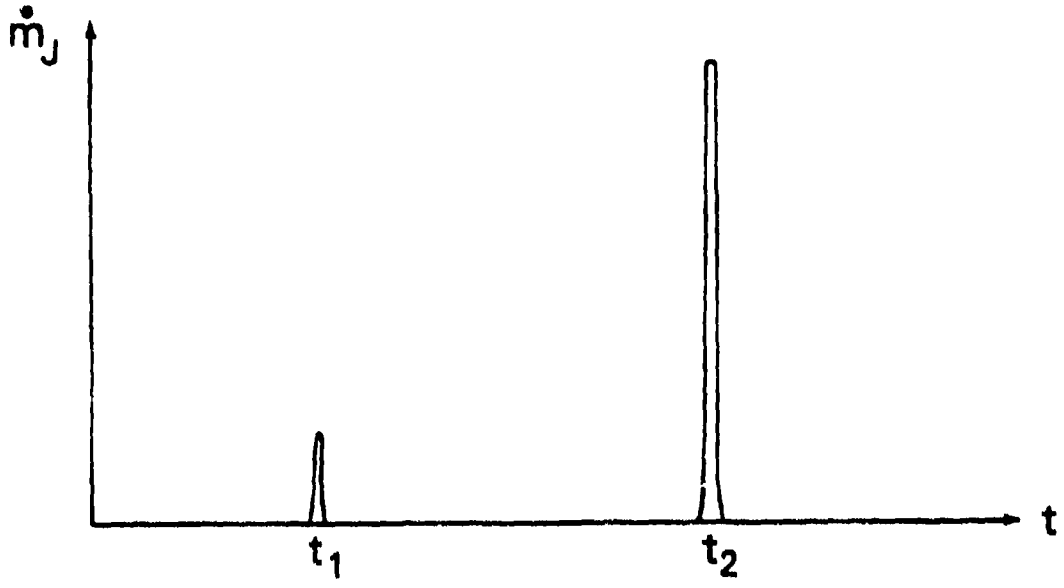

Figure 3

The crossing rate function $\dot{m}_J$ is shown as a function of time, for the example of Figure 2.

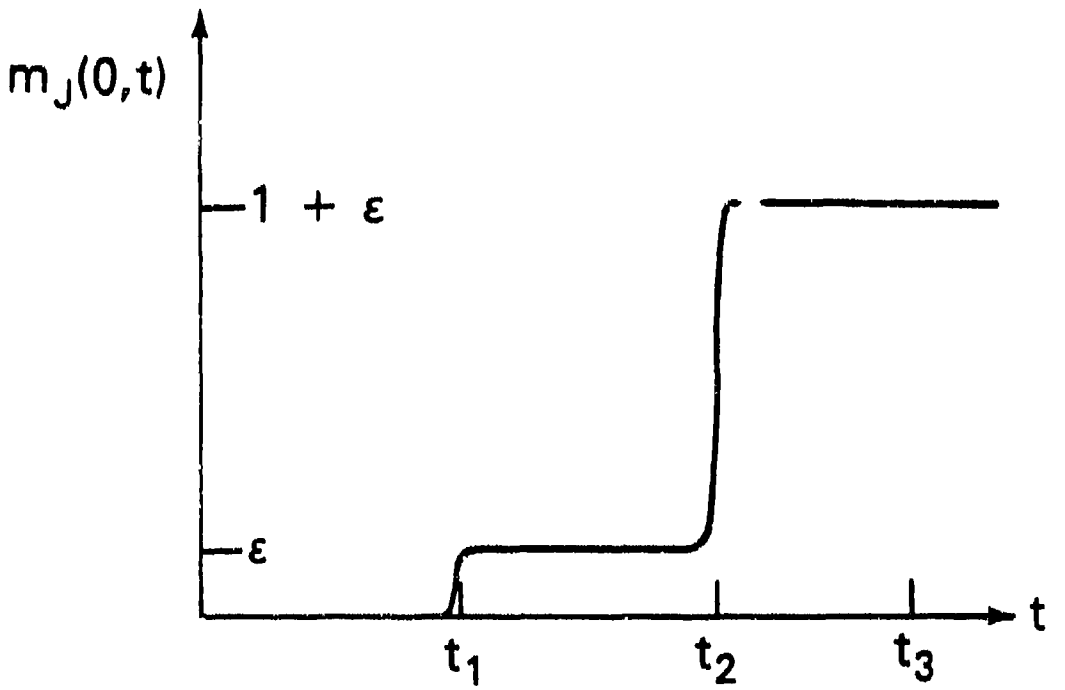

Figure 4

The expected number of threshold crossings m_J is shown as a function of time, obtained as the integral of the crossing rate function $\dot{m}_J$ depicted in Fig. 3. The small jump in m_J at t_1 is associated with the local maximum in $m_y(t)$ at t_1 shown in Fig. 2. The unity increase in m_J at time t_2 also has its corresponding origin in Fig. 2. The absence of a similar effect at t_3 (cf. Fig. 2b) is due to the definition of $\dot{m}_J$ as a positive-slope crossing rate.

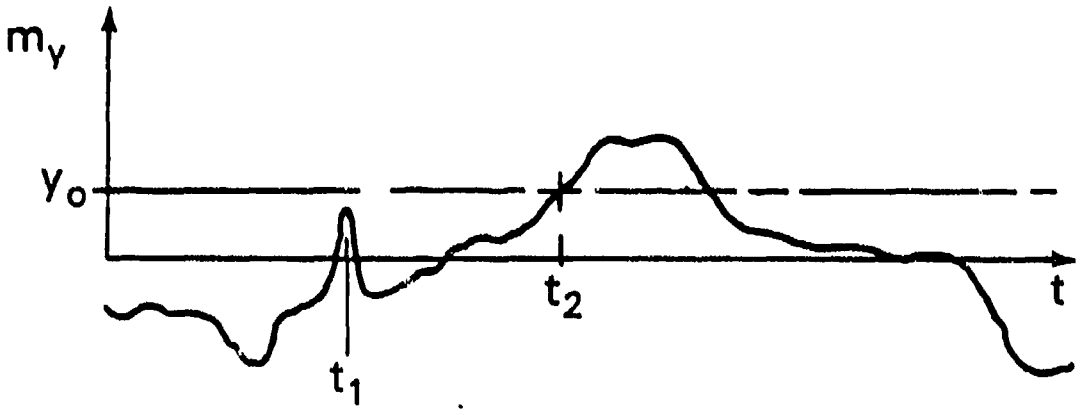

Figure 5

The average current $m_y(t)$ depicted in this figure yields nearly the same curve for the expected number of threshold crossings $m_J(0,t)$ (cf. Fig. 4) as the $m_y(t)$ in Fig. 2. It is assumed only that the peak value and curvature of $m_y(t)$ at time t_1 and the values of t_1, t_2, and y_o are the same in Figs. 2 and 5.

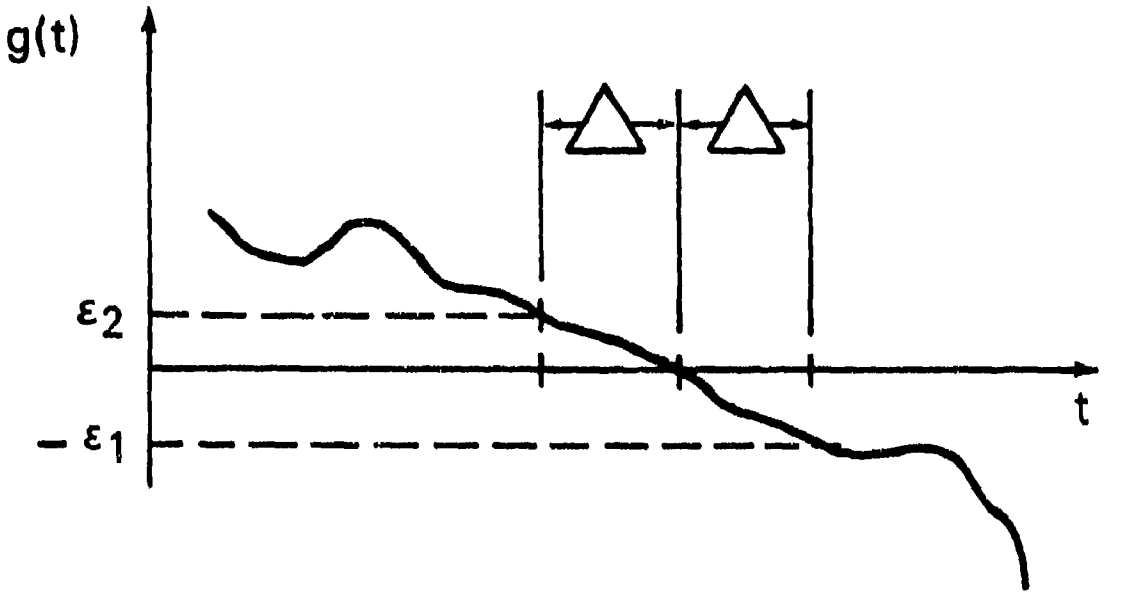

Figure 6

A sample function g(t) of the random process G(t) is depicted as a function of time. The particular sample function chosen has a zero-crossing at time t_o. The time Δ is chosen small enough such that the time interval $|t - t_o| < \Delta$ brackets no zeros of g(t) other than that at t_o.

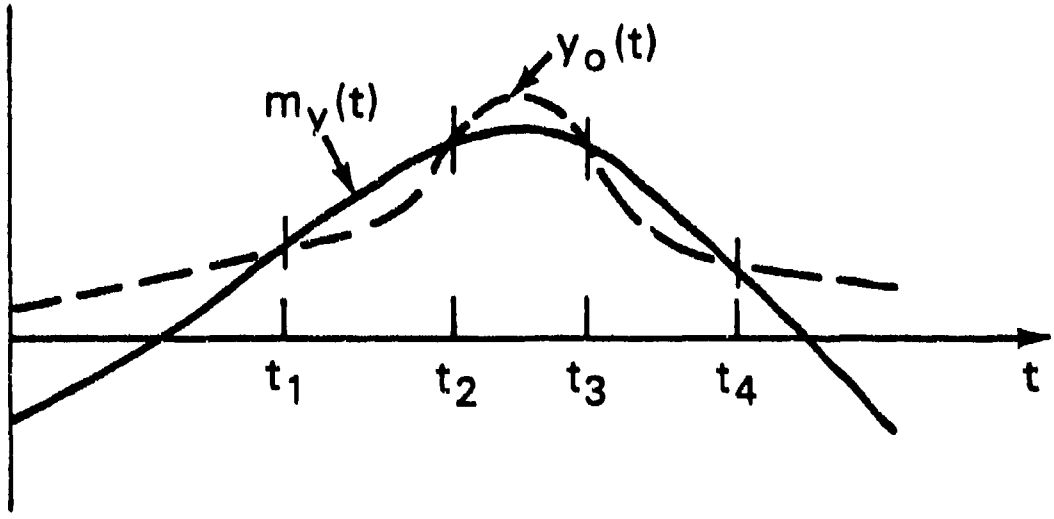

Figure 7

Illustration accompanying eqs. (48)-(50). Functions $y_o(t)$ and $m_y(t)$ are an illustrative threshold function and mean current, respectively. When the domain of integration in eq. (48) is chosen to satisfy constraints (49) and (50), the expected number of threshold crossings m_J is incremented at time t_1, but not at times t_2, t_3, or t_4.

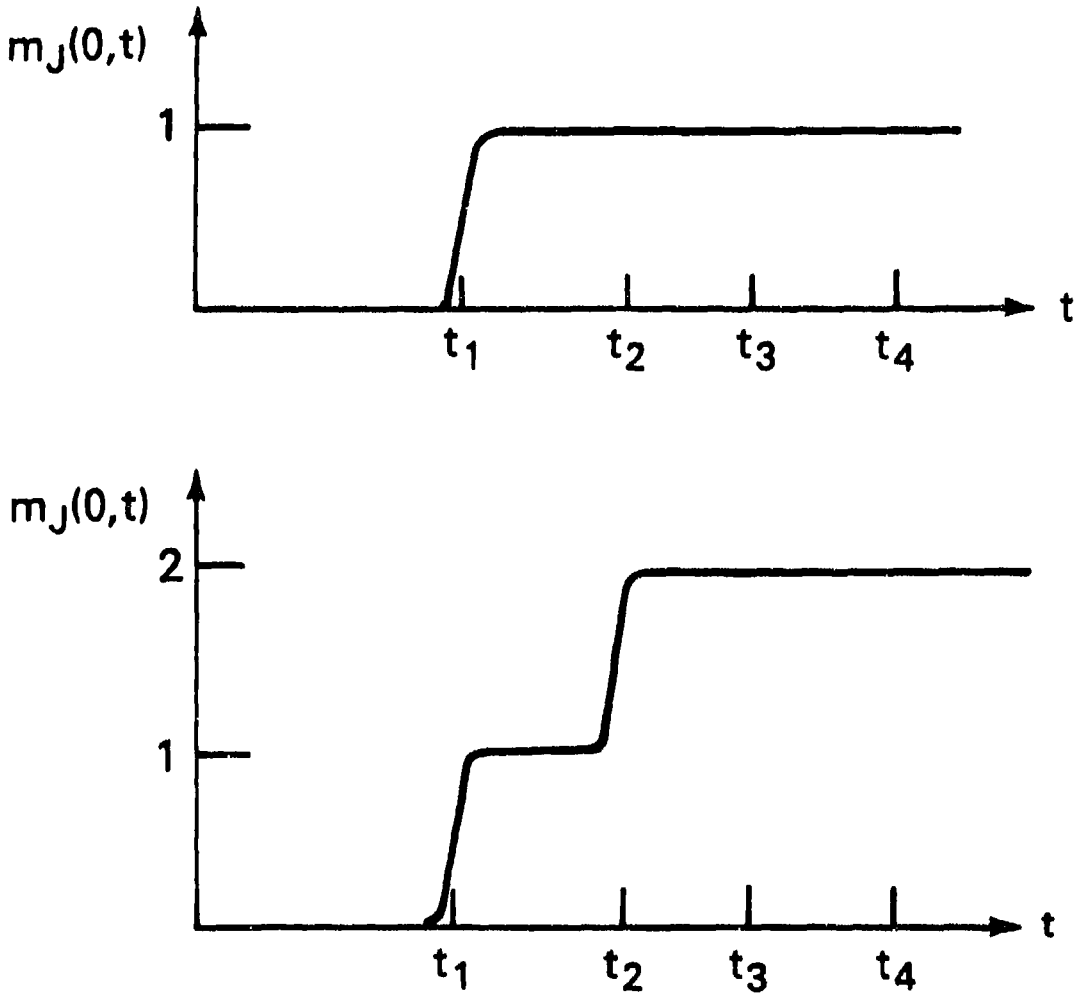

Figure 8

Figures 8a and 8b depict the time development of the expected number of threshold crossings calculated by means of equations (51) and (53), respectively, for the threshold $y_o(t)$ and mean current $m_y(t)$ shown in Fig. 7.

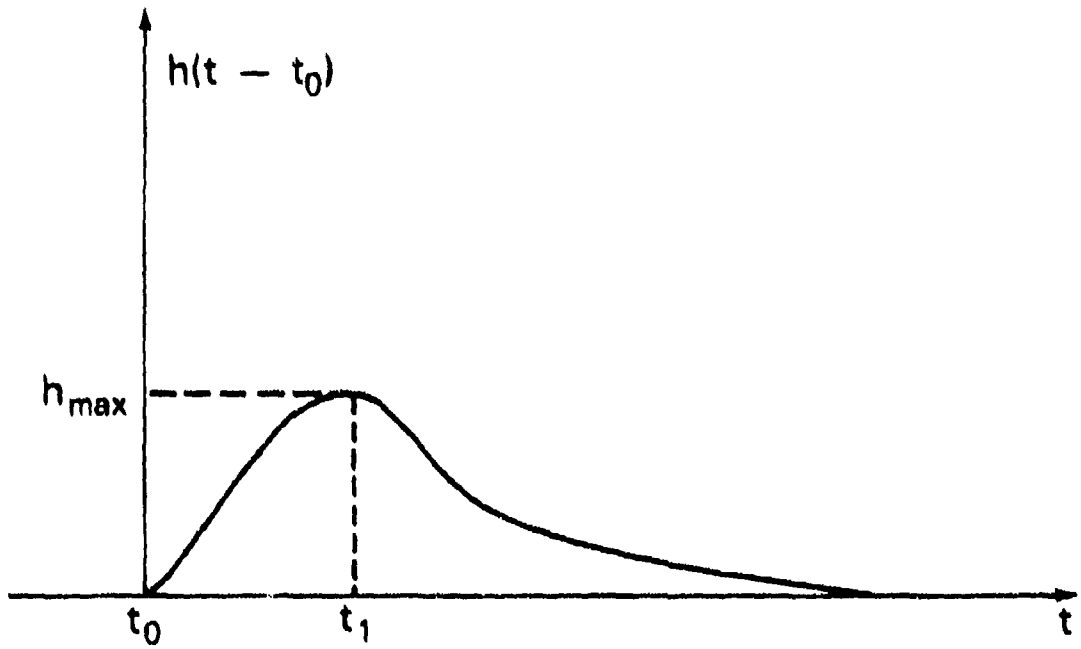

Figure 9

The impulse response of a low-pass post-detector filter is shown as a function of time. The impulse response h(t) assumes its peak value, h_{max}, when its argument is equal to $(t_1 - t_0)$.

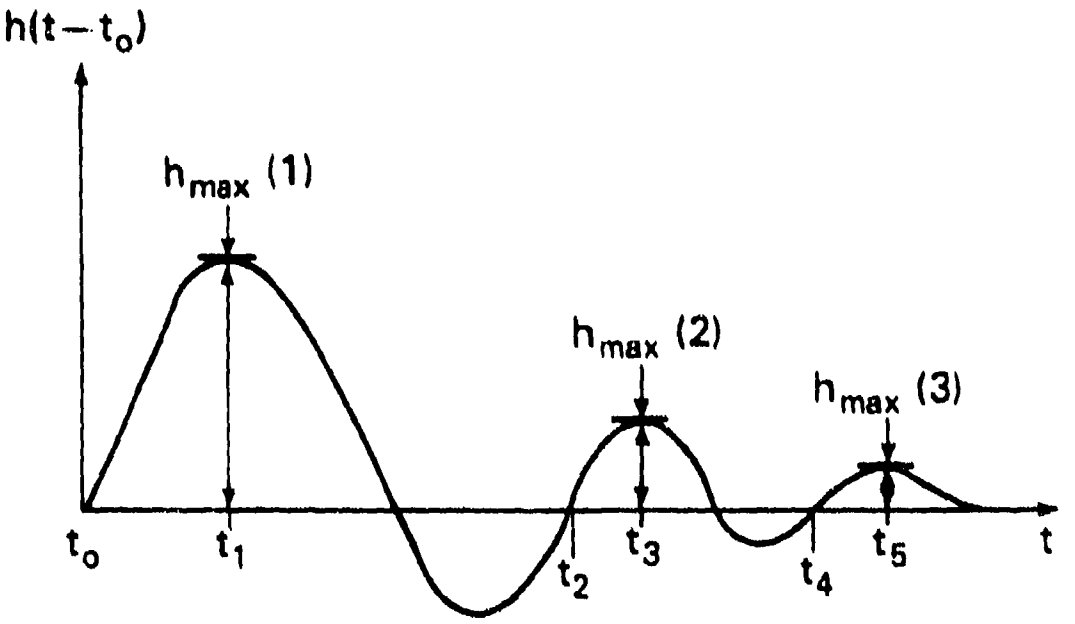

Figure 10

The impulse response of a band-pass post-detector filter is shown as a function of time. The impulse response $h(t-t_o)$ has positive-slope zero crossings at times t_o, t_2, t_4, ... The impulse response has local maxima at the times t_1, t_3, t_5, ...

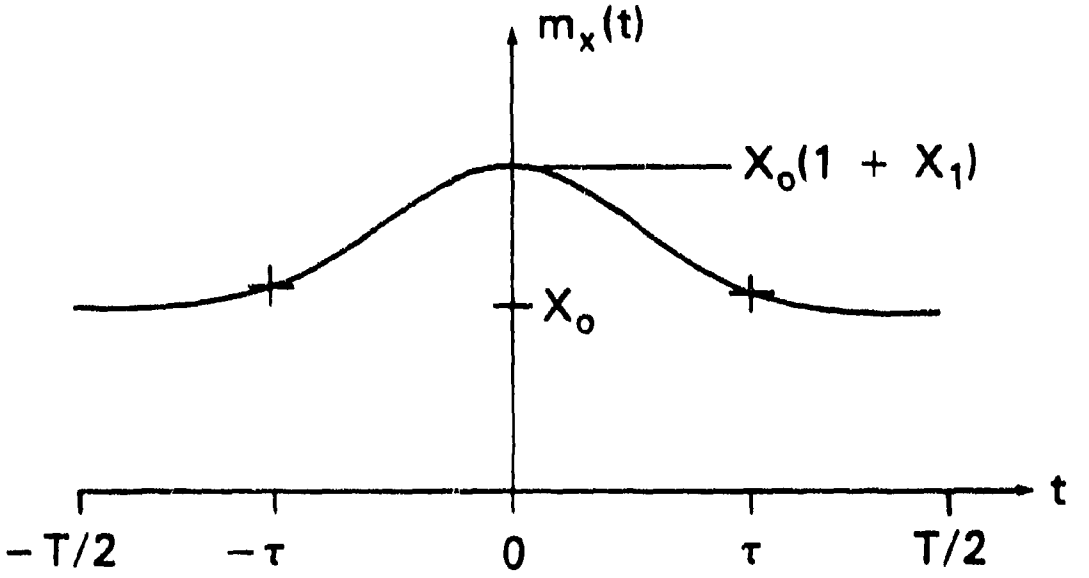

Figure 11

An illustrative plot of the model background current $m_x(t)$ is shown as a function of time. The parametric form of the model $m_x(t)$ is given by eq. (150). The parameters x_o, x_1, and τ, correspond respectively to a constant background level, the object/background peak contrast, and the size of an "object" in the scene. Depending on whether τ is large or small compared to the system dwell time, the model current $m_x(t)$ is representative of a "clutter-like" or a "target-like" object, respectively.

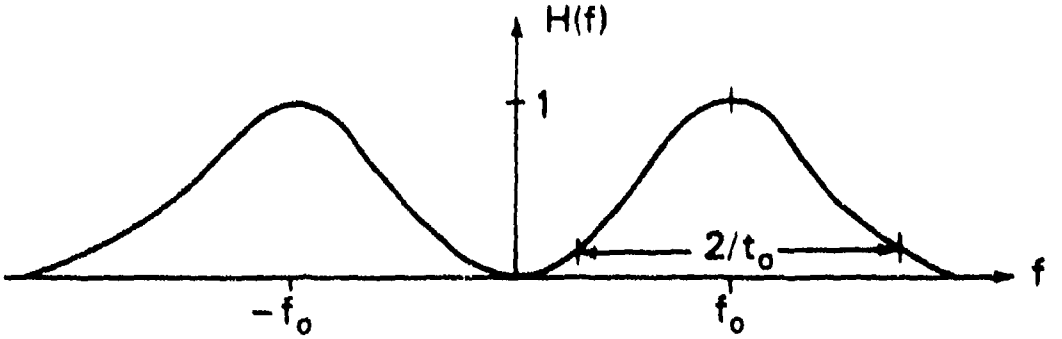

Figure 12

A representative plot of the model filter transfer function H(f) is shown as a function of the electrical frequency. The parametric form of H(f) is given by eq. (151). The parameter f_o is the center frequency of the bandpass characteristic. The parameter t_o is a decay time for the filters' impulse response (cf. eq. 149), and is directly related to the noise bandwidth of the filter by eq. (G-5). The zero-ordinate H(0) of H(f) is determined by the product of f_o and t_o (cf. eq. G-4), and is generally a very small number. The function H(f) is normalized to a peak value of unity.

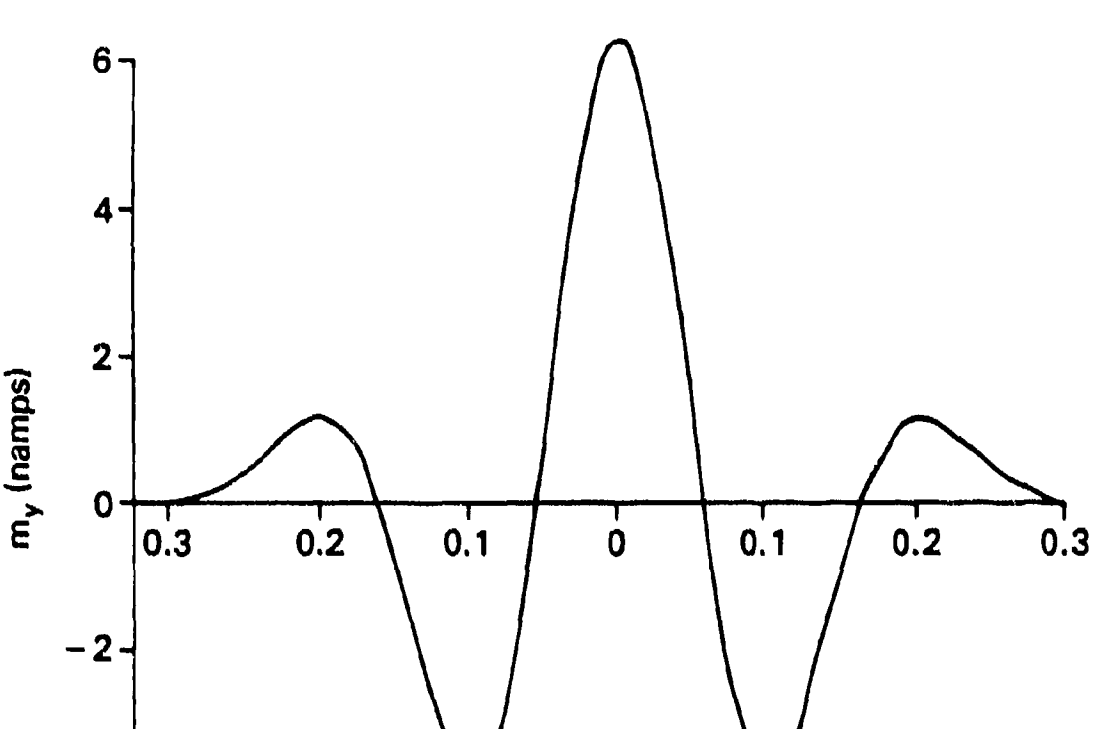

Figure 13

An illustrative evaluation of $m_y(t)$ is plotted as a function of time, for the model background and filter parameters of eqs. (154)-(158). The assumed parametric forms for the model filter impulse response $h(t)$ and the model background $m_x(t)$ are given by eqs. (149) and (150), respectively. The mean current $m_y(t)$ plotted in this figure is defined by eq. (56), and evaluated in terms of $h(t)$ and $m_x(t)$ by means of eq. (73).

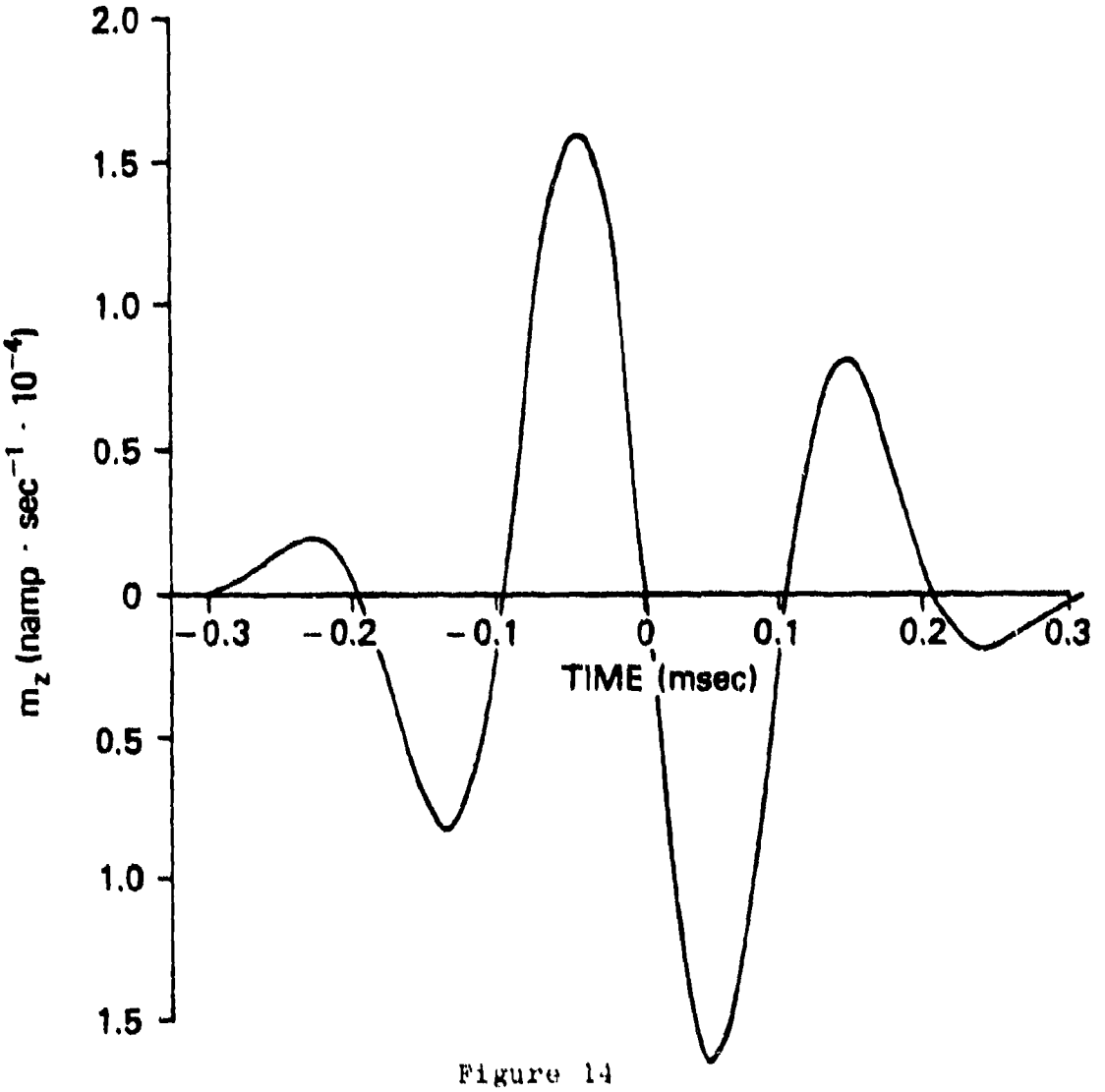

Figure 14

A plot of $m_y(t) \equiv \dot{m}_y(t)$ is shown as a function of time, for the model background and filter parameters of eqs. (154)-(158). This curve is the time derivative of the curve in Figure 13.

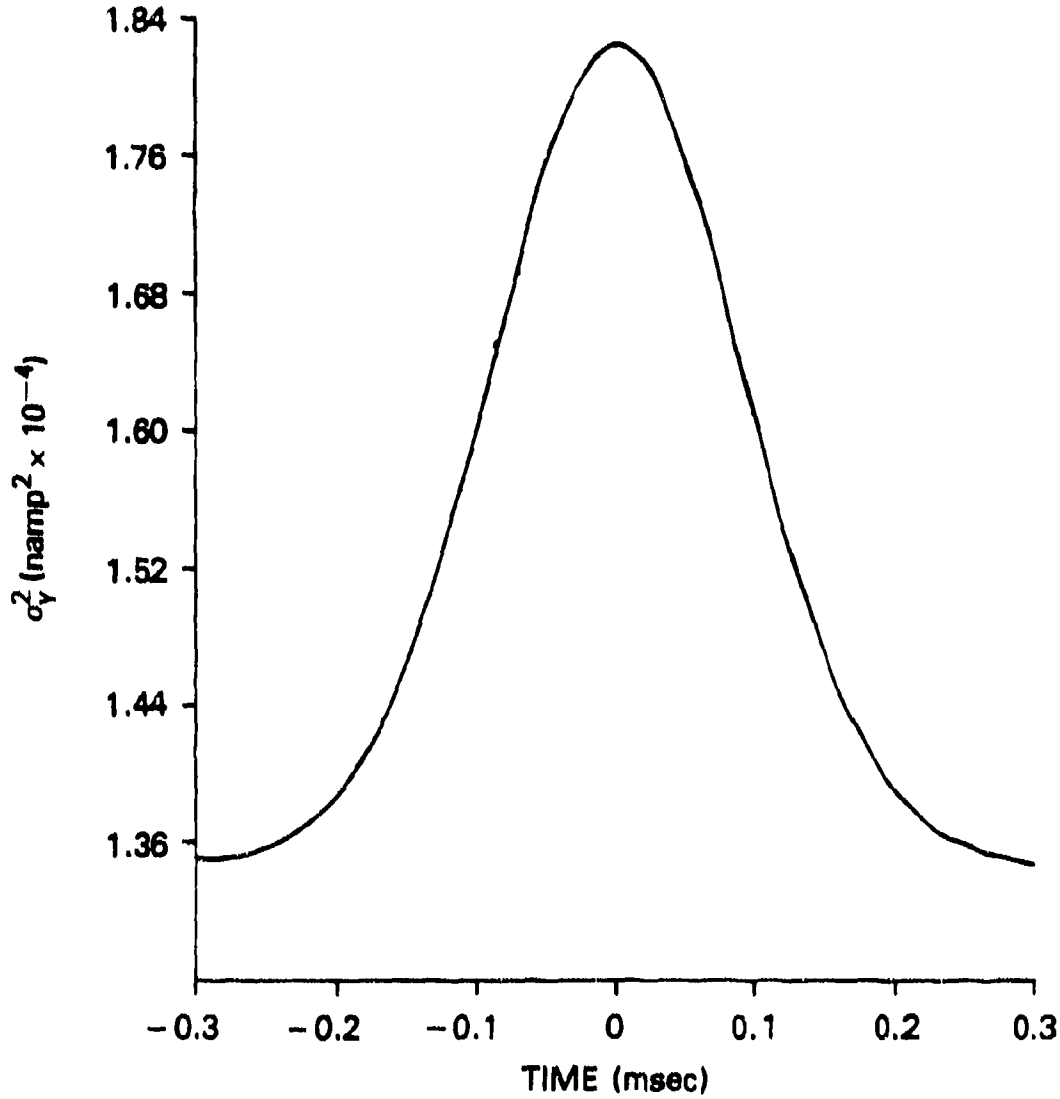

Figure 15

A plot of $\sigma_y^2(t)$ is shown as a function of time, for the model parameters of eqs. (154)-(158). The variance $\sigma_y^2(t)$ of the filtered current Y(t) is defined by eqs. (58), and evaluated in terms of h(t) and $m_x(t)$ by means of eq. (74).

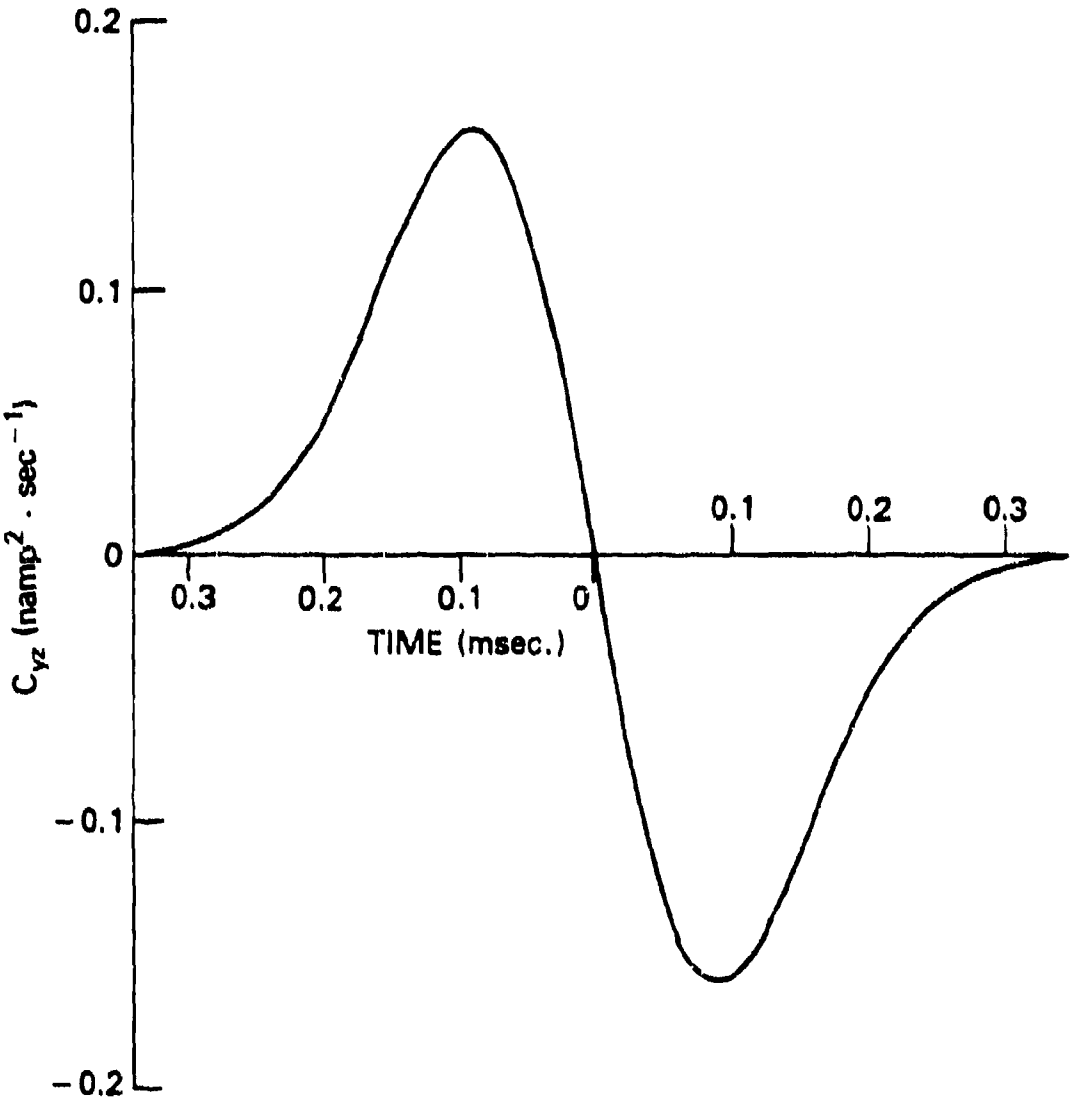

Figure 16

A plot of $C_{YZ}(t) \equiv C_{y\dot{y}}(t)$ is shown as a function of time, for the model parameters of eqs. (154)-(158). The quantity C_{YZ} is the cross-covariance of the filtered current Y(t) and its time derivative (cf. eq. 60), and is evaluated by means of eq. (B-23).

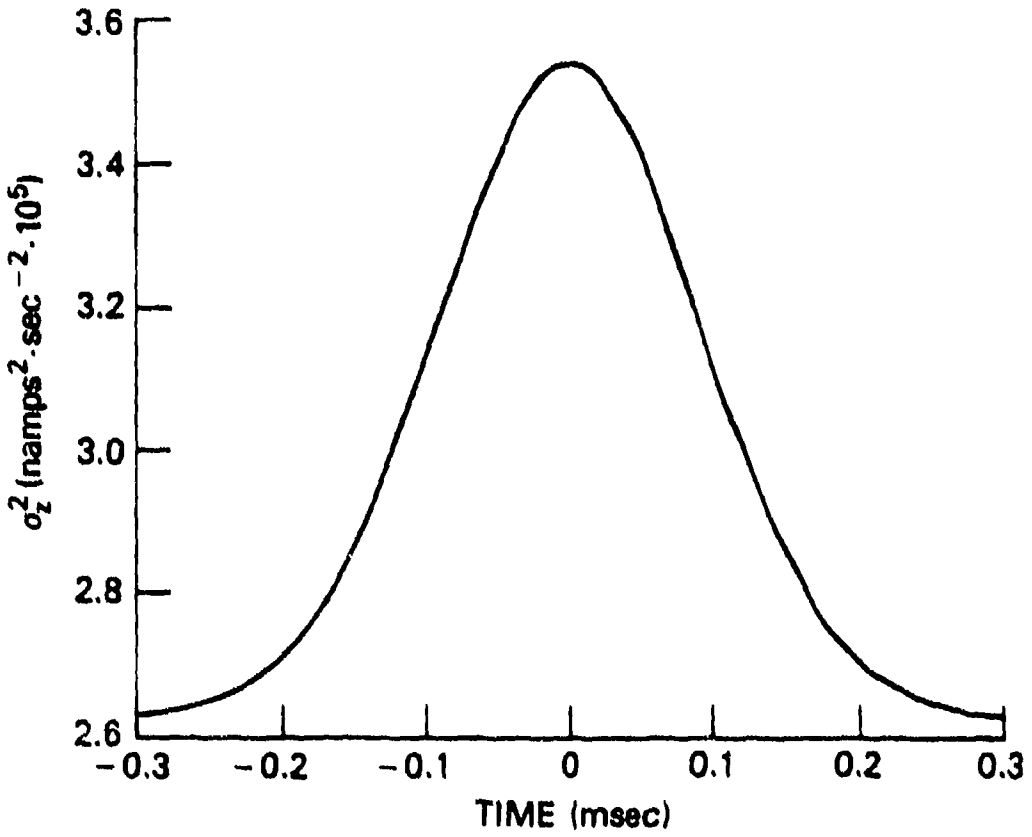

Figure 17

A plot of $\sigma_z^2(t)$ is shown for the model parameters of eqs. (154)-(158). The variance $\sigma_z^2(t)$ of the time derivative of the filtered current is defined by eq. (59), and evaluated by means of eq. (75).

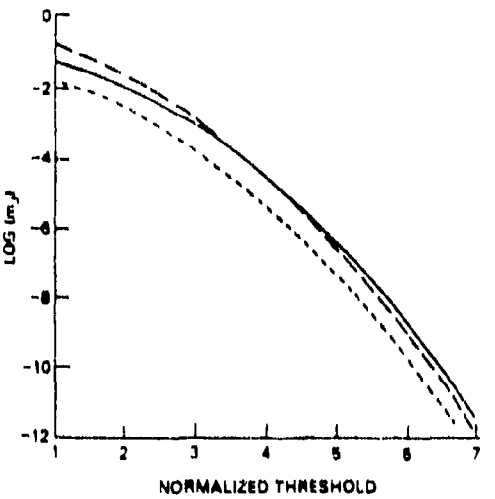

Figure 18

The base ten logarithm of the expected number of threshold crossings m_J is plotted as a function of the normalized threshold level, for the filtered current statistics of Figs. 13-17. The solid curve is the quantity m_J, obtained by integrating eq. (70) numerically. The dotted curve m_A is the asymptotic approximation to m_J given by eq. (166). The dashed curve m_{PS} is the point source approximation to m_J calculated from eq. (170). The two approximations to m_J offer calculational advantages, in that neither m_A nor m_{PS} require numerical integration for their calculation. The basic model background and filter parameters used in calculating these curves are given by eqs. (154)-(158). It follows from the discussion in Appendix G that eqs. (154)-(158) characterize an object matched in angular extent to the instantaneous field-of-view of the scanning sensor, i.e., a "target-like" object. As illustrated in this figure, the point-source approximation m_{PS} provides an excellent approximation to m_J for target-like objects.

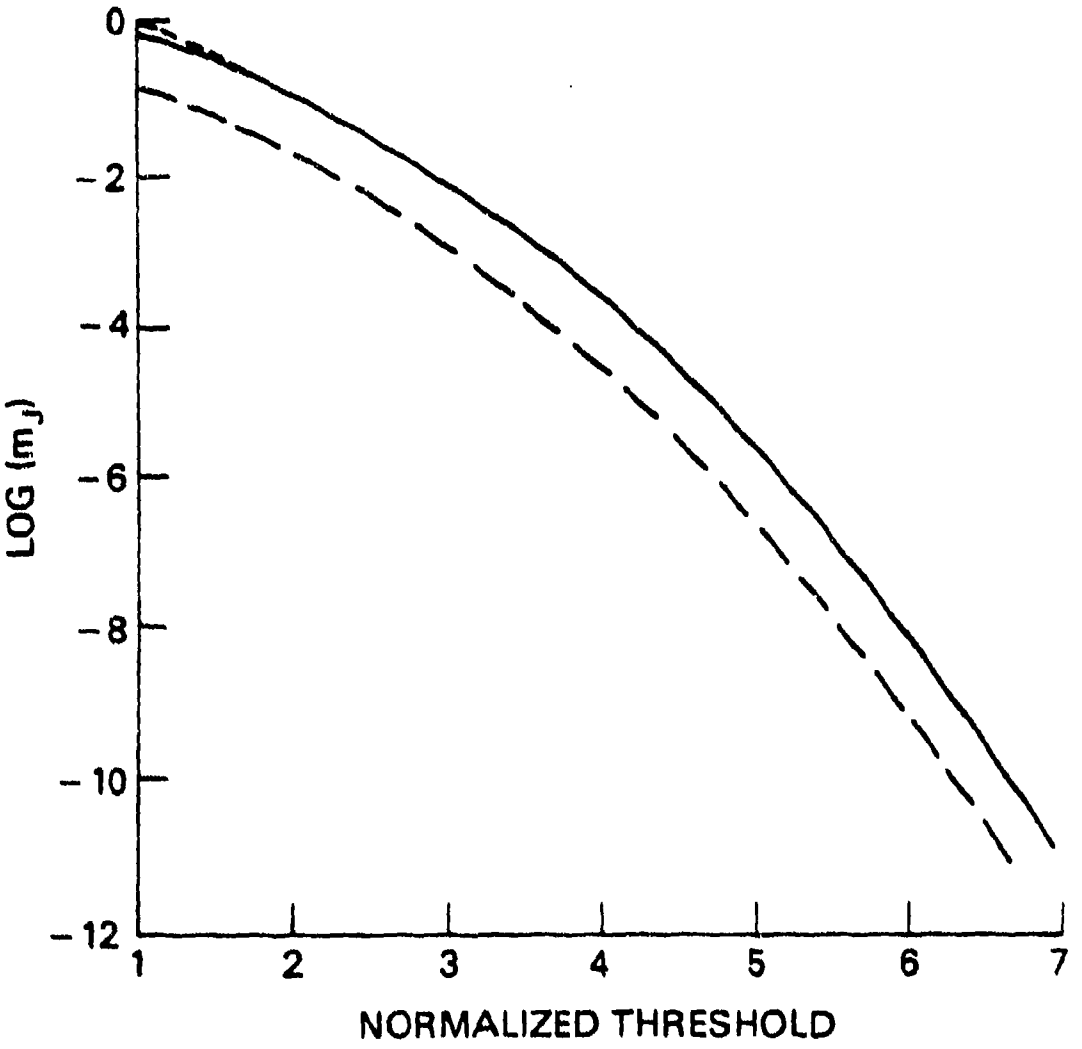

Figure 19

Similar to Fig. 18, except that the field-of-view is now scanned across a "clutter-like" object, five times larger in angular extent than the "target-like" object of Fig. 18. The solid curve, dotted curve, and dashed curve, correspond respectively to the quantities m_J, m_A, and m_{PS}. As illustrated in this figure, the asymptotic approximation m_A provides an excellent approximation to m_J for clutter-like objects.

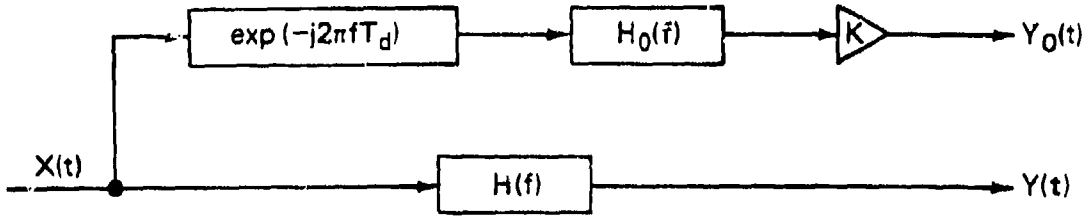

Figure 20

A simple adaptive threshold scheme is illustrated. The transfer function $\exp(-2\pi f\ T_d)$ introduces a delay of T_d seconds, ensuring decorrelation of the random processes Y(t) and $Y_o(t)$ (cf. Fig. 21). The significance of the random currents is seen by inspection of Fig. 1.

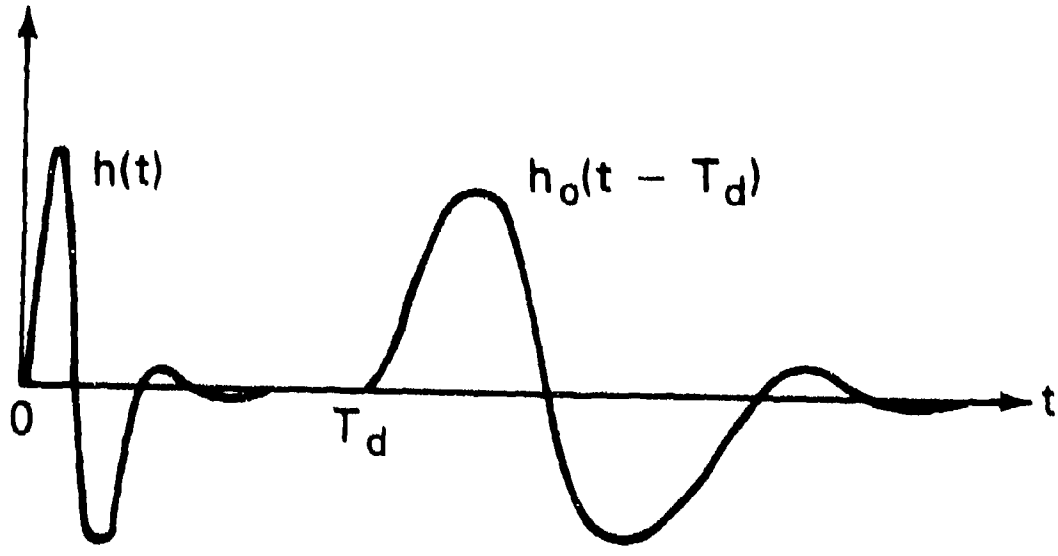

Figure 21

Inspection of this figure shows that the product $h(t)h_o(t-T_d) \approx 0$ when the delay time T_d is chosen sufficiently large. In this case, it follows from eq. (197) that the random processes $Y_o(t)$ and $Y(t)$ are uncorrelated.

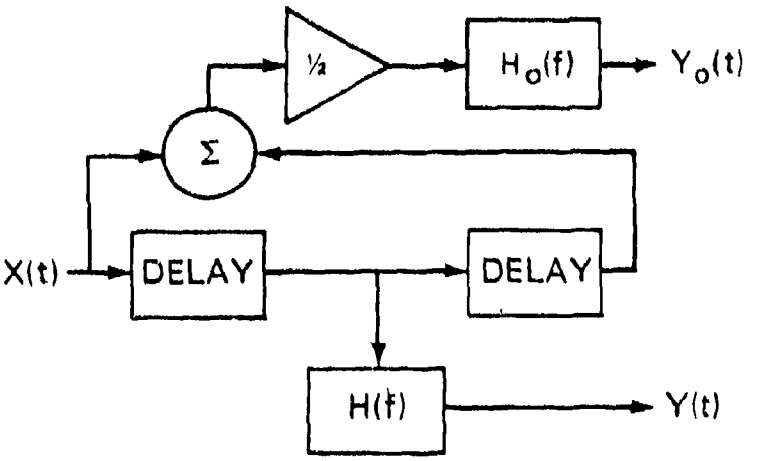

Figure 22

A simple adaptive threshold scheme is illustrated. The delay elements each introduce a delay of T_d seconds. The significance of the random currents X(t), Y(t), and $Y_o(t)$ is seen by inspection of Fig. 1. The block diagram shown here is actually just one part of the threshold processing receiver shown in Fig. 1.

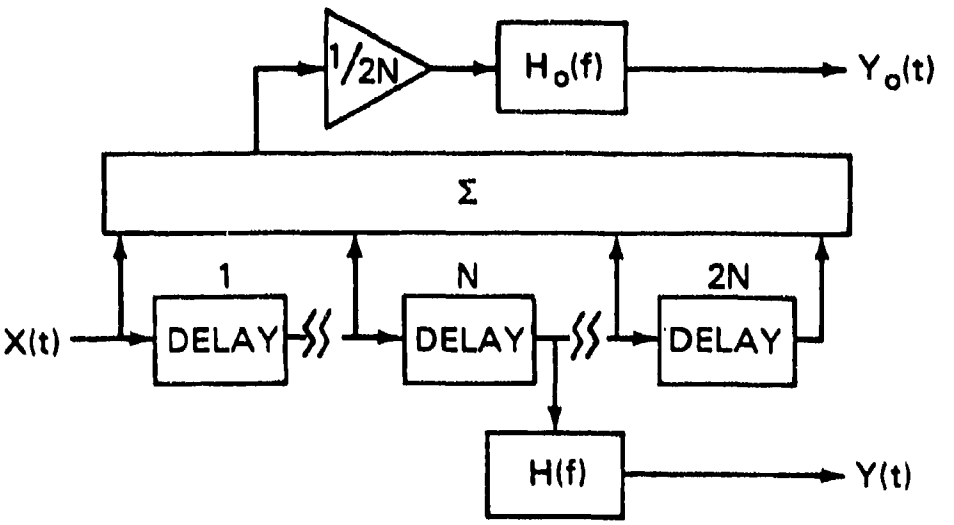

Figure 23

A candidate adaptive threshold scheme is illustrated that generalizes the structure of Fig. 22. The threshold-establishing approach shown here is realized in terms of a tapped delay line with 2N taps. Once again, the significance of X(t), Y(t), and $Y_o(t)$, follows from Fig. 1.

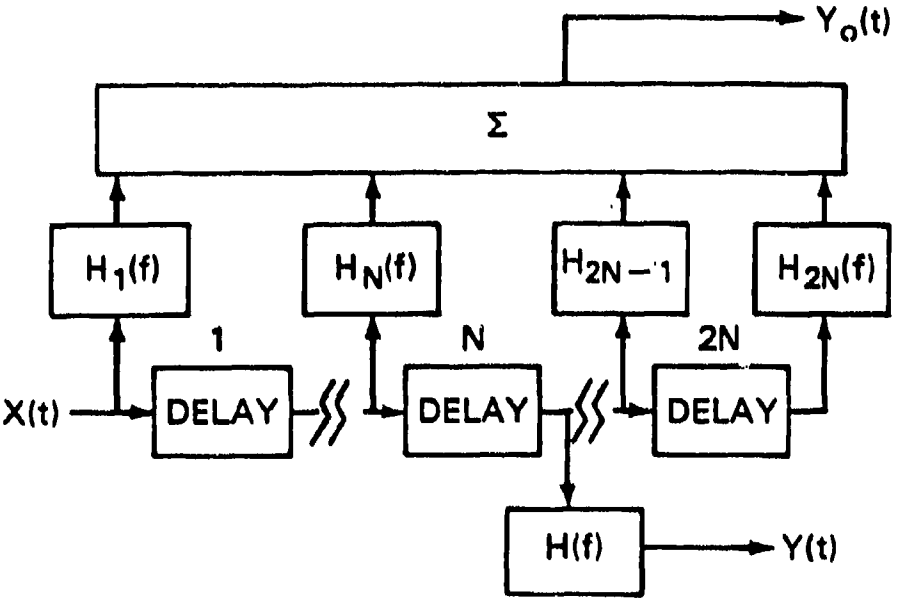

Figure 24

The tapped delay line adaptive threshold scheme shown here generalizes the structure of Fig. 23. The transfer functions $H_n(f)$, n=1,2,...2N at each of the 2N taps of the tapped delay line are de· ı variables, chosen to maximize the receivers' performance against a particular background scene, or set of background scenes. There is no a priori reason why the various delays should be chosen as equal to one another, other than for fabricational simplicity. More generally, additional degrees of freedom are incorporated by allowing these delays to take on distinct values.

APPENDIX A - Calculating the Average Photocurrent from Background Data

1. Objective

The objective of this Appendix is to show how the average value

$$m_X(t) = E\{X(t)\}$$

of the random current X(t) (cf. Fig. 1) can be derived in terms of

a) high spatial resolution radiometric imagery of the infrared scene, in the optical passband of interest

b) the postulated Modulation Transfer Function (MTF) of the optical train of the model system,

c) the quantum efficiency and physical dimensions of the focal plane detectors, and

d) the focal plane scan velocity.

The basic result to be derived is eq. (A-14).

2. The Focal Plane Irradiance

In order to calculate $m_X(t)$, it is first necessary to obtain an expression for the average irradiance $m_E(x,y)$ that would be measured in the focal plane of the model system in terms of the average aperture irradiance $m_{EO}(x,y)$.[1]

---

[1]The aperture irradiance is a random process due to photon noise. Thus, following the usual convention of random process theory, the complete ensemble of aperture irradiance functions is denoted by a capital letter, E(x,y). A single member of the ensemble is denoted by a lower case letter, e(x,y). The capital letter E is used to denote both irradiance and the process of statistical expectation; however, the context of usage should eliminate any possibility of confusing which of these two meanings is meant.

The mean aperture irradiance m_{EO} is characteristic of a particular infrared scene, and may be estimated by means of a radiometric Thermal Imaging System[1,2] (TIS) of higher spatial resolution than the model system. It is also highly desirable that the dwell time of the TIS be much larger than that of the model system, since the analysis requires knowledge of the mean irradiance m_{EO} established by averaging over the photon fluctuation statistics of the incident light.[2]

The spectral filter chosen for use with the TIS should match the combined TIS optical train/photodetector spectral response to that of the model system. This is necessary because there is no way to reliably calculate the irradiance of a scene measured in a waveband $\Delta\lambda_1$ in terms of the irradiance of the same scene measured in a different spectral band $\Delta\lambda_2$.

Once $m_{EO}(x,y)$ has been specified, the "transformed mean aperture irradiance" $E_O(f_x, f_y)$ is obtained as

$$\mathcal{E}_O(f_x, f_y) = \mathcal{F}\{m_{EO}(x,y)\} \tag{A-1}$$

---

[2] A TIS with a dwell time matched to the dwell time of the model system would actually be measuring a single member $e_O(x,y)$ of the ensemble $E_O(x,y)$, rather than the expected value $m_{EO}(x,y)$ of the aperture irradiance. Averaging out the photon noise by either increasing the TIS dwell time or by performing frame addition decreases the noisiness of the TIS image, and improves the goodness of the TIS imagery as an estimate of $m_E(x,y)$.

where

$\mathcal{F}\{.\}$ denotes the Fourier transform of the bracketed quantity

(f_x, f_y) are spatial frequencies corresponding to the space coordinates x and y, respectively

Employing vector notation eq. (A-1) may be written as

$$\mathcal{E}_o(\underset{\sim}{f}) = \mathcal{F}\{m_{EO}(\underset{\sim}{r})\}$$

The transformed focal plane irradiance $\mathcal{E}(\underset{\sim}{f})$ is obtained by multiplying $\mathcal{E}_o(\underset{\sim}{f})$ by the Modulation Transfer Function (MTF) that characterizes the image blurring effect of the model systems' optical train:

$$\mathcal{E}(\underset{\sim}{f}) = MTF(\underset{\sim}{f})\ \mathcal{E}_o(\underset{\sim}{f})\ .\ K_o \qquad (A-2)$$

where K_o is a constant. Assuming the conventional MTF normalization:

$$MTF\ (\underset{\sim}{0}) = 1$$

conservation of energy requires that:

$$K_o = \tau_o/(2f^{\#})^2$$

where:

τ_o = the transmittance of the optics

$f^{\#}$ = the focal length ratio of the optics

Finally, the mean focal plane irradiance is obtained by taking the inverse Fourier transform of $\mathcal{E}(\xi)$:

$$m_E(\underset{\sim}{r}) = \mathcal{F}^{-1}(\mathcal{E}(\xi)) \tag{A-3}$$

3. The Time-Varying Average Photocurrent

The response of a photovoltaic detector centered at position $\underset{\sim}{r}$ in the focal plane may be written as:

$$m_x(\underset{\sim}{r}_0) = \int_{A_{det}} R_I(\underset{\sim}{r}')\, m_E(\underset{\sim}{r}_0+\underset{\sim}{r}')\, d\underset{\sim}{r}' \tag{A-4}$$

where the surface integral extends over the area A_{det} of the detector, and $d\underset{\sim}{r}'$ is an element of surface area (cf. Fig. A.1).

The focal plane irradiance m_E and the mean current m_x in eq. (A-4) are ensemble average values over the photon fluctuation statistics of the light. For the purpose of analysis, the electrical frequency characteristic of the detector has been lumped together with the transfer function of the post-detector filter. Thus, by definition, the current responsivity R_I in eq. (A-4) is independent of the frequency of any temporal modulation that may be imposed on the irradiance.

A "pupil function" $P(\xi')$ is now defined for the detector such that

$$P(\xi') = \begin{cases} 1 & \xi' \in A_{det} \\ 0 & \xi' \notin A_{det} \end{cases} \qquad (A-5)$$

Assuming that the detector has a center of symmetry, so that

$$P(\xi') = P(-\xi')$$

and that the responsivity R_I is uniform on the detector surface, eq. (A-4) becomes

$$m_x(\xi_o) = R_I \int_{A_\infty} P(\xi')\, m_E(\xi_o+\xi')\, d\xi'$$

$$m_x(\xi_o) = R_I \int_{A_\infty} P(-\xi')\, m_E(\xi_o+\xi')\, d\xi' \qquad (A-6)$$

where A_∞ is the infinite focal plane. With the following change of variable

$$\psi = \xi_o + \xi'$$

eq. (A-6) becomes

$$m_x(\xi_o) = R_I \int_{A_\infty} P(\xi_o - \psi)\, m_E(\psi)\, d\psi \qquad (A-7)$$

Defining the following two-dimensional Fourier tranforms:

$$\mathcal{E}(\xi) = \mathcal{F}\{m_E(\xi)\} \tag{A-8}$$

$$P(\xi) = \mathcal{F}\{P(\xi)\} \tag{A-9}$$

Eq (A-7) may be recast with the aid of the Fourier convolution theorem as

$$m_x(\xi_0) = R_I \; \mathcal{F}^{-1}\{P(\xi)\, \mathcal{E}(\xi)\} \tag{A-10}$$

Moreover, it follows from eq. (A-2) that

$$\mathcal{E}(\xi) = MTF(\xi)\, \mathcal{E}_0(\xi) \cdot K_0 \tag{A-11}$$

where

$\mathcal{E}_0(\xi)$ is the spatial Fourier transform of the aperture irradiance, and

$MTF(\xi)$ is the modulation transfer function of the optics.

From (A-10) and (A-11)

$$m_x(\xi_0) = R_I \; \mathcal{F}^{-1}\{MTF'(\xi)\, \mathcal{E}_0(\xi)\} \tag{A-12}$$

where, by definition,

$$MTF'(\xi) \equiv P(\xi)\, MTF(\xi) \cdot K_0 \tag{A-13}$$

For infinitesmal "point detectors" $P(\xi)$ is effectively unity, so that

$$MTF' = MTF \cdot K_o$$

for this special case. More generally, the effect of having a finite detector size can be accounted for by multiplying the MTF of the optical system by the transformed pupil function of the detector, as in Eq. (A-13).

Finally, scanning effects are included by allowing the vector ξ_o in Fig. A.1 to trace the appropriate trajectory. For a uniform scanning rate

$$\xi_o = \chi t$$

where t is the time, and χ is the focal plane scan velocity. Eq. (A-12) then becomes

$$m_x(t) = R_I \int MTF'(\xi) \mathcal{E}_o(\xi) \exp(j2\pi\xi \cdot \chi t) d\xi \qquad (A-14)$$

The current responsivity R_I may be written as:

$$R_I = ne/h\nu \qquad (A-15)$$

where

h = Planck's constant (joule-sec./photon)

h = Planck's constant $\left[\frac{\text{joule-sec.}}{\text{photon}}\right]$

ν = optical frequency $\left[\text{sec}^{-1}\right]$

η = quantum efficiency $\left[\frac{\text{photoelectrons}}{\text{incident photons}}\right]$

e = electronic charge $\left[\frac{\text{coulombs}}{\text{electron}}\right]$

The focal plane scan velocity in eq. (A-14) is given by:

$$|\dot{\chi}| = \frac{w}{t_d} \qquad \text{(A-16)}$$

where

w = the detector width $\left[\text{cm}\right]$

t_d = system dwell time $\left[\text{sec}\right]$

It may be shown from eq. (A-16) that:

$$|\dot{\chi}| = 2\pi\, f\#D_{ap}/T_F \qquad \text{(A-17)}$$

where:

$f\#$ = the focal length ratio of the optics $\left[\text{dimensionless}\right]$

D_{ap} = the diameter of the optical aperture $\left[\text{cm}\right]$

T_F = system frame time $\left[\text{sec.}\right]$

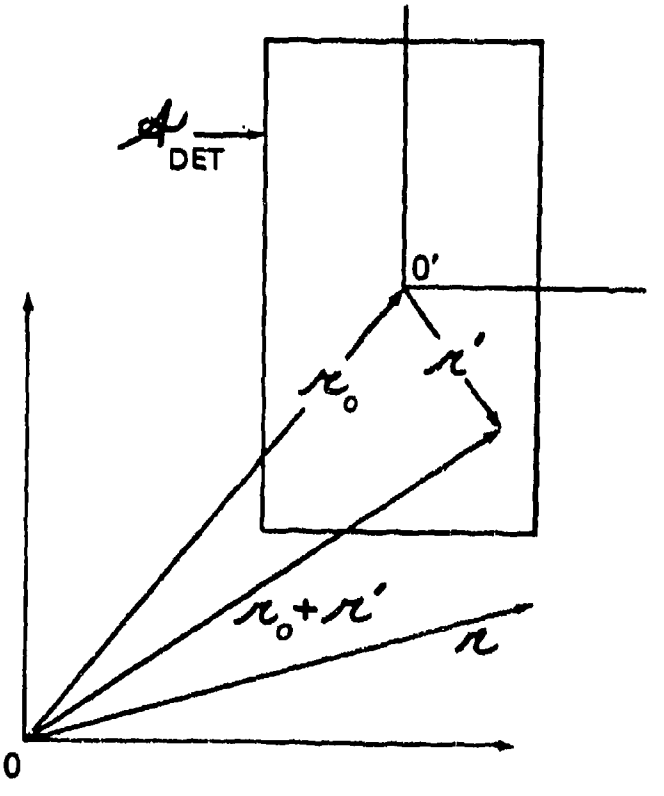

Fig. A.1 Focal Plane Geometry

The focal plane irradiance $m_E(r)$ is stationary in the coordinate system with origin 0. Vector r_o locates the center of a detector of area A_{det}. For scanning sensors, r_o is a function of time.

APPENDIX B. NOISE CURRENT CORRELATION FUNCTIONS

The object of this Appendix is to verify eqs. (73)-(76) which are needed to evaluate eq. (70) for the threshold crossing rate $\dot{m}_J(t)$.

The starting point for this discussion is the linear system input/output relation between the random processes X(t) and Y(t) (cf. Figure 1):

$$Y(t) = \int_{-\infty}^{\infty} d\mu \; X(\mu)h(t-\mu) \tag{B-1}$$

It follows directly from (B-1) that:

$$C_{YY}(t_1,t_2) = \int\int_{-\infty}^{\infty} d\mu d\lambda \; C_{XX}(\lambda,\mu)\; h(t_1-\lambda)\; h(t_2-\mu) \tag{B-2}$$

where the covariances C_{YY} and C_{XX} are defined by

$$C_{YY}(t_1,t_2) \equiv E\{[Y(t_1)-m_y(t_1)]\,[Y(t_2)-m_y(t_2)]\} \tag{B-3}$$

$$C_{XX}(\lambda,\mu) \equiv E\{[X(\lambda)-m_x(\lambda)]\;[X(\mu)-m_x(\mu)]\} \tag{B-4}$$

and where

$$m_y(t) \equiv E\{Y(t)\} \tag{B-5}$$

$$m_x(t) \equiv E\{X(t)\} \tag{B-6}$$

With the definition

$$Z(t) \equiv \dot{Y}(t) \tag{B-7}$$

it follows from eq. (B-3) that

$$C_{YZ}(t_1,t_2) = \partial_{t_2}\{C_{yy}(t_1,t_2)\} \tag{B-8}$$

and

$$C_{ZZ}(t_1,t_2) = \partial_{t_1}\partial_{t_2}\{C_{yy}(t_1,t_2)\} \tag{B-9}$$

From eqs. (B-2), (B-8) and (B-9)

$$C_{YZ}(t_1,t_2) = \int_{-\infty}^{\infty}\int d\mu d\lambda\ C_{xx}(\lambda,\mu)\ h(t_1-\lambda)\ \partial_{t_2}h(t_2-\mu) \tag{B-10}$$

$$C_{ZZ}(t_1,t_2) = \int_{-\infty}^{\infty}\int d\mu d\lambda\ C_{xx}(\lambda,\mu)\ \partial_{t_1}h(t_1-\lambda)\ \partial_{t_2}h(t_2-\mu) \tag{B-11}$$

Setting $t_1=t_2=t$ in eqs. (B-10) and (B-11), and noting that

$$C_{ZZ}(t,t) = \sigma_z^2(t) = E\{Z^2(t)\} - m_z^2(t) \tag{B-12}$$

it follows that

$$C_{YZ}(t,t) = \int_{-\infty}^{\infty}\int d\mu d\lambda\ C_{xx}(\lambda,\mu)h(t-\lambda)\ \partial_t h(t-\lambda) \tag{B-13}$$

$$\sigma_z^2(t) = \int_{-\infty}^{\infty}\int d\mu d\lambda\ C_{xx}(\lambda,\mu)\ \partial_t h(t-\lambda)\ \partial_t h(t-\mu) \tag{B-14}$$

An expression for $C_{xx}(\lambda,\mu)$ is now required before the analysis can be carried any further.

Setting $t_1=t_2=t$ in eq. (B-2), and noting that

$$C_{yy}(t,t) = \sigma_y^2(t) = E\{Y^2(t)\} - m_y^2(t) \qquad \text{(B-15)}$$

it follows that

$$\sigma_y^2(t) = \int_{-\infty}^{\infty}\int d\mu d\lambda\ C_{xx}(\lambda,\mu)h(t-\lambda)h(t-\mu) \qquad \text{(B-16)}$$

However, an adaptation of eq. (4.3.13) on p. 115 of ref. (12) leads to:

$$\sigma_y^2(t) = e\int_{-\infty}^{\infty} d\mu\ h^2(t-\mu)\ m_x(\mu) \qquad \text{(B-17)}$$

where e is the electronic charge. Consistency between eqs. (B-16) and (B-17) requires that

$$C_{xx}(\lambda,\mu) = e\ m_x(\mu)\ \delta(\lambda-\mu) \qquad \text{(B-18)}$$

where $\delta(.)$ is the Dirac delta function. Covariance functions like eq. (B-18) are characteristic of non-stationary white noise.[20] From eqs. (B-13), (B-14), and (B-18),

$$C_{YZ}(t,t) = e\int_{-\infty}^{\infty} d\mu\ h(t-\mu)\ \partial_t h(t-\mu)\ m_x(\mu) \qquad \text{(B-19)}$$

$$\sigma_z^2(t) = e \int_{-\infty}^{\infty} d\mu \left[\partial_t h(t-\mu)\right]^2 m_x(\mu) \qquad \text{(B-20)}$$

Noting that

$$h(t-\mu)\, \partial_t h(t-\mu) = \tfrac{1}{2}\, \partial_t\, h^2(t-\mu) \qquad \text{(B-21)}$$

it follows from eqs. (B-19) and (B-21) that

$$C_{YZ}(t,t) = \tfrac{1}{2}\, e\, \partial_t \{ \int_{-\infty}^{\infty} d\mu\, h^2(t-\mu)\, m_x(\mu)\} \qquad \text{(B-22)}$$

From (B-17) and (B-22)

$$C_{YZ}(t,t) = \tfrac{1}{2}\, \partial_t\{\sigma_y^2(t)\} = \sigma_y(t)\, \dot{\sigma}_y(t) \qquad \text{(B-23)}$$

Defining r(t) as

$$r(t) = C_{YZ}(t,t) \left[\sigma_y(t)\sigma_z(t)\right]^{-1} \qquad \text{(B-24)}$$

it follows from (B-23) and (B-24) that

$$r(t) = \{\dot{\sigma}_y(t)/\sigma_z(t)\} \qquad \text{(B-25)}$$

Taking the expected value of both sides of eq. (B-1) leads to the result

$$m_y(t) = \int_{-\infty}^{\infty} d\mu\, m_x(\mu)\, h(t-\mu) \qquad \text{(B-26)}$$

Taking the time derivative of (B-1):

$$\dot{Y}(t) = Z(t) = \int_{-\infty}^{\infty} d\mu \; X(\mu) \; \partial_t h(t-\mu) \tag{B-27}$$

Taking the expected value of both sides of (B-27):

$$m_z(t) = \int_{-\infty}^{\infty} d\mu \; m_x(\mu) \; \partial_t h(t-\mu)$$

I.e.,

$$m_z(t) = \partial_t \{ \int_{-\infty}^{\infty} d\mu \; m_x(\mu) \; h(t-\mu) \} \tag{B-28}$$

From eqs. (B-26) and (B-28)

$$m_z(t) = \dot{m}_y(t) \tag{B-29}$$

Defining the convolution operator as in eq. (77), eqs. (B-26), (B-17), (B-20), (B-29), and (B-25) may be written as:

$$m_y(t) = h(t) \bullet m_x(t) \tag{B-30}$$

$$\sigma_y^2(t) = e \; h^2(t) \bullet m_x(t) \tag{B-31}$$

$$\sigma_z^2(t) = e[\dot{h}(t)]^2 \bullet m_x(t) \tag{B-32}$$

$$m_z(t) = \dot{m}_y(t) \tag{B-33}$$

$$r(t) = \{\dot{\sigma}_y(t)/\sigma_z(t)\} \tag{B-34}$$

Equations (B-30)-(B-34) are identical to eqs. (73)-(76).

Appendix C. Relationships Between FAR, P_D, and m_J

1. The Relationship Between FAR and m_J

The complete description of an IRST sensors' performance under a given set of operational conditions requires the simultaneous specification of both the False Alarm Rate (FAR) and the Probability of Detection (P_D) for a "target" within the sensors' field of view. However, both "false alarms" and target detections are manifested as threshold crossings by the signal processor. Thus, the object of this Appendix is to relate the traditional IRST performance measures, P_D and FAR, to the expected number of threshold crossings m_J over prescribed intervals of time.

It is assumed that the average current $m_x(t)$ is known* on an interval of time $|t| < T/2$

The expected number of threshold crossings on the interval $|t| < T/2$ is defined as $m_J(O,T)$. Defining the false alarm rate as the expected number of threshold crossings per "reference interval" T_{ref}, the following relationship obtains between FAR and m_J :

$$FAR = (T_{ref}/T)\, m_J(O,T) \qquad (C\text{-}1)$$

---

*The quantity $m_x(t)$ may be specified a priori, or it may be calculated in terms of the radiance of a particular background scene (as discussed in Appendix A).

For example, if FAR is defined as the average number of false alarms per week, T_{ref} is set equal to the number of seconds in one week; if FAR is defined as the average number of false alarms per system dwell time, then T_{ref} is set equal to the dwell time (again expressed in units of seconds).

It is implicitly assumed in eq. (C-1), that the scene under observation does not include a target, so that each threshold crossing that occurs gives rise to a "false alarm".

2. The Relationship Between P_D and m_J: First-Order Approximation

Although not as straight-forward as eq. (C-1), a relationship between P_D and m_J can also be established.

As prelude to the definition of P_D, a "decision interval" T_D is first defined. The interval T_D is presumed to bracket the entire period of time during which the current Y(t) manifests target-induced fluctuations.

Assuming that a target is present in the scene, the number of threshold crossings that occur during the interval T_D is defined as the integer random variable J. The discrete probability density function of J is denoted as $f_J(j)$.

The probability of detection P_D is now defined as the probability that one or more threshold crossings occur during the decision interval:

$$P_D = \sum_{j=1}^{\infty} f_J(j) \qquad (C-2)$$

(The likelihood of a background-induced crossing during T_D has been neglected). Unfortunately, the problem of obtaining a formulation for f_J appears to be quite difficult.[23] The focus of this paper has been on the development of formulations for the expected number of threshold crossings

$$m_J \equiv E\{J\} = \sum_{j=1}^{\infty} j f_J(j) \qquad \text{(C-3)}$$

In order to establish a relationship between P_D and m_J, eqs. (C-2) and (C-3) are written as:

$$P_D = f_J(1) + \sum_{j=2}^{\infty} f_J(j) \qquad \text{(C-4)}$$

$$m_J = f_J(1) + \sum_{j=2}^{\infty} j f_J(j) \qquad \text{(C-5)}$$

Assuming that the probability of two or more threshold crossings is negligible during the decision interval T_D, eqs. (C-4) and (C-5) can be estimated as:

$$P_D \approx f_J(1) \qquad \text{(C-6)}$$

$$m_J \approx f_J(1) \qquad \text{(C-7)}$$

It follows from (C-6) and (C-7) that

$$P_D \simeq m_J(O,T_d) \qquad \text{(C-8)}$$

According to eq. (C-8), the expected number of threshold crossings during the decision interval T_D provides a good estimate of the detection probability P_D, so long as the probability of two or more crossings during T_D is negligible.

3. The Relationship Between P_D and m_J: Infinite Contrast Point Targets

An alternate approach is now taken to the problem of establishing the relationship between m_J and P_D. The discussion that follows is based on the analysis of Section IV, and will lead to the same result as before - namely, that the expected number of threshold crossings during the decision interval provides a reasonable estimate for P_D.

It is shown in Section IV that for BLIP sensors and unresolved targets:

$$m_J = 1 - \Phi(u_{min}) \qquad \text{(C-9)}$$

where $\Phi(.)$ is the Gaussian distribution function

$$\Phi(u) = (2\pi)^{-\frac{1}{2}} \int_{-\infty}^{u} \exp(-v^2/2)dv \qquad \text{(C-10)}$$

and

$$u_{min} \equiv \left[y_o - m_y(t_{max})\right] / \sigma_y(t_{max}) \qquad \text{(C-11)}$$

where t_{max} is the time at which the mean current $m_y(t)$ assumes its peak value.

Eq. (C-9) is equal to the exceedance probability of a Gaussian random variable having a mean and variance of $m_y(t_{max})$ and $\sigma_y^2(t_{max})$, respectively. As such, eq. (C-9) is a relatively straightforward generalization of the procedure conventionally used to define P_D.[24] Once again, one is encouraged to interpret m_J as a reasonable approximation to P_D.

4. The Relationship Between P_D and m_J: Proposal for a Second-Order Approximation

The first-order approximation to P_D discussed in Section C.2 is based on the following logic:

a) The methods discussed in Section IV of this paper are used to obtain a value for m_J, the first moment (i.e., the average value) of the random variable J.

b) Following eqs. (C-5) and (C-7), m_J is used as an estimate for $f_J(1)$.

c) The estimate for $f_J(1)$ established in b) is substituted into the truncated summation for P_D, eq. (C-6).

It appears only reasonable that an improved estimate could be obtained for P_D if the variance σ_J^2 of J were known in addition to the mean m_J of J. It will now be shown how knowledge of σ_J^2 can be used to calculate a second-order approximation for P_D (compare with (C-6)):

$$P_D \approx f_J(1) + f_J(2) \qquad \text{(C-12)}$$

Unfortunately, the technique described in this section for calculating the second-order approximation to P_D cannot be implemented until a formulation for σ_J^2 is developed analagous to the formulation for m_J in Section III. In this connection, it is noted that Bendat has derived an equation for the crossing count variance of stationary processes.[27] His result (cf. also ref. (23)) is far more complicated than the analagous eq. (E-8) for m_J. Thus a generalization of Bendat's result for σ_J^2 to the case of nonstationary processes and stochastic threshold functions may prove to be a difficult problem.

It is now assumed that a formulation for σ_J^2 can be obtained, analagous to the development for m_J in Section III. Analagous to eq. (C-3):

$$\sigma_J^2 \equiv \left\{ \sum_{j=1}^{\infty} j^2 \, f_J(j) \right\} - m_J^2 \qquad \text{(C-13)}$$

Substituting eq. (C-3) into (C-13) leads to the following expression for σ_J^2:

$$\sigma_J^2 = f_J(1) \left[1-f_J(1)\right] + 4f_J(2) \left[1-f_J(1)-f_J(2)\right] + E_J \qquad \text{(C-14)}$$

where

$$E_J \equiv \sum_{j=3}^{\infty} j^2 f - 2 \left[f(1) + 2f(2)\right] \sum_{j=3}^{\infty} jf - \left[\sum_{j=3}^{\infty} jf\right]^2 \qquad \text{(C-15)}$$

Assuming that the probability of three or more threshold crossings is negligible during the decision interval, eqs. (C-3) and (C-14) are approximated as:

$$m_J \approx f_J(1) + 2f_J(2) \tag{C-16}$$

$$\sigma_J^2 \approx f_J(1)\left[1-f_J(1)\right] + 4f_J(2)\left[1-f_J(1)-f_J(2)\right] \tag{C-17}$$

Calculation of m_J according to the method of section III, and an analagous calculation for σ_J^2, enables eqs. (C-16) and (C-17) to be solved for approximations to $f_J(1)$ and $f_J(2)$. The second-order approximation to P_D is then obtained by means of eq. (C-12).

If eq. (C-12) is found to yield an appreciably different result than eq. (C-8), third-order or even higher order approximations to P_D may be required; otherwise, the first-order eq. (C-8) is then verified as a good approximation for P_D.

APPENDIX D. CRAMÉR AND LEADBETTER'S EQUATION

Cramér and Leadbetter[14] have derived the following equation for the rate of positive slope zero crossings of a non-stationary Gaussian random process Y(t) (cf. ref. (14), eq. (13.3.2)):

$$\dot{m}_{CL}(t;0) = \left(\frac{\sigma_{\dot{z}}}{\sigma_y}\right) (1-r^2)^{\frac{1}{2}} \phi\left(\frac{m_y}{\sigma_y}\right) \{\phi(\eta) + \eta\Phi(\eta)\} \tag{D-1}$$

where

$$\eta \equiv \left[\sigma_z(1-r^2)^{\frac{1}{2}}\right]^{-1}\left[\dot{m}_y - \left(\frac{\sigma_z r m_y}{\sigma_y}\right)\right] \tag{D-2}$$

and the quantities m_y, σ_y, σ_z, and r are defined as in eq. (70).

On p. 288 of ref. (14) the statement is made that the mean rate at which Y(t) crosses a curve $y_o(t)$ can be obtained from eq. (D-1) simply by making the substitution

$$m_y \rightarrow (m_y - y_o) \tag{D-3}$$

in eq. (D-1).

From eqs. (D-1) - (D-3)

$$\dot{m}_{CL}(t;y_o) = \left(\frac{\sigma_z}{\sigma_y}\right) (1-r^2)^{\frac{1}{2}} \phi(u)\{\phi(p_1) + p_1\Phi(p_1)\} \tag{D-4}$$

with p_1 defined by eq. (67).

Eq. (D-4) is similar, but not identical, to eq. (70). The relationship between eq. (D-4) and eq. (70) will now be explained, and it will be shown that there is an assumption implicit in (D-4) that limits the range of its validity.

Two alternative formulations for the curve crossing rate are derived in Section III.B.

a) Assuming that both conditions (49) and (50) must be satisfied before a threshold crossing can be "counted" by the processor, the resulting expression for the crossing rate is given by eq. (51).

b) Assuming that only condition (50) need be satisfied before a threshold crossing can be counted by the processor, the expression for $\dot{m}_J$ is given by eq. (53).

It is now proposed that a third type of processor might be constructed, sensitive only to those threshold crossings for which

$$\dot{y}(t) > \dot{y}_o(t) \tag{D-5}$$

I.e., it is now assumed that the processor requires the satisfaction of inequality (49), but not (50). It then follows from eqs. (48), (D-5), and (52), that:

$$\dot{m}_J(t) = I(\infty) - I(\dot{y}_o) \tag{D-6}$$

From eqs. (D-6), (63), and (67)-(69):

$$\dot{m}_J(t) = \left(\frac{\sigma_z}{\sigma_y}\right)(1-r^2)^{\frac{1}{2}}\,\phi(u)\,\{\phi(p_1) + p_1\Phi(p_1)\} \tag{D-7}$$

Noting that eqs. (D-4) and (D-7) are identical, it follows that assumption (D-5) must be implicit in Cramer and Leadbetter's prescription for calculating the curve crossing rate.

An asymptotic analysis of eq. (D-4) similar to that of Section III.D.3 leads to:

$$m_{CL}(t;y_o) \simeq \mu(\dot{m}_y - \dot{y}_o) \qquad \text{(D-8)}$$

analagous to eq. (115). It follows from (D-8) that the mean crossing count m_{CL} is sensitive to all threshold crossings for which $\dot{m}_y > \dot{y}_o$. For example, m_{CL} is incremented by unity both at time t_1 and time t_3 in Fig. 7. Thus, the asymptotic character of m_{CL} reflects the requirement (D-5), as expected.

Appendix E - Introduction to Scanning Sensors and Adaptive Threshold Detectors

1. Scanning Sensors Operating Against Uniform Scenes

a. Current Statistics

When the sensor of Fig. 1 scans across a uniform background scene, the output current Y(t) is "statistically stationary". The meaning of statistical stationarity will now be discussed, as background to the discussion of non-uniform scenes and non-stationary processes that follows in the next section.

It is assumed that the sensor is scanned and re-scanned over the same scene, and that there are no changes in either the scene or the sensor from one scan to the next.

The current y(t) during the course of any one particular scan is called a "sample function" of the random process Y(t). (The process Y(t), in turn, may be thought of as the infinite ensemble of possible sample functions.) The current sample function obtained on the n^{th} scan is designated y(t;n). We now consider a particular one of these sample functions, y(t;1), depicted in Fig. E.1a.

The time variations in y(t;l) have their origin in the time-of-arrival fluctuations of the individual photons incident on the detector.* Thus, the fluctuations in y(t;l) are independent of the scan velocity and are present regardless of whether the sensor is scanning or motionless.

---

*If successive photons arrived at uniform, or otherwise predictable, time increments the arrival time of the "next" photon would be predictable in advance - in violation of the Heisenberg uncertainty principle. Thus, even nominally constant-intensity sources give rise to random photocurrents. This kind of noise is often called "photon fluctuation noise" or "quantum noise". When the quantum noise associated with the background light is the dominant noise type in the sensor, the sensor is said to be operating in the "Background Limited Performance" (BLIP) regime.

The average current at a particular instant of time t_o may be defined as the "ensemble average":

$$m_y(t_o) = \lim_{N\to\infty} \left\{\frac{1}{N} \sum_{n=1}^{N} y(t_o;n)\right\} \qquad \text{(E-1)}$$

In order for Y(t) to be a stationary process it is necessary that $m_y(t)$, as defined in eq. (E-1), be independent of time. Thus,

$$m_y(t_o) = m_y(t_1)$$

where the times t_o and t_1 are totally arbitrary (cf. Fig. E.1). Similarly, the mean-square deviation of Y(t) from its average value (i.e., the "variance" of Y) may be defined at each instant of time as

$$\sigma_y^2(t) \equiv \lim_{N\to\infty} \frac{1}{N} \sum_{n=1}^{N} \left[y(t;n) - m_y(t)\right]^2 \qquad \text{(E-2)}$$

The variance σ_y^2, like the mean m_y, is independent of time for stationary processes.

Eqs. (E-1) and (E-2) are satisfactory for illustrating the concept of "ensemble averaging"; however, it is desireable to have a different means for actually calculating the values of m_y and σ_y^2 in terms of standard background and sensor parameters.

It is first necessary to define the average value m_x of the current X(t) (cf. Fig. 1):

$$m_x = \eta e Q_B \qquad \text{(E-3)}$$

where

η = quantum efficiency of the detector $\left[\frac{\text{electrons}}{\text{photon}}\right]$

e = electronic charge $\left[\frac{\text{coulombs}}{\text{electron}}\right]$

Q_B = average background photon flux $\left[\frac{\text{photons}}{\text{sec}}\right]$

It may be shown that for sensors operating in the BLIP regime the mean value and variance of Y(t), originally defined by eqs. (E-1) and (E-2), can be calculated in terms of m_x as follows:

$$m_y = H(0)\, m_x \qquad \text{(E-4)}$$

$$\sigma_y^2 = 2em_x\Delta f \qquad \text{(E-5)}$$

where H(0) is the zero-ordinate of the transfer function H(f) (cf. Fig. 1), and Δf is the noise bandwidth of H(f). For bandpass H(f), H(0)=0. It follows from eq. (D-4) that m_y=0 for this case.

Since the scene is spatially uniform, the average photon flux Q_B is independent of time. It follows from eqs. (E-3) - (E-5) that the mean m_y and variance σ_y^2 are also independent of time, justifying the claim of stationarity for the current Y(t).

Assuming that the transfer function H(f) is normalized as follows:

$$\max_{f} H(f) = 1 \tag{E-6}$$

the noise bandwidth Δf in eq. (E-5) may be calculated from the equation:

$$\Delta f = \int_{0}^{\infty} |H(f)|^2 \, df \tag{E-7}$$

b. Crossing Rates for Constant Threshold Detection

It is now assumed that the signal processor of Fig. 1 is implemented such that the threshold y_o is equal to a constant. The constant threshold y_o is depicted on the sample function plots of Fig. E.1. A brief outline will now be given of a method for calculating the average number of times that the random process Y(t) crosses the threshold during a time interval of duration T seconds. (The relationship between the mean number of crossings m_J and the usual search set performance parameters P_D and FAR is discussed in Appendix C.)

The expected number of crossings $m_J(0,T)$ may be written in terms of the crossing rate $\dot{m}_J$ as:

$$m_J(0,T) = \dot{m}_J T \tag{E-8}$$

According to Rice,[13] $\dot{m}_J$ may be calculated as

$$\dot{m}_J = \dot{m}_{Jo} \exp(-u^2/2) \tag{E-9}$$

where

$$\bar{m}_{Jo} \equiv \left[\frac{1}{\Delta f} \int_0^\infty f^2 \, |H(f)|^2 df\right]^{\frac{1}{2}} \tag{E-10}$$

with Δf given by (E-7). Also,

$$u \equiv (y_o - m_y)/\sigma_y \tag{E-11}$$

with m_y and σ_y given by eqs. (E-4) and (E-5).

The quantity u defined by eq. (E-11) may be thought of as a normalized threshold level.

It follows from eq. (E-9) that the expected number of threshold crossings drops off rapidly as the threshold level is increased.

2. Scanning Sensors Operating Against Non-Uniform Scenes

a. Current Statistics

It is now assumed that the sensor of Fig. 1 is scanned a number of times over the same non-uniform scene, and that there are no changes in either the scene or the sensor from one scan to the next. A number of sample functions of the resulting current process Y(t) are depicted in Fig. E2.

Once again, the ensemble average mean and variance of Y(t) are defined by eqs. (E-1) and (E-2). However, as will now be discussed, Y(t) is now a non-stationary process, i.e., m_y and σ_y^2 are functions of time.

It is assumed that the infrared scene encompasses regions of blue sky and clouds where

Q_{BS} = average photon flux incident on the detector when blue sky is being observed.

Q_C = average photon flux incident on the detector when cloud is being observed.

The photon flux Q in eq. (E-3) is seen to be a function of time: Q takes on the value Q_C when a cloud is in the field of view, and a different value Q_{BS} when the scanning field of view includes only blue sky. Thus, the process Y(t) is non-stationary when the scene is non-uniform, since the mean and variance of Y(t) are seen from eqs. (E-3) - (E-5) to be functions of time.*

The time-varying mean value $m_y(t)$ is superposed as a dashed curve on each of the sample functions y(t) depicted in Fig. E.2.

---

*For the present, it suffices to say that the forms of eqs. (E-4) and (E-5) indicate that a time-varying m_x must give rise to time varying m_y and σ_y^2. However, it should be noted that eqs. (E-4) and (E-5) are only strictly valid for stationary processes, i.e., for time-invariant m_x. Thus, for a given time-varying $m_x(t)$, the correct values of m_y and σ_y^2 cannot generally be calculated from (E-4) and (E-5). Generalizations of (E-4) and (E-5) strictly valid for both stationary and non-stationary processes are given by eqs.(6) and (7).

b. Crossing Rates for Constant Threshold Detection

The performance of a constant threshold signal processor (cf. Fig. 1) against a non-uniform scene can be characterized in terms of the quantity:*

$$m_J(O,T) = \int_{T_o} \dot{m}_J(t)dt \qquad \text{(E-12)}$$

where T_o is the time interval $|t| < T/2$, and where $m_J(O,T)$ is the number of times that the current $Y(t)$ can be expected to cross the threshold level y_o during the time interval T_o. Eq. (E-12) is a straightforward generalization of eq. (E-8), to allow for the possibility of time-variable threshold crossing rates $\dot{m}_J$.

As long as the time variation of $m_x(t)$ is slow compared to the time variation of the impulse response $h(t)$ of the post-detector filter (cf. Fig. 1), a good estimate for $\dot{m}_J(t)$ can be obtained from eq. (E-9).

---

*Cf. Appendix C for a discussion of the relationship of $m_J(O,T)$ to the usual IRST performance parameters P_D and FAR.

The following steps are then followed in calculating $m_J(0,T)$:

(i) The time-varying mean current $m_x(t)$ is derived from the time-varying photon irradiance $Q(t)$ by means of eq. (E-3). (A detailed derivation of $m_x(t)$ in terms of the background radiance distribution is provided in Appendix A.)

(ii) Estimates of $m_y(t)$ and $\sigma_y^2(t)$ are obtained from eqs. (E-4) and (E-5). (More rigorously, eqs. (6) and (7) may be used to obtain $m_y(t)$ and $\sigma_y^2(t)$.)

(iii) Eq. (E-11) is evaluated for $u(t)$.

(iv) Eq. (E-9) is evaluated for $\dot{m}_J(t)$.

(v) Eq. (E-12) is evaluated for $m_J(0,T)$.

Numerical examples following the above prescription typically show that the crossing rate function $\dot{m}_J(t)$ is extremely sharply peaked (cf. Fig. E.3). Consequently, appreciable contributions to $m_J(0,T)$ only accrue in the near neighborhood of points such as t_p in Fig. E.3. It is shown in Section III.D that eq. (E-12) may be approximated as:

$$m_J(0,T) \approx \dot{m}_J(t_p)\ \delta t_p \qquad \text{(E-13)}$$

with $\dot{m}_J(t_p)$ obtained from eq. (E-9). The quantity δt_p is the effective interval of time during which $m_y(t)$ remains in the near neighborhood of its peak value, from the standpoint of crossing rate calculations. An expression for δt_p is derived in Section III.D (cf. eq. 16 or eq. 96).

The implications of eq. (E-13) for system performance are illustrated with the aid of Fig. E.4.

The large, relatively slowly varying maximum centered at t_p in Fig. E.4 is presumed to have its origin in the background scene. The narrower, lower amplitude spike centered at t_o in Fig. E.4 is presumed to be due to a "target".

It follows from eqs. (E-13) and (E-9) that the likelihood of a clutter-induced threshold crossing grows rapidly as the threshold level y_o in Fig. E.4 is lowered. It follows from the analysis in Section III.D that a clutter-induced threshold crossing (i.e., a "false alarm") becomes a virtual certainty when the threshold level actually intercepts the mean current $m_y(t)$. There is apparently no way for the constant threshold processor to detect the target peak at t_o without also incurring a false alarm arising from the clutter peak centered at t_p.

C. Crossing Rates for Ideal (CFAR) Adaptive Threshold Detection

The performance of an adaptive threshold processor is illustrated with the aid of Fig. E.5.

The processor is presumed to have some means for deriving high-confidence estimates for $m_y(t)$ and $\sigma_y(t)$, defined as $\hat{m}_y$ and $\hat{\sigma}_y$, respectively. When $m_y(t)$ is "slowly-varying" the processor establishes $y_o(t)$ as:

$$y_o(t) = \hat{m}_y(t) + K_{AT}\,\hat{\sigma}_y(t) \qquad \text{(E-14)}$$

The threshold is interpolated through periods of "rapidly varying" $m_y(t)$ by means of a smoothing filter. (cf., for example, the neighborhood of t_o in Fig. E.5). The adaptive threshold constant K_{AT} in eq. (E-14) is a design parameter.

From eqs. (E-11) and (E-14)

$$u(t) = K_{AT}\left[\hat{\sigma}_y(t)/\sigma_y(t)\right] + \left[\hat{m}_y(t) - m_y(t)\right]/\sigma_y(t) \qquad \text{(E-15)}$$

When the estimation errors are sufficiently small

$$\hat{\sigma}_y(t) \approx \sigma_y(t) \qquad \text{(E-16)}$$

$$\hat{m}_y(t) \approx m_y(t)$$

it follows from (E-15) that

$$u(t) \approx K_{AT} \qquad \text{(E-17)}$$

Thus, u(t) is rendered time-invariant by the adaptive threshold processor when there is no rapidly-varying target contribution to $m_y(t)$. When there are no targets in the scene, the mean current $m_y(t)$ is assumed to be slowly-varying, and the expected number of crossings during the time interval T_o may be calculated from eqs. (E-9), (E-12), and (E-17), as:

$$m_J(O,T) = \int_{T_o} \dot{m}_{Jo} \exp\left(-K_{AT}^2/2\right) dt \qquad \text{(E-18)}$$

Since both $\dot{m}_{Jo}$ and K_{AT} are time-invariant, eq. (E-18) becomes

$$m_J(O,T) = \dot{m}_{Jo} \exp\left(-K_{AT}^2/2\right) T \qquad \text{(E-19)}$$

Eq. (E-19) has the same form as the crossing rate expression for uniform scenes, eq. (E-8).

The kind of processor just described has been called a Constant False Alarm Rate (CFAR) processor, since the threshold crossing rate is now independent of time, i.e., a crossing is no more likely to occur when scanning a region of non-uniform background than when scanning a region of uniform background. E.g., with reference to Fig. E.5, the crossing rate is now no greater at t_p than at any other time.

It should be borne in mind that the CFAR processor is a non-realizable ideal: it has been assumed that the processor is able to estimate the quantities $m_y(t)$ and $\sigma_y(t)$ to as high a precision as desired. Generally, errors in the estimated values for m_y and σ_y are unavoidable, giving rise to appreciable time-dependence in eq. (E-15) for u(t).

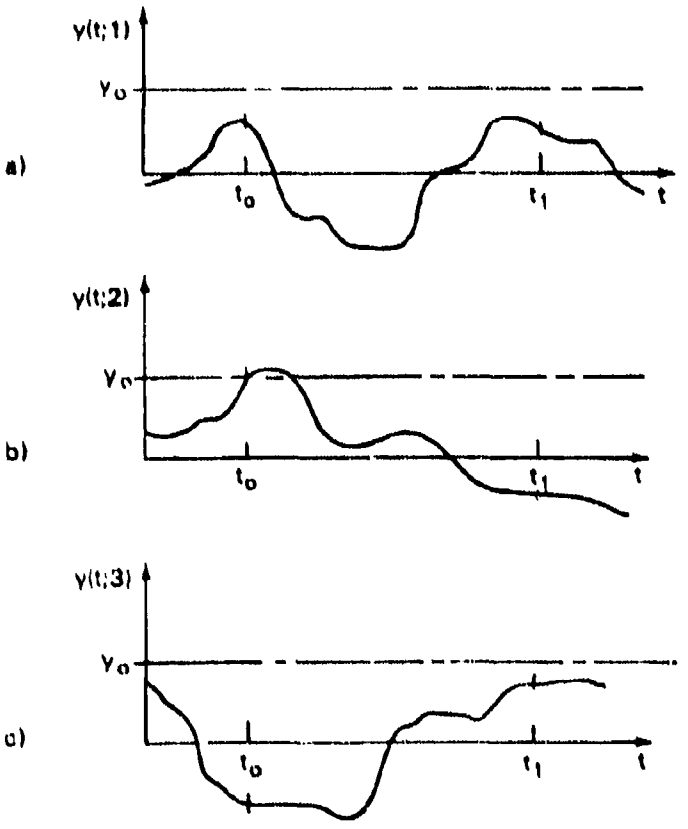

Figure E.1

Three sample functions of the random current Y(t) are shown as functions of time. The current Y(t) is taken at the output of the post-detector filter as the sensor is scanned over a uniform scene (cf. Fig. 1). The sample functions are designated y(t;n), n=1,2,3,... The sample functions display random time variations caused by time-of-arrival fluctuations of the individual photons incident on the detector. Since the current Y(t) is stationary, the ensemble average mean value (variance) defined by eq. (E-1) (eq. E-2) is the same at time t_0 as at time t_1, where times t_0 and t_1 are arbitrary.

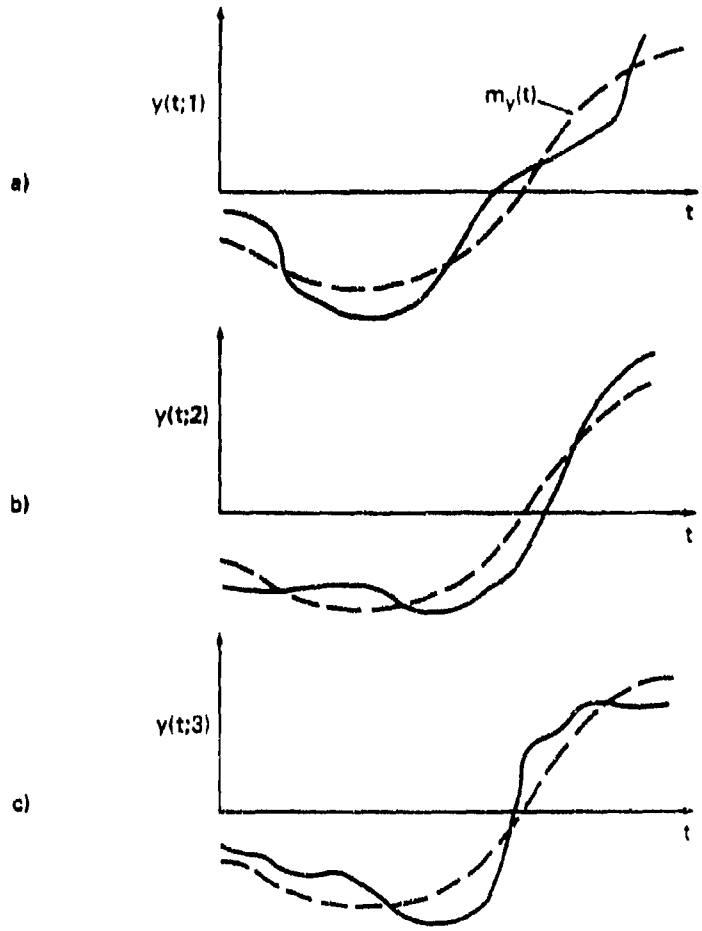

Figure E.2

Three sample functions of the random current Y(t) are shown as functions of time. This figure is similar to Fig. E.1, except the sensor is now presumably scanned over a non-uniform scene. The time-varying ensemble average $m_y(t)$ of Y(t) is shown as a dashed curve superposed on each of the three depicted sample functions (solid curves). The ensemble average m_y is still defined by eq. (E-1); however, the fact that m_y is now a function of time implies that Y(t) is now a nonstationary random process.

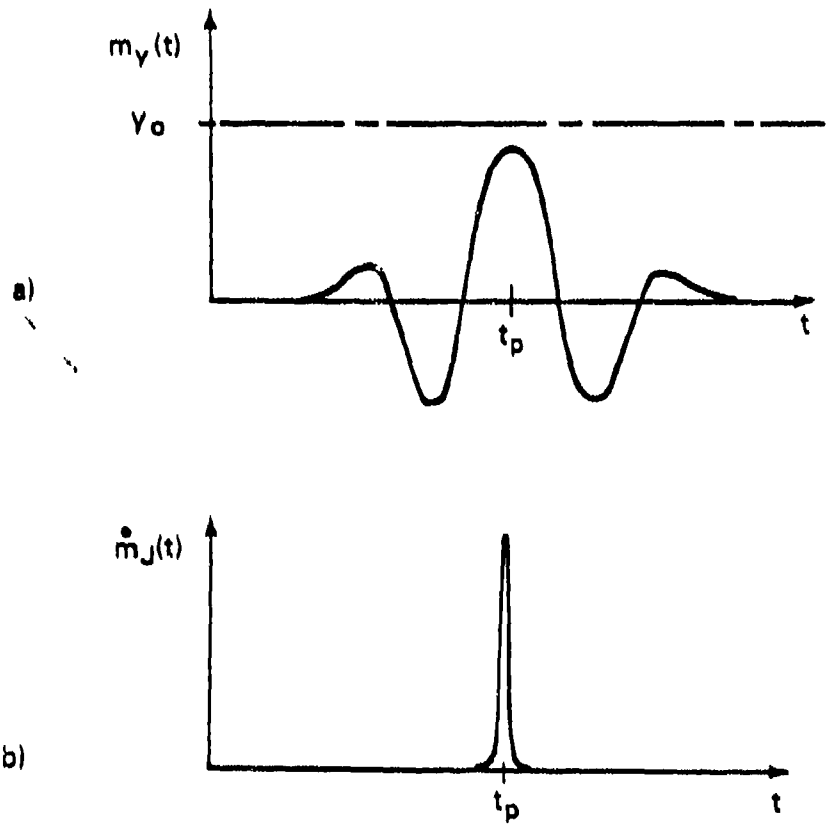

Figure E.3

Part a) is an illustrative plot of $m_y(t)$ Vs. t, where m_y is the mean value of the filtered current Y(t) (cf. Fig. 13). Also shown is a constant threshold current y_o, lying above the peak value of m_y. The function $m_y(t)$ takes on its peak value at the time t_p.

Part b) is a plot of the threshold crossing rate $\dot{m}_J(t)$ corresponding to the threshold y_o and mean current $m_y(t)$ of part a). The entire contribution to the crossing rate integral, eq. (E-12), accrues in the very near neighborhood of t_p.

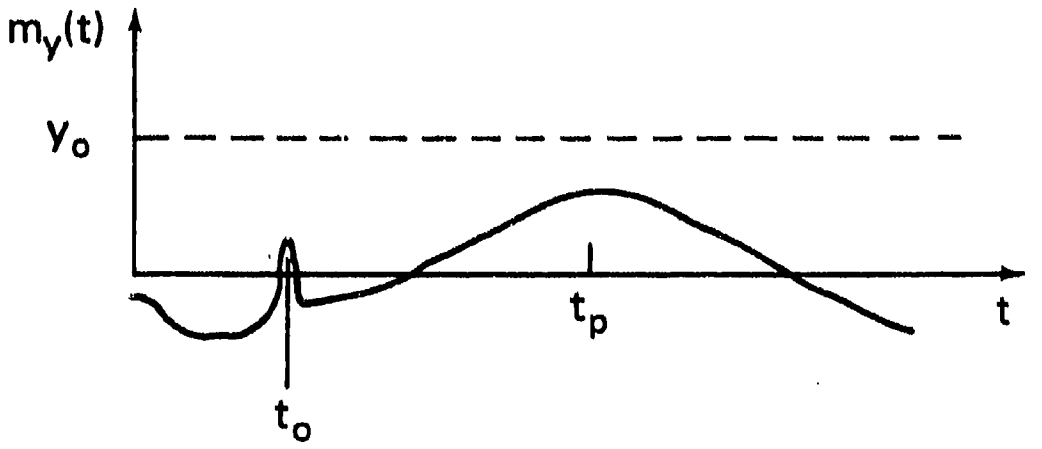

Figure E.4

This figure illustrates a critical shortcoming of constant threshold processing. The slowly varying maxima centered at t_p presumably has its origin in the non-uniform background scene. The narrower, lower amplitude spike centered at t_o is due to a target. The likelihood of a false alarm (i.e., a clutter-induced threshold crossing) grows rapidly as the threshold level y_o is reduced. There is no way for the constant threshold processor to detect the target peak at t_o without also incurring a false alarm arising from the clutter peak centered at t_p.

A plot of the threshold crossing rate $\dot{m}_J(t)$ corresponding to this figure would show that the probability of a false alarm is far greater at time t_p than at any other time.

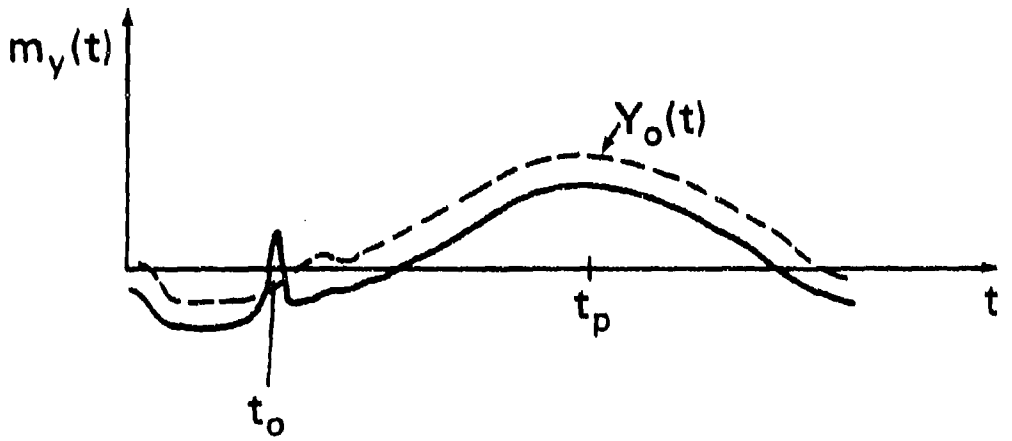

Figure E.5

This figure illustrates an important potential advantage that accrues to the use of adaptive threshold processing. The mean current $m_y(t)$ is the same as for Fig. E.4, with a clutter peak centered at time t_p, and a lower-amplitude target spike centered at time t_o. The adaptive threshold $y_o(t)$ is presumably able to accurately track the slowly varying background signal, but not the more rapidly varying target signal. Thus, target detection is assured, while the probability of a false alarm is kept acceptably small. As contrasted with the situation of Fig. E.4, the probability of a false alarm is now no greater in the neighborhood of time t_p than at any other time.

APPENDIX F. THE EDGEWORTH CORRECTION TO $\hat{m}_J$

The objective of this Appendix is to estimate the relative error in $\hat{m}_J$ due to the assumption of a strictly Gaussian probability density function for the current Y(t) (cf. Fig. 1):

$$f_y(y) = \sigma_y^{-1} \phi\left(\frac{y-m_y}{\sigma_y}\right) \qquad \text{(F-1)}$$

where $\phi(.)$ is the Gaussian density function, m_y is the mean value of Y(t), and σ_y^2 is the variance of Y(t), defined respectively by eqs. (F-3), (56), and (58).

It will be shown that the assumption of non-stationary Gaussian statistics for the filtered current Y(t) is totally justifiable, for typical sensor parameters and background radiances.

The starting point for this analysis is a truncated Edgeworthseries expansion [13] of $f_y(y)$, as appropriate for describing Poisson shot noise processes Y(t):*

$$f_y(y) = \sigma_y^{-1} \phi(u) - (\lambda_y/6\sigma_y^4)\, \phi^{(3)}(u) \qquad \text{(F-2)}$$

---

*Strictly speaking, Y(t) is a conditional Poisson shot noise, with a wideband thermal level density function. However, it is well known that such processes may be modeled as constant level Poisson shot processes when the response time of the detector is very long compared with the coherence time of the incident light. (cf. Ref. (12))

where

$$\phi(u) = (2\pi)^{-\frac{1}{2}} \exp(-u^2/2) \tag{F-3}$$

$$\phi^{(n)}(u) = d^n \phi(u)/du^n \tag{F-4}$$

$$u = (y-m_y)/\sigma_y \tag{F-5}$$

$$m_y = h(t) \ast\ast m_x(t) \tag{F-6}$$

$$\sigma_y^2 = e\, h^2(t) \ast\ast m_x(t) \tag{F-7}$$

$$\lambda_y = e^2\, h^3(t) \ast\ast m_x(t) \tag{F-8}$$

The quantities e, h(t), and $m_x(t)$, in eqs. (F-6)-(F-8) are defined following eq. (76). Eqs. (F-7) and (F-8), the variance and third semi-invariant of the nonstationary process Y(t), are adapted from Ref. (12).

From eqs. (F-2)-(F-4):

$$f_y(y) \approx \sigma_y^{-1} \phi(u) \{1 + \epsilon_y\} \tag{F-9}$$

where the error term ϵ_y is given by

$$\epsilon_y = (\lambda_y/6\sigma_y^3) \{u(u^2-3)\} \tag{F-10}$$

According to eq. (F-10), the relative error increases as u^3; however, it follows from eqs. (F-3) and (F-9) that the density function f_y is of negligible amplitude for large values of u. It will now be assumed that values of u greater than eight are of no importance, since

$$f_y(y) = \mathcal{O}\{\exp(-32)\} = \mathcal{O}(10^{-14}), \quad u=8 \tag{F-11}$$

In order to establish a reasonable upper bound for ε_y, the value u=8 will be used in eq. (F-10):

$$\varepsilon_y < 500\ (\lambda_y/6\sigma_y^3) \tag{F-12}$$

Also,

$$(\lambda_y/\sigma_y^3) < (\lambda_{y\ max}/\sigma_{y\ min}^3) \tag{F-13}$$

where, from eqs. (F-7) and (F-8):

$$\sigma_{y\ min}^2 = e\ m_{x\ min} \int_{-\infty}^{\infty} h^2(t)dt \tag{F-14}$$

$$\lambda_{y\ max} = e^2\ m_{x\ max} \int_{-\infty}^{\infty} h^3(t)dt \tag{F-15}$$

From (F-14) and (F-15):

$$\lambda_{y\ max}\ \sigma_{y\ min}^{-3} = (m_{x\ max}/m_{x\ min})(m_{x\ min}/e)^{-\frac{1}{2}}\ \chi \tag{F-16}$$

where

$$\chi \equiv \left[\int_{-\infty}^{\infty} h^3(t)dt\right]\left[\int_{-\infty}^{\infty} h^2(t)dt\right]^{-3/2} \qquad \text{(F-17)}$$

The number of photoevents per second is now defined as:

$$\nu \equiv m_{x\ min}/e \qquad \text{(F-18)}$$

Assuming that the scene brightness doesn't change by more than a factor of two from one dwell time to another:

$$(m_{x\ max}/\ m_{x\ min}) < 2 \qquad \text{(F-19)}$$

From eqs. (F-12), (F-13), (F-16), (F-18), and (F-19):

$$\varepsilon_y < 200\ \nu^{-\frac{1}{2}}\chi \qquad \text{(F-20)}$$

It is easy to show that for a rectangular-shaped h(t) of duration τ_D, eq. (F-17) becomes

$$\chi = \tau_D^{-\frac{1}{2}} \qquad \text{(F-21)}$$

where τ_D is the system dwell time. From (F-20) and (F-21):

$$\varepsilon_y < 200(\nu\tau_D)^{-\frac{1}{2}} \qquad \text{(F-22)}$$

For a current of 100 namps and a dwell time of 160 μsec. (cf. eqs. (154) and (G-14)) the number of photoelectrons per dwell time is given by:

$$\nu\tau_D = \frac{10^{-7}\ \text{coul.sec}^{-1}}{1.6\text{x}10^{-19}\ \text{coul.electron}^{-1}\ (1.6\text{x}10^{-4}\ \text{sec})}$$

I.e.,

$$\nu\tau_D = 10^8 \qquad \text{(F-23)}$$

From eqs. (F-22) and (F-23):

$$\varepsilon_y < 0.02 \qquad \text{(F-24)}$$

In general, eq. (F-21) greatly over-estimates the value of χ, and the corresponding upper bound for ε_y is much smaller than indicated by eq. (F-24). This is because h(t) is the impulse response of a bandpass filter, taking on negative values as well as positive values. Thus, there is cancellation in the numerator of eq. (F-17).

It will now be shown that the relative error in $f_y(y)$ can be used as an estimate for the relative error in $\hat{m}_J$. This point is most easily illustrated by employing eq. (D-6) for $\hat{m}_J$. However, either of the crossing rate expressions (51) or (53) could be used instead, at the expense of complicating some of the equations.

From eqs. (D-6) and (52):

$$\dot{m}_J(t) = \int_{\dot{y}_o}^{\infty} (z-\dot{y}_o)\, f_{y\dot{y}}\,(y_o,z)\, dz \qquad \text{(F-25)}$$

For the numerical examples that have been worked thus far (such as those of Section V), it has been found that the correlation coefficient of Y(t) and $\dot{Y}(t)$ is much smaller than unity:

$$r(t) << 1 \qquad \text{(F-26)}$$

where r(t) is defined by eq. (B-24). Since it has just been shown that Y(t) has very nearly a Gaussian density function, and since uncorrelated Gaussian variates are statistically independent, it follows that

$$f_{y\dot{y}}(y_o,z) \approx f_y(y_o)\, f_{\dot{y}}(z) \qquad \text{(F-27)}$$

From eqs. (F-25) and (F-27):

$$\dot{m}_J(t) = f_y(y_o) \int_{\dot{y}_o}^{\infty} (z-\dot{y}_o)\, f_{\dot{y}}(z)dz \qquad \text{(F-28)}$$

Substituting eq. (F-9) into eq. (F-28), it is seen that ε_y provides an estimate for the relative error in $\dot{m}_J$, as well as the relative error in f_y.

APPENDIX G. PARAMETER CHOICE RATIONALE FOR EQUATIONS (149) AND (150)

The object of this Appendix is to describe a rationale for choosing the background and filter parameters x_o, x_1, τ, f_o, and t_o (cf. eqs. (149) and (150)).

It is common IRST design practice[4] to choose the noise bandwidth of the post-detector filter as follows:

$$\Delta f = (2\tau_T)^{-1} \tag{G-1}$$

where

Δf = noise bandwidth of the post-detector filter

τ_T = the time required for the scanning sensor to sweep across a target.

It is not difficult to show that

$$\tau_T = \alpha_T T_F / 2\pi \tag{G-2}$$

where

α_T = the angular extent of a typical target, at the desired detection range (radians)

T_F = the system "frame time," i.e., the time required for the sensor to complete a full 360° azimuthal sweep.

It may be shown that for the transfer function H(f) of eq. (151), the noise bandwidth is given by:

$$\Delta f = (t_o\sqrt{2})^{-1}\left[1 + \exp\left(-2\pi f_o^2 t_o^2\right)\right] \qquad \text{(G-3)}$$

Assuming that

$$H(0) = 2\exp\left(-\pi f_o^2 t_o^2\right) << 1 \qquad \text{(G-4)}$$

it follows from eq. (G-3) that

$$\Delta f \approx (t_o\sqrt{2})^{-1} \qquad \text{(G-5)}$$

Eq. (G-5) is the justification for referring to t_o as a "noise bandwidth parameter" of the post-detector filter.

From eqs. (G-1) and (G-5):

$$t_o = \tau_T\sqrt{2} \qquad \text{(G-6)}$$

Assuming, for example, that

$$\alpha_T = 1 \text{ mrad.} \qquad \text{(G-7)}$$

$$T_F = 1 \text{ sec.}$$

it follows from eqs. (G-2) and (G-6) that

$$\tau_T = 159 \text{ μsec.} \qquad \text{(G-8)}$$

and

$$t_o = 225. \text{ μsec.} \qquad \text{(G-9)}$$

Assuming (somewhat arbitrarily) that

$$H(O) = 10^{-3} \tag{G-10}$$

it follows from eq. (G-4), (G-9), and (G-10) that

$$f_o = 6.91 \text{ kHz} \tag{G-10}$$

Thus, a rationale has been provided for choosing the filter parameters f_o and t_o of eq. (149).

To complete the problem specification, it remains to choose values for the parameters of eq. (150):

τ = the time required for the sensor to scan across the object

x_o = background brightness parameter (amperes)

x_1 = object contrast parameter (dimensionless)

Analagous to eq. (G-2):

$$\tau = \alpha_o T_F / 2\pi \tag{G-11}$$

where

α_o = object angular extent (radians)

The form of eq. (150) is general enough to describe both "target-like" and "clutter-like" objects. Target-like objects are defined by:

$$\alpha_o \leq \alpha_T \tag{G-12}$$

Clutter-like objects are defined by:

$$\alpha_o > \alpha_T \tag{G-13}$$

It follows from eqs. (G-2), (G-8), and (G-11) that the parameter value

$$\tau = 159 \text{ μsec.} \tag{G-14}$$

corresponds to a target-like object $\alpha_o = \alpha_T$.

The value for x_o in eq. (150) is obtained as follows:

$$x_o = R_I \, P_{opt} \tag{G-15}$$

where

x_o = uniform background current (amperes)

R_I = current responsivity (amperes/watt)

P_{opt} = optical power incident on a single detector (watts)

The optical power P_{opt} in eq. (G-15) is calculated as:

$$P_{opt} = L_B \, A_{ap} \, \omega \tag{G-16}$$

where

L_B = in-band background radiance (watts cm^{-2}. sr^{-1})

A_{ap} = area of the telescope aperture (cm^2)

ω = instantaneous field-of-view (sr)

The current responsivity R_I in eq. (G-15) is calculated as:

$$R_I = \frac{\eta e}{h\nu} \qquad \text{(G-17)}$$

where

η = quantum efficiency (photoelectrons · (incident photon)$^{-1}$)

e = electronic charge (coulombs (electron)$^{-1}$)

h = Planck's constant (joule sec (photon)$^{-1}$)

ν = optical frequency (sec.$^{-1}$)

It follows from eq. (G-17) and the numerical values of e and h that:

$$R_I = 0.8\eta\bar{\lambda} \qquad \text{(G-18)}$$

where

$\bar{\lambda}$ = average optical wavelength (μm)

It follows from eq. (G-15), (G-16), and (G-18) that

$$x_o = 134 \text{ namps.} \qquad \text{(G-19)}$$

for the following assumed parameter values:

$$A_{ap} = 500 \text{ cm}^2$$

$$\omega = \alpha^2 = 10^{-6} \text{ sr.}$$

$$\eta = 0.6$$

$$\bar{\lambda} = 4.0 \text{ } \mu\text{m}$$

and

$$L_B = 0.14 \text{ mw cm}^{-2} \text{ sr}^{-1} \qquad \text{(G-20)}$$

The value of background radiance given by eq. (G-20) was obtained by integrating Fig. 1 of Ref. (28) over the wavelength band 3-5 μm.

The assumed value of peak object contrast, eq. (155), was chosen arbitrarily. It is not difficult to calculate the value of apparent contrast radiant intensity corresponding to given values of x_o and x_1.